THE UNIVERSITY OF WESTERN ONTARIO

DEPARTMENT OF PHYSICS

MOLECULAR EXCITATION GROUP

LONDON LOCI OF DIATOMIC MOLECULAR SPECTRA

by

MARY FRANCES MURTY

October 8, 1964

CONDON LOCI OF DIATOMIC MOLECULAR SPECTRA

by

Mary Frances Murty

Submitted in partial fulfillment

of the requirements for the degree of

Master of Science

Faculty of Graduate Studies

The University of Western Ontario

London, Canada

1964

Approved for the
Department of Physics
by the Advisory Committee

R. W. Nicholls

H. D. Ferguson

Peter A. Fraser

Approved for the
Department of Physics
by the Examining Committee

Charles W. Cunningham

Peter A. Fraser

W. H. Wehlau

Date: Oct 8/64

ABSTRACT

26046

The geometry in the v'v" plane of Condon loci of diatomic molecular band systems is studied. Using both simple harmonic and Morse potential models it is shown that for most band systems the largest contribution to the overlap integral of the vibrational wave functions of a transition is from the coincidence of a single pair of antinodes of the wave functions. The coincidence of a pair of terminal antinodes describes the primary Condon locus, while the coincidence of a terminal and an internal antinode describes a subsidiary Condon locus in cases where the loci are nested.

A single pair of coinciding antinodes does not control the magnitude of the overlap integral in band systems where Δr_e is either very small (< 0.01 Å) or very large (> 0.3 Å). Thirteen band systems are examined with Δr_e ranging from zero to 0.4 Å.

It is shown that the location of strong bands in the v'v" plane can be predicted with reasonable accuracy without the computation of Franck-Condon factors.

Author

ACKNOWLEDGEMENTS

The author wishes to convey her sincere thanks to Dr. R. W. Nicholls who suggested this problem, for his supervision and encouragement, and for making available his computations of Franck-Condon factors.

Grateful thanks are extended to Dr. P. A. Fraser and Dr. H. I. S. Ferguson for helpful discussions.

The author also wishes to thank Dr. P. A. Forsyth, Head of the Department of Physics, for making available the facilities of the department.

The assistance of Mr. J. Radema and Mr. T. Davidson in the preparation of diagrams, and of Miss K. Tritjak in computational work is gratefully acknowledged.

This work has been supported by a research contract from the Department of Defence Production, and by research grants from the National Research Council of Canada, the National Aeronautics and Space Administration (NSG-349), the United States Air Force Office of Scientific Research (AF-AFOSR62-236) and the United States Air Force Cambridge Research Center (AF 19(628)-2820). This support is gratefully acknowledged.

TABLE OF CONTENTS

ABSTRACT iii

ACKNOWLEDGEMENTS iv

LIST OF TABLES viii

LIST OF FIGURES x

Chapter 1. The Franck-Condon Principle in Diatomic Molecular Spectroscopy 1

1.1 Introduction 1

1.2 The Intensity Distribution in Band Systems of Diatomic Molecules - Condon Loci 4

1.3 The Franck-Condon Principle and Franck-Condon Factors 4

Chapter 2. Concepts 9

2.1 Band Intensities and Franck-Condon Factors 9

2.2 Suggested Identity of Condon Loci 15

2.3 Geometry of the Primary Condon Locus 17

Chapter 3. Condon Loci and the Simple Harmonic Molecular Potential Model 18

3.1 The Simple Harmonic Oscillator Model of a Diatomic Molecule 18

3.2 Reduction of Antinode Position to Algebraic Form 21

3.3 Coincidence of Antinode Pairs 23

3.4 Form of the Loci of Antinode Coincidence 27

3.5 Detailed Examination of Representative Types of Transition 31

3.5.1 MgH $C^2\Pi \rightarrow X^2\Sigma$ and $A^2\Pi \rightarrow X^2\Sigma$ 31

3.5.1a Comparison of Overlap Integral with Antinode Coincidence 40

3.5.2 CO $A^1\Pi \rightarrow X^1\Sigma$ Fourth Positive System .. 42

3.5.3 C_2 $B^3\Pi \rightarrow X^3\Pi$ Fox-Herzberg System 46

3.6 Additional Remarks on the Geometry of the Primary Condon Locus 46

3.7 A Simple Method of Finding the Subsidiary Condon Loci 51

Chapter 4. Condon Loci and the Morse Potential Model 54

4.1 The Morse Model of a Diatomic Molecule 54

4.2 Wave Functions, Overlap Integrals and Franck-Condon Factors 56

4.3 Reduction of Antinode Position to Algebraic Form 56

4.4 Graphical Method for Locating the Coincidence of Antinode Pairs 57

4.5 Loci of Antinode Coincidence 57

4.6 Detailed Examination of Representative Types of Transition 59

4.6.1 MgO $B^1\Sigma \rightarrow X^1\Sigma$ Green System 59

4.6.2 CO $A^1\Pi \rightarrow X^1\Sigma$ Fourth Positive System .. 64

4.6.3 C_2 $B^3\Pi \rightarrow X^3\Pi$ Fox-Herzberg System 64

Chapter 5. Conclusions 70

Appendix 1. Further Results of the Examination of Condon Loci Using the Simple Harmonic Oscillator Model 72

A1.1 CH^+ $A^1\Pi \rightarrow X^1\Sigma$ 73

A1.2 CO^+ $A^2\Pi \rightarrow X^2\Sigma$ Comet Tail System 76

A1.3 O_2 $B^3\Sigma_u^- \rightarrow X^3\Sigma_g^-$ Schumann-Runge System 82

A1.4 GaI $A^3\Pi \rightarrow X^1\Sigma$ System A 82

Appendix 2. Further Results of the Examination of Condon Loci Using the Morse Oscillator Model 90

A2.1 N_2^+ $B^2\Sigma^+_u \leftarrow N_2X^1\Sigma^+_g$ Rydberg System 90

A2.2 MgO $B^1\Sigma \rightarrow A^1\Pi$ Red System 94

A2.3 CO^+ $A^2\Pi \rightarrow X^2\Sigma$ Comet Tail System 94

A2.4 N_2^+ $C^2\Sigma^+ \leftarrow N_2X^1\Sigma^+_g$ 100

A2.5 N_2^+ $D^2\Pi_g \leftarrow N_2X^1\Sigma^+_g$ 100

A2.6 O_2 $B^3\Sigma_u^- \rightarrow X^3\Sigma_g^-$ Schumann-Runge System 105

A2.7 GaI $A^3\Pi \rightarrow X^1\Sigma$ System A 105

REFERENCES 112

VITA 114

LIST OF TABLES

Table 1.1 Band Intensities of MgO B → A 5

3.1 Empirical Constants Describing Antinode Loci 22

3.2 Data for Transitions Examined with SHO Model 29

3.3 Observed Bands of MgH C → X 32

3.4 Observed Bands of MgH A → X 32

3.5 Overlap Integrals of MgH C → X 34

3.6 Overlap Integrals of MgH A → X 34

3.7 Examination of Contributions to Overlap Integral of MgH C → X 38

3.8 Overlap Integrals of CO A → X 43

3.9 Observed Bands of CO A → X 44

3.10 Observed Bands of C_2 B → X 47

3.11 Overlap Integrals of C_2 B → X 47

4.1 Data for Transitions Examined with Morse Model 60

4.2 Band Intensities of MgO B → X 61

4.3 Franck-Condon Factors for MgO B → X 62

4.4 Franck-Condon Factors for CO A → X 65

4.5 Franck-Condon Factors for C_2 B → X 67

A1.1 Observed Bands of CH^+ A → X 74

A1.2 Overlap Integrals of CH^+ A → X 74

A1.3 Examination of Contributions to Overlap Integral of CH^+ A → X 77

A1.4 Band Intensities of CO^+ A → X 78

A1.5 Overlap Integrals of CO^+ A → X 80

A1.6 Band Intensities of O_2 B → X 83

A1.7 Overlap Integrals of GaI A → X 86

A1.8 Band Intensities of GaI A → X 87

A2.1 Franck-Condon Factors for $N_2^+B \rightarrow N_2X$ 92

A2.2 Franck-Condon Factors for MgO B → A 95

A2.3 Band Intensities of MgO B → A 96

A2.4 Franck-Condon Factors for CO^+ A → X 98

A2.5 Franck-Condon Factors for $N_2^+C \rightarrow N_2X$ 101

A2.6 Franck-Condon Factors for $N_2^+D \rightarrow N_2X$ 103

A2.7 Franck-Condon Factors for O_2 B → X 106

A2.8 Franck-Condon Factors for GaI A → X 109

LIST OF FIGURES

Figure 1.1a	Franck-Condon Factor $q_{v'v''}$ Surface for MgO ($B^1\Sigma \rightarrow A^1\Pi$) Band System	3
1.1b	Condon Loci for MgO ($B^1\Sigma \rightarrow A^1\Pi$) Band System	3
2.1	Vibrational Wave Function, v = 5	13
2.2	Overlapping of pairs of antinodes	14
2.3	Reduced Vibrational wave function	16
	2.3a even vibrational quantum number	
	2.3b odd vibrational quantum number	
3.1	Antinode loci of simple harmonic oscillator	20
3.2	Nomenclature of antinode coincidence on potential energy diagram	26
3.3	Positioning of antinode coincidence on v'v" plane for $r_e'' < r_e'$	26
3.4	Transition illustrating primary locus	28
3.5	Segments of primary locus	28
3.6	Loci of coincidence of antinode pairs, MgH C → X ..	35
3.7	Loci of coincidence of antinode pairs, MgH A → X .	36
3.8	Progression plots of overlap integral of MgH C→X .	37
3.9	Loci of coincidence of antinode pairs, CO A → X ...	45
3.10	Loci of coincidence of antinode apirs, C_2 B → X ...	48
3.11	Primary Condon locus	50
3.12	Approximate loci of coincidence of antinode pairs, CO A →X	53

4.1 Potential energy of a Morse diatomic molecule 55

4.2 Antinode positions of CO^+ A and X states 58

4.3 Loci of coincidence of antinode pairs, MgO B→X ... 63

4.4 Loci of coincidence of antinode pairs, CO A→X ... 66

4.5 Loci of coincidence of antinode pairs, C_2B→X 68

Al.1 Loci of coincidence of antinode pairs, CH^+ A→X ... 75

Al.2 Loci of coincidence of antinode pairs, CO^+ A→X ... 81

Al.3 Loci of coincidence of antinode pairs, O_2 B→X 84

Al.4 Loci of coincidence of antinode pairs, GaI A→X ... 88

A2.1 Loci of coincidence of antinode pairs, N_2^+ B←N_2X ... 93

A2.2 Loci of coincidence of antinode pairs, MgO B→A ... 97

A2.3 Loci of coincidence of antinode pairs, CO^+ A→X ... 99

A2.4 Loci of coincidence of antinode pairs, N_2^+C←N_2X 102

A2.5 Loci of coincidence of antinode pairs, N_2^+D←N_2X 104

A2.6 Loci of coincidence of antinode pairs, O_2 B→X 107

A2.7 Loci of coincidence of antinode pairs, GaI A→X ... 110

CHAPTER I

THE FRANCK-CONDON PRINCIPLE IN DIATOMIC MOLECULAR SPECTROSCOPY

1.1 Introduction

The interpretation of emission and absorption intensity measurements of atomic and molecular spectra is an important part of contemporary astrophysics, space physics and laboratory atomic and molecular physics.

Spectral intensities are controlled, apart from population and energy quantum factors, by the transition strength S. In the general case this is the square of the quantum mechanical matrix element of the dipole moment,

$$S = \left| \int \psi_u^* M \psi_L \, d\tau \right|^2 . \qquad (1.1)$$

In the case of one rotational line of a diatomic molecular spectrum it is

$$S_{uL} = S_{\Lambda'' J''}^{\Lambda' J'} \; R_e^2 (\bar{r}_{v'v''}) \; q_{v'v''} , \qquad (1.2)$$

where $S^{\Lambda' J'}_{\Lambda'' J''}$ is the Hönl-London factor or line strength, $R_e(r)$ is the electronic transition moment which can be related to the "band-system strength", and $q_{v'v''}$ is the Franck-Condon factor or band strength. The Hönl-London factors are well known simple polynomials of J and Λ. The electronic transition moment is the matrix element of the electric dipole moment with respect to the two electronic wave functions involved:

$$R_e(r) = \int \psi^{*}_{u,el} \; M_{el} \, \psi_{L,el} \; d\tau_{el} \quad . \tag{1.3}$$

The Franck-Condon factor is the square of the overlap integral of the vibrational wave functions involved:

$$q_{v'v''} = \left| \int \psi_{v'} \, \psi_{v''} \; dr \right|^2 \quad . \tag{1.4}$$

This factor exerts the dominating control on the distribution of integrated band intensities over a band system. The Franck-Condon factor array may be represented as a three-dimensional surface (see fig. 1.1a) which is strongly undulatory with a series of ridges often roughly symmetrical about the line $v' = v''$. The ridges represent the potentially strong bands. The projection of the ridges on the $v'v''$ plane is a series of nested open curves (see fig. 1.1b) called Condon loci.

It is the purpose of this thesis to discuss the circumstances which control the geometrical properties of the loci. Such a study has obvious applications to the identification of molecular spectra and to the prediction of the positions of other strong bands of a system which is only known fragmentarily.

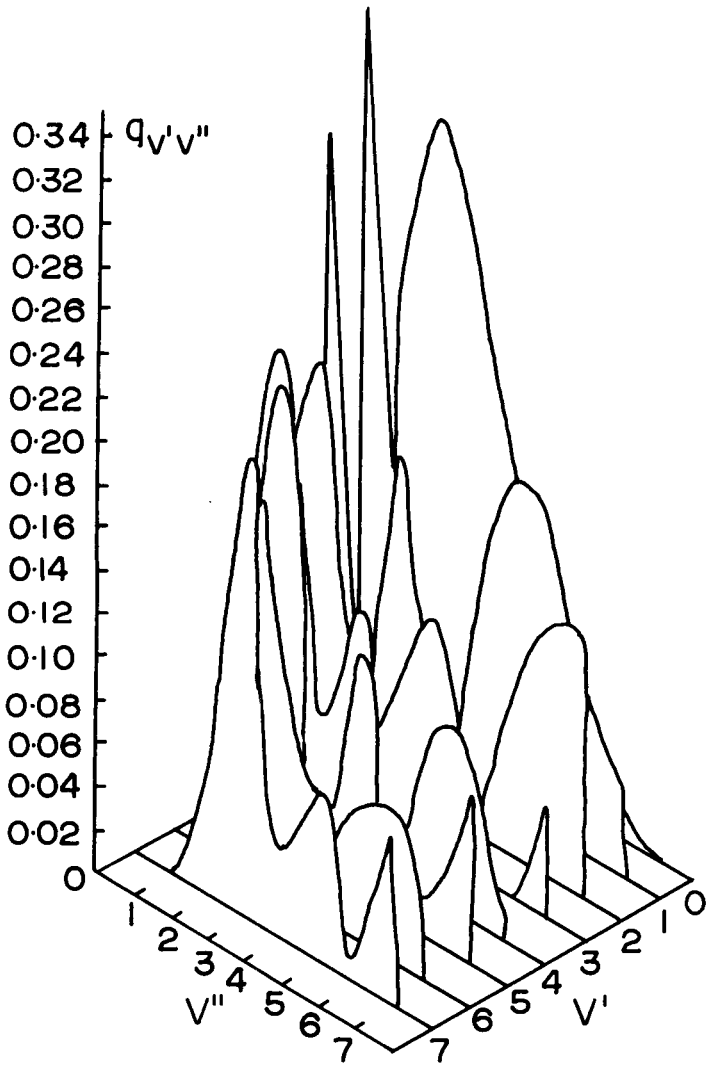

Fig.1.1a

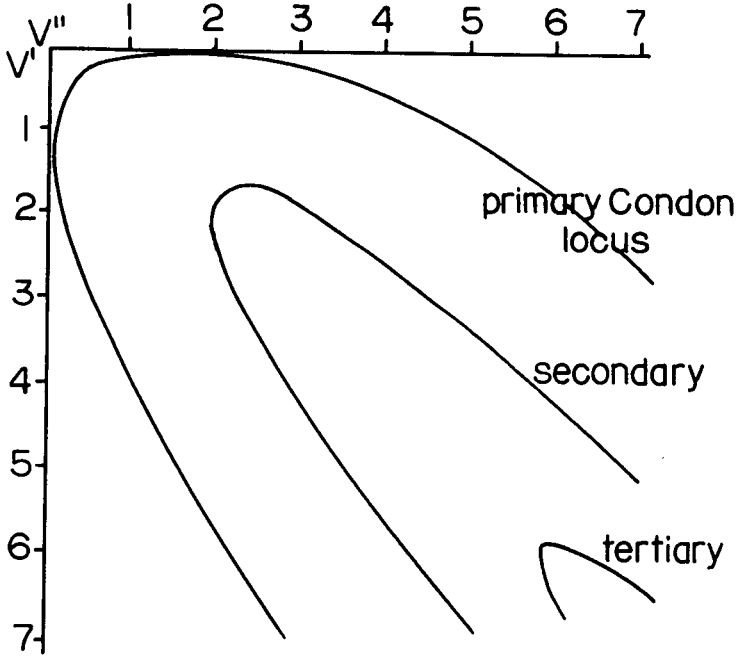

Fig.1.1b

Franck-Condon factor surface and Condon loci for MgO B $^1\Sigma \rightarrow$ A $^1\Pi$ band system

1.2 The Intensity Distribution in Band Systems of Diatomic Molecules - Condon Loci

If the observed bands of a system are placed in a two-dimensional array of vibrational quantum numbers v' and v'' (Deslandres Table), it is noticed that for nearly all transitions the most intense fall on distinct quasi-parabolic loci. The successive loci lie one inside the other and are said to be nested. The outermost locus relates to the strongest bands of the system and is known as the primary Condon locus. The inner loci are the subsidiary Condon loci. The loci are clearly illustrated in table 1.1 by the intensity array of the MgO $B^1\Sigma - A^1\Pi$ system. For some transitions the loci degenerate into a single diagonal line. Further, for a few other transitions the loci appear as parallel diagonal lines, the main diagonal ($v' = v''$) relating to the most intense bands.

The loci of intense bands are close to the loci of high Franck-Condon factors, the proximity being governed by the accuracy of the vibrational model used in their calculation.

1.3 The Franck-Condon Principle and Franck-Condon Factors

The mechanism of photodissociation of a diatomic molecule was discussed qualitatively by Franck (1926) in a study of the strongest bands of a system. He explained that a spontaneous electronic transition affects neither the position nor the momentum of the nuclei directly, for the electronic rearrangements occur much more rapidly than nuclear rearrangements. Thus the instantaneous internuclear separation and nuclear momentum remain unchanged in a

Table 1.1

Band Intensities of MgO B→A (Mahanti 1932)

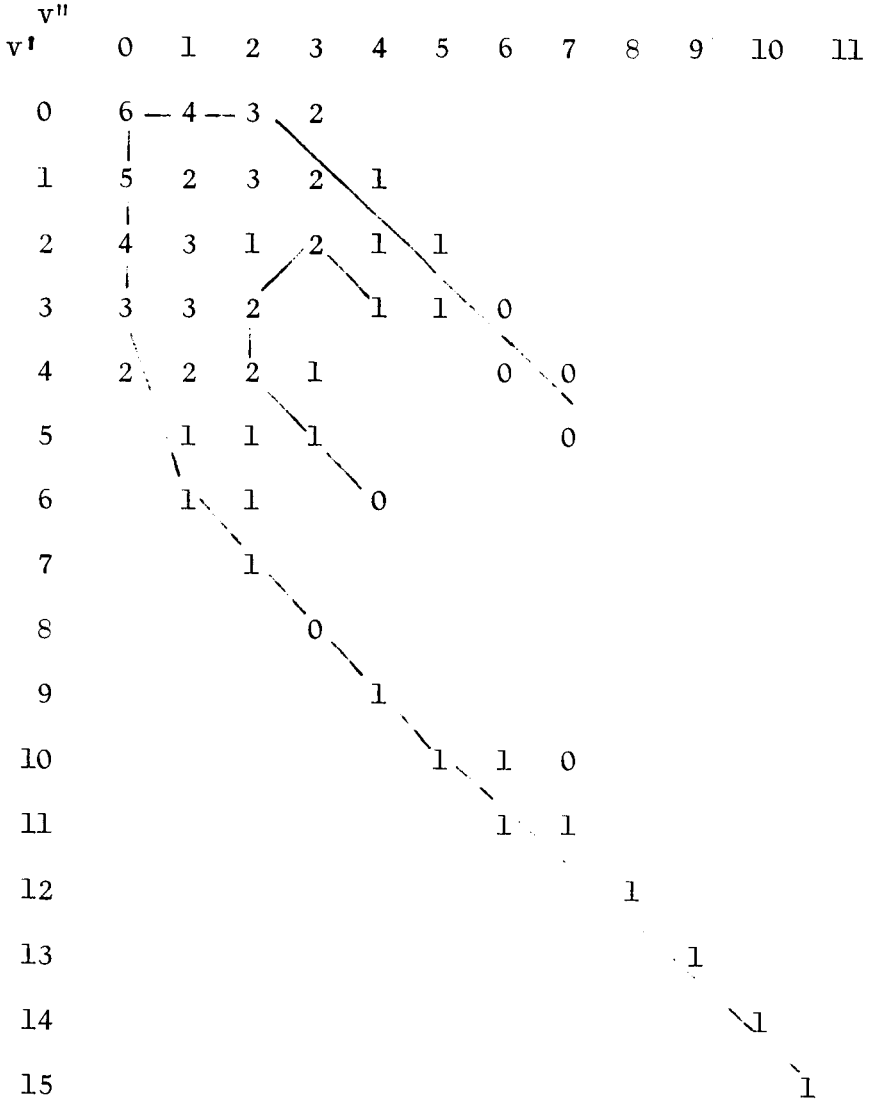

spontaneous transition. Such a transition is represented (fig. 1.2) as a vertical line from a point on the lower curve to a point on the upper curve on a potential energy diagram. The respective points on the potentials are the classical turning points of the vibrational motion.

Condon (1926) qualitatively extended the theory to band systems in emission showing that the preferred bands lie on a quasi-parabolic locus on the v'v" plane (the Condon Parabola). Jenkins et al. (1927) found that most of the observed β bands of NO lie close to the predicted Condon Parabola. A few bands however were found to lie inside this locus, and no explanation was advanced at the time. Condon (1947) recalls that following the introduction of wave mechanical ideas by Schrödinger he was able (Condon 1928) to associate the intensity of a band with the square of the overlap integral of the vibrational wave functions of the initial and final states, i.e. $I \propto \left| \int \psi_{v'} \psi_{v''} \, dr \right|^2$. Later Bates (1952) suggested that it be called the Franck-Condon factor. It is often denoted symbolically by $q_{v'v''}$ as in eq. 1.4.

Franck-Condon factor arrays have been calculated for a large number of transitions for a variety of molecular potential functions using many different methods, e.g. by Hutchisson (1930), Wehrli (1934), Gaydon and Pearse (1939), Pillow (1949), Aiken (1951), Jarmain et al (1955), Nicholls (1962a), Jarmain (1963) and Flinn et al (1964) to name only a few. In all cases, except those studied by Wehrli, large values of the factor were found to lie on nested loci and to

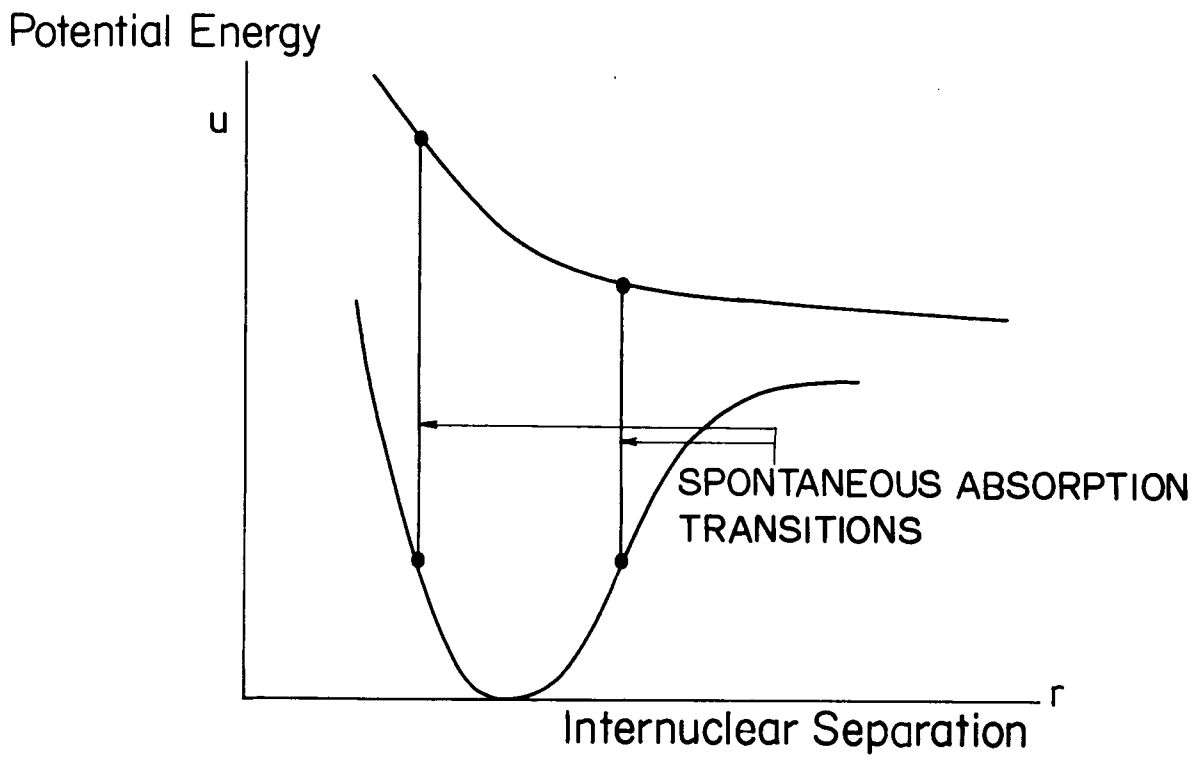

Fig.I.2 Photodissociation

be associated with strong bands, the outer one being called the primary Condon locus and the inner ones subsidiary Condon loci, though in sone cases the loci were confined to the $v' = v''$ diagonal. The study by Wehrli was of the simple harmonic oscillator model, the initial and final states having the same equilibrium internuclear separation. In this case there is complete cancellation in the overlap integral of pairs of vibrational wave functions of odd difference in vibrational quantum number. Wehrli concluded that this situation is not in accordance with the classical Franck-Condon Principle. It follows that this case is not in accordance with the semi-quantum form of the principle discussed in this thesis.

The following chapters of this thesis show the relevance of the Franck-Condon factor to the intensity of a spectral band and the distribution of intensity in a band system. The semi-quantum form of the Franck-Condon Principle advanced to account for the geometrical aspects of the distribution in the $v'v''$ plane is discussed, and examined for a number of band systems using simple harmonic and Morse molecular models.

CHAPTER 2

CONCEPTS

2.1 Band Intensities and Franck-Condon Factors

The concept of transition probability which controls spectral intensities is reviewed in this chapter. The distribution of intensity in a band system of a diatomic molecule is controlled in a large part by the degree of overlap between the vibrational wave functions of the upper and lower levels of the transition as asserted by the Franck-Condon Principle and explained in the introduction.

The intensity I_{uL} of radiation of the energy quantum E_{uL} emitted from an optically thin gas is proportional to the probability of this transition, the population of the upper state N_u, and the energy quantum. Thus

$$I_{uL} = A_{uL} N_u E_{uL} , \qquad (2.1)$$

where A_{uL} is the Einstein A coefficient, the spontaneous transition probability.

The Einstein A coefficient is defined (see Allen 1962) in terms of the line strength S_{uL} by

$$g_u A_{uL} = \frac{64\pi^4}{3hc^3} \nu_{uL}^3 S_{uL} \qquad (2.2)$$

where g_u is the statistical weight of the upper state, u, ν_{uL} is the frequency of the quantum of energy E_{uL}, and S_{uL} is the transition strength which may be separated into parts dependent on the electronic and vibrational motion and the rotational motion viz.

$$S_{uL} = S_{v'v''} S^{J'\Lambda'}_{J''\Lambda''} \qquad (2.3)$$

$S_{v'v''}$ is known as the band strength and is given as

$$S_{v'v''} = \left| \int \psi_{v'} R_e(r) \psi_{v''} dr \right|^2 , \qquad (2.4)$$

where $R_e(r) = \int \psi^*_{u,el}(\underline{r}_i , r) M_{el} \psi_{L,el}(\underline{r}_i, r) d\tau_{el}$. (2.5)

$S^{J'\Lambda'}_{J''\Lambda''}$ is known as the Hönl-London factor and has been tabulated for all important transitions as simple functions of J and Λ (see Herzberg 1950). However in the discussion of integrated band intensities $\sum_{J''} S^{J'\Lambda'}_{J''\Lambda''}$ and $\sum_{J'} S^{J'\Lambda'}_{J''\Lambda''}$ are required. They are the statistical weights of the J' and J'' levels respectively and equal to $2J' + 1$ and $2J'' + 1$. The statistical weight of the upper state, g_u, may be expressed in terms of the electronic statistical weight, d_u:

$$g_u = d_u (2J' + 1). \qquad (2.6)$$

Hence for one rotational line of a spectrum eq. 2.2 may be written

$$A^{uv'J'}_{Lv''J''} = \frac{64\pi^4}{3hc^3 d_u(2J'+1)} \nu^3 {}^{uv'J'}_{Lv''J''} S_{v'v''} S^{J'\Lambda'}_{J''\Lambda''} \qquad (2.7)$$

and an A coefficient for a band defined as

$$A_{v'v''} = \sum_{J'} \sum_{J''} A^{uv'J'}_{Lv''J''} \tag{2.8}$$

$$= \frac{64\pi^4}{3hc^3 d_u} \sum_{J'} \left[\frac{\nu^3 \, {}^{uv'J'}_{Lv''J''}}{2J' + 1} \sum_{J''} S_{v'v''} \, S^{J'\Lambda'}_{J''\Lambda''} \right] \tag{2.9}$$

$$= \frac{64\pi^4}{3hc^3 d_u} \nu^3_{v'v''} \left| \int \psi_{v'} R_e(r) \psi_{v''} \, dr \right|^2 \tag{2.10}$$

where $\nu_{v'v''}$ is an average frequency for the v'v'' band. Fraser (1954) showed that although the electronic transition moment varies markedly with r, an r-centroid, $\bar{r}_{v'v''}$ may be defined so that

$$\left| \int \psi_{v'} R_e(r) \psi_{v''} \, dr \right|^2 = R_e^2 (\bar{r}_{v'v''}) \left| \int \psi_{v'} \psi_{v''} \, dr \right|^2 \tag{2.11}$$

$$= R_e^2 (\bar{r}_{v'v''}) \; q_{v'v''} \tag{2.12}$$

where $q_{v'v''}$ is the Franck-Condon factor.

The integrated intensity of a band is thus

$$I_{v'v''} = \frac{64\pi^4}{3c^3 d_u} \nu^4_{v'v''} N_{v'} \; R_e^2(\bar{r}_{v'v''}) \; q_{v'v''} \tag{2.13}$$

where $N_{v'}$ is the population of the upper level v'. The Franck-Condon factor varies from band to band by many orders of magnitude, dominating the effect on the intensity of the distribution of population among the levels v' and the variation of the wavelength over a band system.

The values of v' and v'' of strong bands define the Condon loci on the v'v'' plane (table 1.1 and fig. 1.1). In cases where the loci are nested the outer (primary Condon locus) is closely associated with the equivalence of turning points of the classical vibrational

motion because of the large contribution to the overlap integral of the aligned terminal antinodes of the vibrational wave functions ψ_v. These functions, ψ_v, are oscillatory with v+1 antinodes (fig. 2.1). The terminal loops are considerably larger than the internal loops, because ψ has greater "wavelength" in the terminal region than elsewhere. This means that the area under a terminal loop is greater than that under an internal loop.

The nomenclature used to specify an antinode is shown in fig. 2.1. The antinode position is denoted by r with two subscripts. The first is either 1 or 2 depending on whether the antinode is closest to the left or right-hand turning point of the vibrational motion. The second subscript is the number, p, of the antinode counting inwards from the terminal antinode. The terminal, or primary, antinodes are thus $r_{1,1}$ and $r_{2,1}$; the secondary $r_{1,2}$ and $r_{2,2}$; the pth $r_{1,p}$ and $r_{2,p}$.

An antinode of a vibrational wave function of one electronic state lying at the same internuclear distance as one of another state will make a large contribution to the overlap integral (fig. 2.2a) particularly if the loops are large and of comparable wavelength (fig. 2.2b). The overlap integral of the two wave functions will be additionally augmented if other antinodes of the two wave functions exist in the same region of internuclear separation (fig. 2.2c).

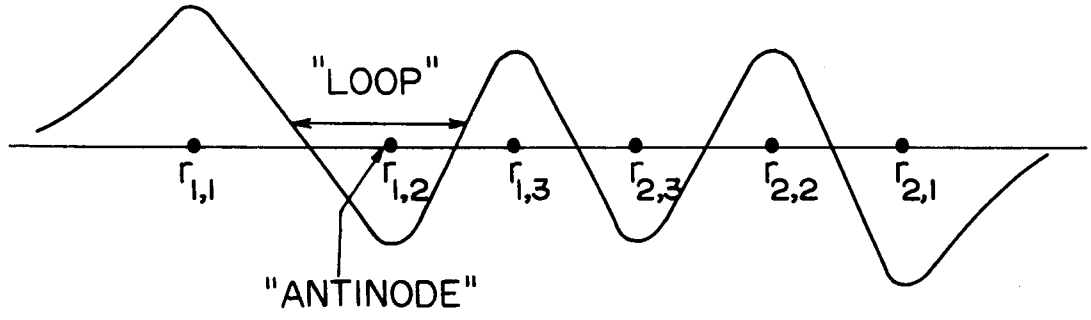

Fig.2.1 Vibrational wave function, v=5

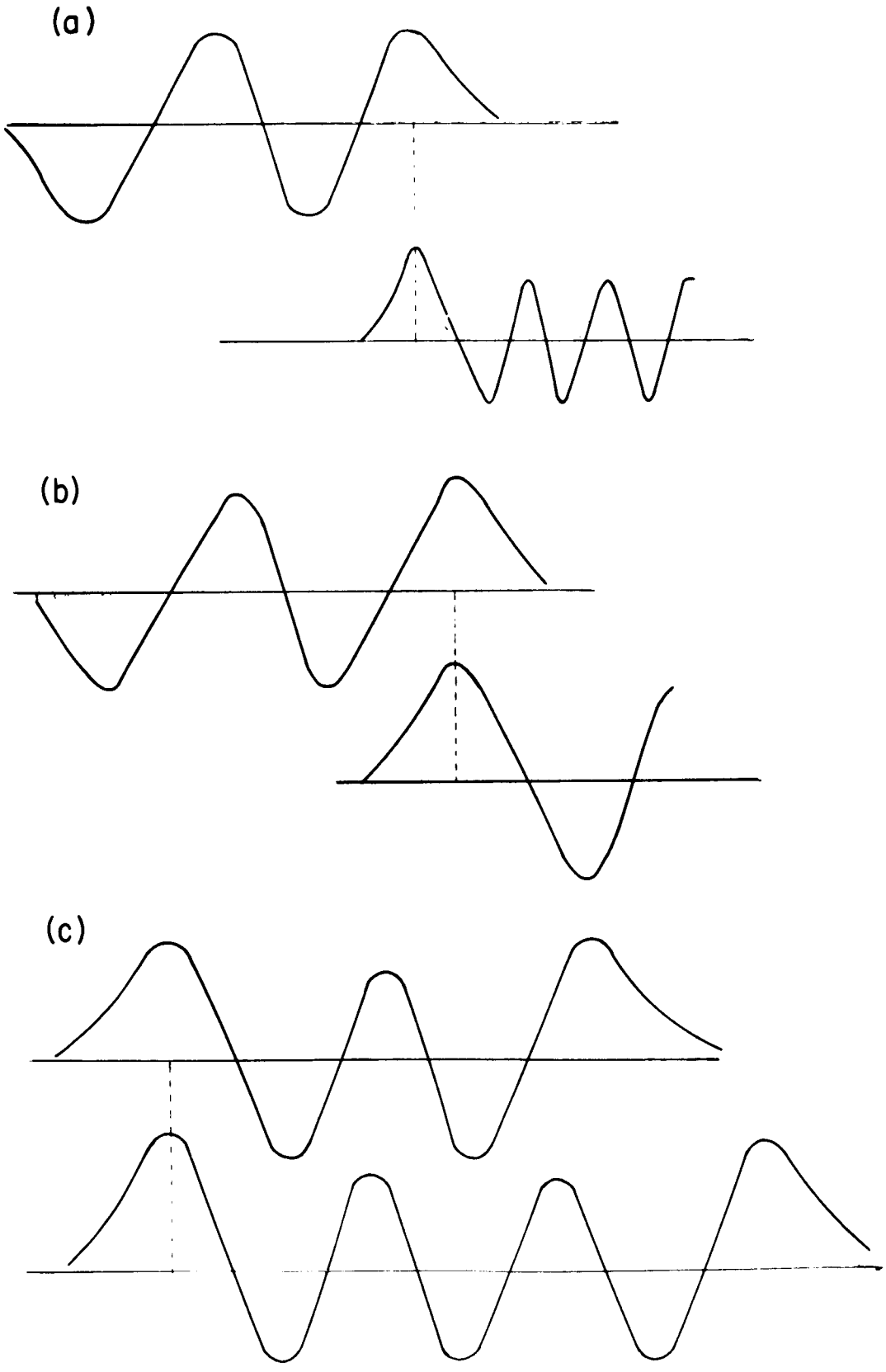

Fig. 2.2 Overlapping of pairs of antinodes (see text)

2.2 Suggested Identity of Condon Loci

The subsidiary Condon loci have a very similar geometrical appearance to the primary Condon locus. As previously mentioned the primary locus is the result of the large contribution to the overlap integral by the coincidence of terminal antinodes. It is suggested (Nicholls 1963a) that there is a similar association of antinode pairs giving the systematic behaviour of the Franck-Condon factors and the regular geometrical appearance of the subsidiary Condon loci. Each subsidiary locus is thought to be associated with the coincidence of a terminal antinode of one vibrational wave function with an internal antinode of a vibrational wave function of the other state of the transition; the pth locus being associated with a pth antinode.

The geometrical study of Condon loci is thus based on the calculation of the loci in the $v'v''$ plane of the coincidence of antinode pairs given by the condition $r'_{1 \text{ or } 2,\ p} = r''_{1 \text{ or } 2,\ 1}$ or $r'_{1 \text{ or } 2,\ 1} = r''_{1 \text{ or } 2,\ p}$ where $p = 1, 2, 3 \ldots$ and denotes the order of the locus. The coincidence of pairs of internal antinodes ($r'_{1 \text{ or } 2,\ p'} = r''_{1 \text{ or } 2,\ p''}$, $p' = 2, 3 \ldots$, $p'' = 2, 3 \ldots$) will not describe new loci on the $v'v''$ plane, but will lie close to the loci described above and give additional contributions to the overlap integral.

The above treatment is equivalent to treating each vibrational wave function as a series of delta functions of unit value at the antinodes, and zero elsewhere. This is illustrated by fig. 2.3

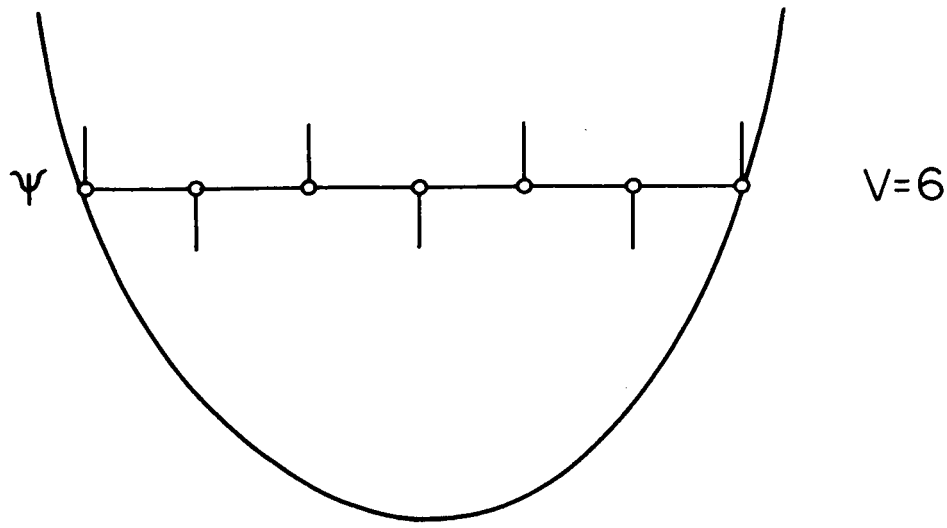

(a) even vibrational quantum number

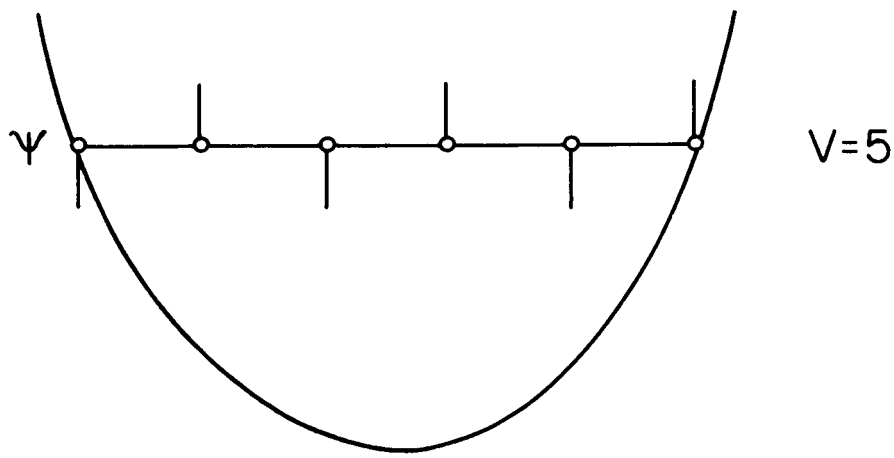

(b) odd vibrational quantum number

Fig. 2.3 Reduced vibrational wave functions

which shows both even and odd vibrational wave functions thus reduced. The wave function is now given by

$$\begin{aligned} \psi_v &= 0 \text{ when } r \neq r_{1 \text{ or } 2,\ p} \\ &= (-1)^{p+1} \text{ when } r = r_{1 \text{ or } 2,\ p}\text{ , v even} \\ &= (-1)^{p} \text{ when } r = r_{1,\ p}\text{ , v odd} \\ &= (-1)^{p+1} \text{ when } r = r_{2,\ p}\text{ , v odd} \end{aligned} \tag{2.14}$$

Calculation of the coincidence of antinodes will in general yield non-integral values of vibrational quantum numbers. These are unrealistic but a high value of overlap integral can be expected in the surrounding region on the v'v" plane.

2.3 Geometry of the Primary Condon Locus

The geometry of primary Condon loci using a simple harmonic potential has been discussed by Manneback (1951) and Nicholls (1962b). They have shown that the width of the skewed displaced parabola resulting from the coincidence of turning points is a function of the equilibrium internuclear separation, and that the inclination of the locus to the main diagonal is a function of the harmonic oscillator frequencies. No similar study has been made of subsidiary loci, or of the loci resulting from anharmonic potentials due to the algebraic difficulties. We have however studied the general form of the loci calculated according to Nicholls' suggestion (1963a) for a wide range of Δr_e and ω_e'/ω_e'' values for both simple harmonic and Morse potentials.

CHAPTER 3

CONDON LOCI AND THE SIMPLE HARMONIC MOLECULAR POTENTIAL MODEL

3.1 The Simple Harmonic Oscillator Model of a Diatomic Molecule

The simplest possible assumption about the form of the vibrations in a diatomic molecule is that each atom moves towards or away from the other in simple harmonic motion. Such a motion of the two atoms is equivalent to the harmonic vibration of a single mass point having the reduced mass (μ) of the molecule about an equilibrium position (r_e). The wave functions of this vibration are well known (Pauling and Wilson 1935) and have been tabulated by Gaydon and Pearse (1939) and Pillow (1949). Sixty-four arrays of vibrational overlap integral based on SHO wave functions have been calculated by Aiken (1951) and discussed by Manneback (1951). The simple harmonic oscillator model is thus very suitable for our study of the systematics of antinode coincidence and Condon loci.

The Schrödinger wave equation of a simple harmonic system is:

$$\frac{d^2\psi}{dx^2} + \frac{8\pi^2}{h^2}\mu\,(E - 2\pi^2\mu\upsilon^2 x^2) = 0 \qquad (3.1)$$

where $x = r - r_e$, the displacement of the mass point from the

equilibrium position, and ν is the vibrational frequency of the motion. The eigenvalues of 3.1 are

$$E(v) = h\nu\,(v + \tfrac{1}{2}) \qquad (3.2)$$

where v is the vibrational quantum number taking integral values (0, 1, 2 ...) only. The eigenfunctions of 3.1 are known to be the Hermite orthogonal functions (see Pauling and Wilson 1935)

$$\psi_v(x) = N_v \exp\left(-\frac{\xi^2}{2}\right) H_v(\xi)\,, \qquad (3.3)$$

where $$\xi = \sqrt{\alpha}\,x\,, \qquad (3.4)$$

$$\alpha = \frac{4\pi^2}{h}\mu\nu = \frac{4\pi^2 c}{h}\mu\omega_e\,, \qquad (3.5)$$

$$N_v = \left\{\left(\frac{\alpha}{\pi}\right)^{\frac{1}{2}} \frac{1}{2^v\, v!}\right\}^{\frac{1}{2}}\,, \text{ the normalising constant} \qquad (3.6)$$

and $$H_v = (-1)^v e^{\xi^2} \frac{d^v}{d\xi^2} e^{-\xi^2}\,, \text{ the Hermite polynomial of order } v \qquad (3.7)$$

The energy level diagram showing the potential energy, the vibrational levels and the wave functions for a few levels of a simple harmonic oscillator are shown in fig. 3.1. Antinode positions of the wave functions are joined and the quasi-parabolic curves labelled with the appropriate value of p (see also fig. 2.1).

It must be emphasized that the simple harmonic oscillator model is of limited application. It is a realistic representation of the motion of a diatomic molecule only close to the equilibrium position and at low values of vibrational quantum number.

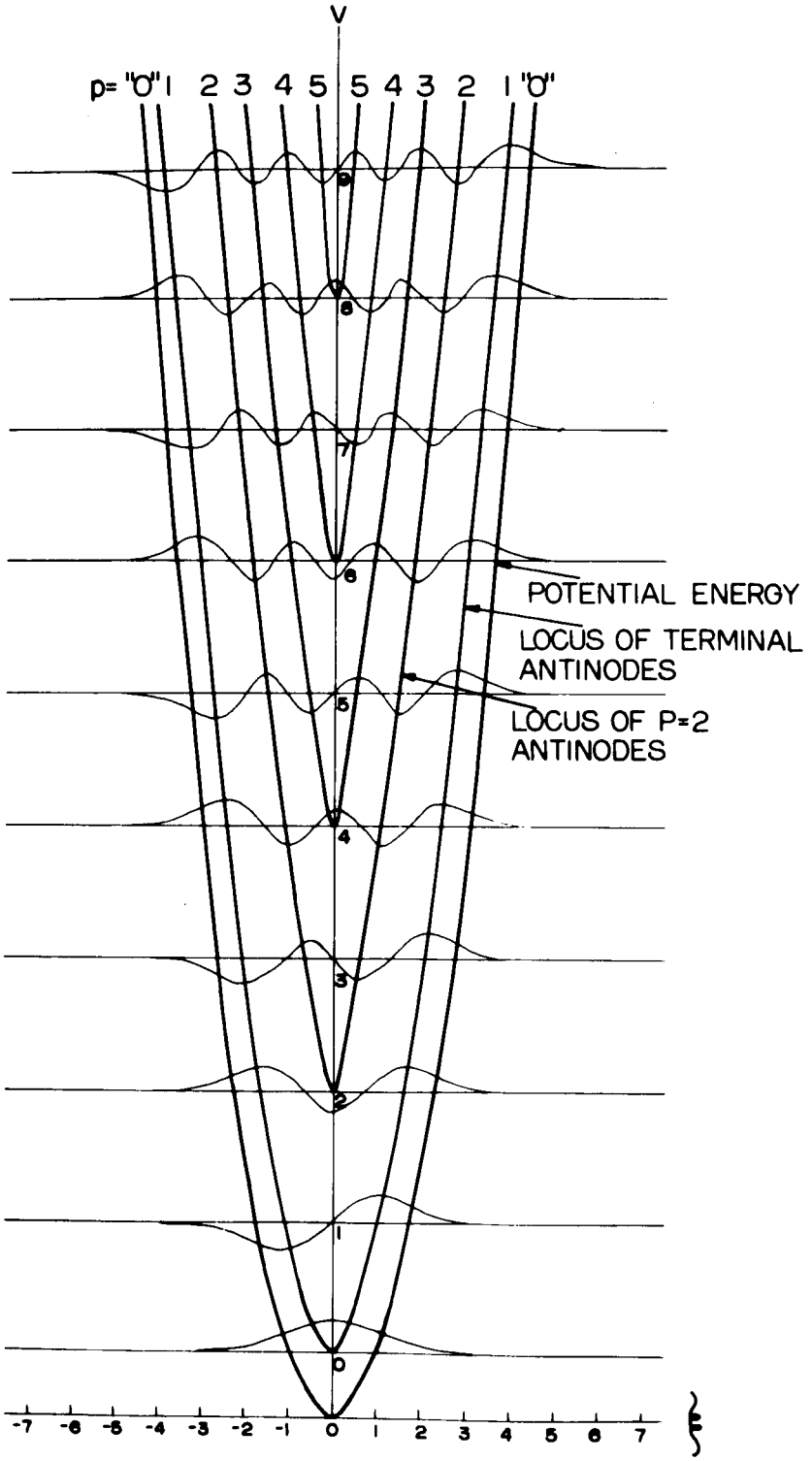

$$|\xi|^2 = k\omega_e(r - r_e)^2$$

$$V - b_p = a_p|\xi|^{n_p}$$

Fig.3.1 Antinode loci of simple harmonic oscillator

3.2 Reduction of Antinode Position to Algebraic Form

In our study it was necessary to specify algebraically the position of an antinode of a vibrational wave function in order that the coincidence of pairs of antinodes could be calculated. Attempts to find analytical relations from the wave functions having proved fruitless, empirical equations of the antinode loci shown on fig. 3.1 have been developed by Nicholls (1963b). For values of p = 1, 2, 3 ... 8 an expression has been found of the form

$$v - b_p = a_p \left| \xi \right|^{n_p} \quad , \tag{3.8}$$

or

$$\left| \xi \right| = \left\{ \frac{v - b_p}{a_p} \right\}^{1/n_p} \quad , \tag{3.9}$$

where a_p, b_p and n_p are the empirical constants given in table 3.1 derived by fitting log-log plots to eq. 3.8. From eqs. 3.4, 3.5 and 3.8

$$\frac{v - b_p}{a_p} = (k\,\omega_e)^{n_p/2} (r - r_e)^{n_p} \quad , \tag{3.10}$$

where $k = \frac{4\pi^2 c}{h} \mu$. (3.11)

The position r of the pth antinode is therefore

$$r_{\substack{1,p \\ 2,p}} = r_e \mp \frac{1}{(k\,\omega_e)^{\frac{1}{2}}} \left\{ \frac{v - b_p}{a_p} \right\}^{1/n_p} \tag{3.12}$$

The former case of eq. 3.12 (r_1,p) applies when $r < r_e$ (i.e. antinodes to the left) and the latter ($r_{2,p}$) when $r > r_e$ (i.e. antinodes to the right).

Table 3.1

Empirical Constants Describing Antinode Loci

P	b_P	a_P	n_P
1	0	0.809	1.79
2	2	1.80	1.38
3	4	2.29	1.28
4	6	2.79	1.17
5	8	3.03	1.14
6	10	3.42	1.1
7	12	3.51	1.0
8	14	3.57	1.0

3.3 Coincidence of Antinode Pairs

It is our aim to assess the validity of the approximate form of the Franck-Condon Principle which considers the vibrational wave function as a series of delta functions at the antinodes and predicts large values of the overlap integral when there is alignment (i.e. equality of r) between one delta function of each level of the transition. The primary locus of high Franck-Condon factors on the v'v" plane is known to be associated with the alignment of primary antinodes. This suggests that the secondary locus may be associated with the alignment of a primary and a secondary antinode; the pth locus with the alignment of a primary and pth antinode. We shall therefore calculate the loci on the v'v" plane of these cases of coincidence and compare them with the Condon loci exhibited in tables of overlap integrals.

The position of the pth antinode of the upper state is $r'_{1,p'}$ (left) or $r'_{2,p'}$ (right) which is given by equation 3.12

$$r'_{\substack{1,p' \\ 2,p'}} = r'_e \mp \frac{1}{(k\omega'_e)^{\frac{1}{2}}} \left\{ \frac{v' - b_{p'}}{a_{p'}} \right\}^{1/n_{p'}} \tag{3.13}$$

Similarly the pth antinode of the lower state is at

$$r''_{\substack{1,p'' \\ 2,p''}} = r''_e \mp \frac{1}{(k\omega''_e)^{\frac{1}{2}}} \left\{ \frac{v'' - b_{p''}}{a_{p''}} \right\}^{1/n_{p''}} \tag{3.14}$$

The approximate form of the Franck-Condon Principle under consideration requires the calculation of v' and v" values when the condition

$$r'_{1 \text{ or } 2,p'} = r''_{1 \text{ or } 2,p''} \tag{3.15}$$

is applied, i.e.

$$r_e' \pm \frac{1}{(k\omega_e')^{\frac{1}{2}}} \left\{\frac{v' - b_{p'}}{a_{p'}}\right\}^{1/n_{p'}} = r_e'' \mp \frac{1}{(k\omega_e'')^{\frac{1}{2}}} \left\{\frac{v'' - b_{p''}}{a_{p''}}\right\}^{1/n_{p''}} \quad (3.16)$$

$$\text{or } \pm\Delta r_e = \pm \frac{1}{(k\omega_e')^{\frac{1}{2}}} \left\{\frac{v' - b_{p'}}{a_{p'}}\right\}^{1/n_{p'}} \pm \frac{1}{(k\omega_e)^{\frac{1}{2}}} \left\{\frac{v'' - b_{p''}}{a_{p''}}\right\}^{1/n_{p''}} \quad (3.17)$$

The pth locus described above is defined by eq. 3.17 where $p' = 1$, $p'' = p$, and $p' = p$, $p'' = 1$, $p = 1, 2, 3 \ldots$. (This is alignment of a primary and a pth antinode). Eq. 3.17 then becomes

$$\pm\Delta r_e = \pm \frac{1}{(k\omega_e')^{\frac{1}{2}}} \left\{\frac{v' - b_{1,p}}{a_{1,p}}\right\}^{1/n_{1,p}} \pm \frac{1}{(k\omega_e'')^{\frac{1}{2}}} \left\{\frac{v'' - b_{p,1}}{a_{p,1}}\right\}^{1/n_{p,1}} \quad (3.18)$$

$$\text{or } \pm\Delta r_e = \pm K' V_{1,p}^{\alpha_{1,p}} \pm K'' V_{p,1}^{\alpha_{p,1}} \quad (3.19)$$

where

$$K = \frac{1}{(k\omega_e)^{\frac{1}{2}}} \quad (3.20)$$

$$V = \frac{v - b}{a} \quad (3.21)$$

and

$$\alpha = \frac{1}{n} \quad . \quad (3.22)$$

For $p \neq 1$, eq. 3.19 contains the eight identities of eq. 3.15. Only six of these are physically achievable. When $r_e'' < r_e'$ the six cases are:

a)
$$\begin{cases} r'_{1,1} = r''_{1,p} \\ |\Delta r_e| = + K' V_1'^{\alpha_1} - K'' V_p''^{\alpha_p} \end{cases}$$

b)
$$\begin{cases} r'_{1,p} = r''_{1,1} \\ |\Delta r_e| = + K' V_p'^{\alpha_p} - K'' V_1''^{\alpha_1} \end{cases}$$

$$
\begin{aligned}
c &\begin{cases} r'_{1,1} = r''_{2,p} \\ |\Delta r_e| = + K' V_1'^{\alpha_1} + K'' V_p''^{\alpha_p} \end{cases} \\
d &\begin{cases} r'_{1,p} = r''_{2,1} \\ |\Delta r_e| = + K' V_p'^{\alpha_p} + K'' V_1''^{\alpha_1} \end{cases} \\
e &\begin{cases} r'_{2,1} = r''_{2,p} \\ |\Delta r_e| = - K' V_1'^{\alpha_1} + K'' V_p''^{\alpha_p} \end{cases} \\
f &\begin{cases} r'_{2,p} = r''_{2,1} \\ |\Delta r_e| = - K' V_p'^{\alpha_p} + K'' V_1''^{\alpha_1} \end{cases}
\end{aligned}
\qquad (3.23)
$$

The untenable cases are

$$r'_{2,1} = r''_{1,p} \quad \text{and} \quad r'_{2,p} = r''_{1,1}$$

since we have stipulated $r''_e < r'_e$. The possible coincidence cases, a - f of eq. 3.23, are illustrated in the transition of fig. 3.2 and in the Deslandres diagram of fig. 3.3 which shows the segmented loci. The distinctness of the segments of the loci has been exaggerated. There is however no discontinuity of slope at the junction of segments, the slope becoming rapidly zero or infinity very close to the junction.

For an electronic transition in which $r''_e > r'_e$ the letters on fig. 3.3 would be transposed as follows:

$$a \longleftrightarrow e \qquad \text{and} \qquad b \longleftrightarrow f \ .$$

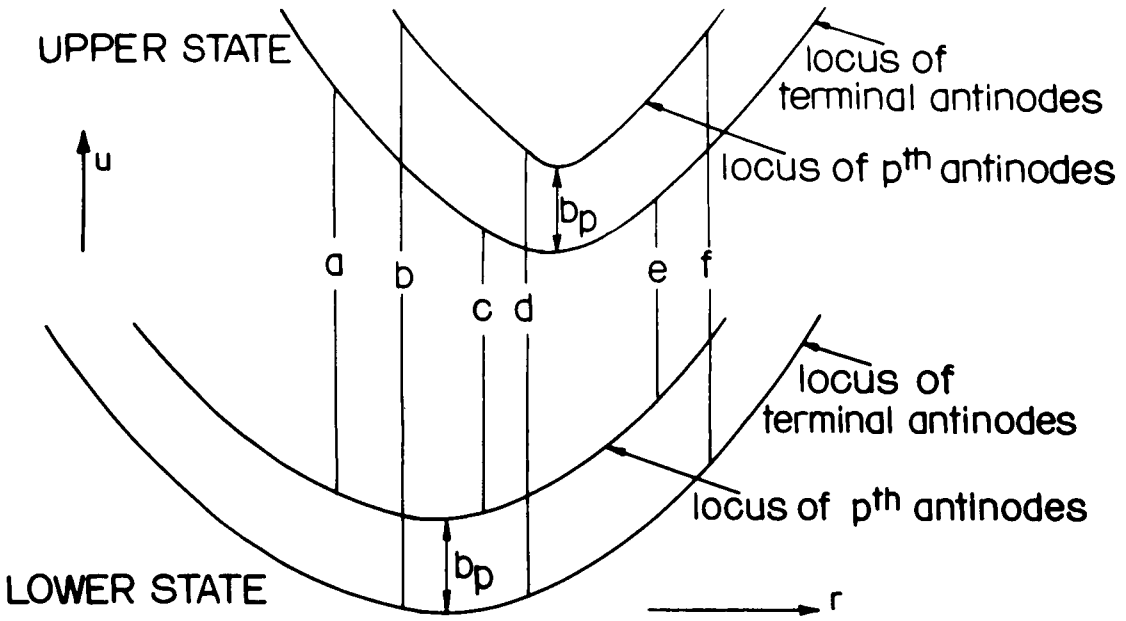

Fig.3.2 Nomenclature of antinode coincidence on potential energy diagram for $r_e'' < r_e'$

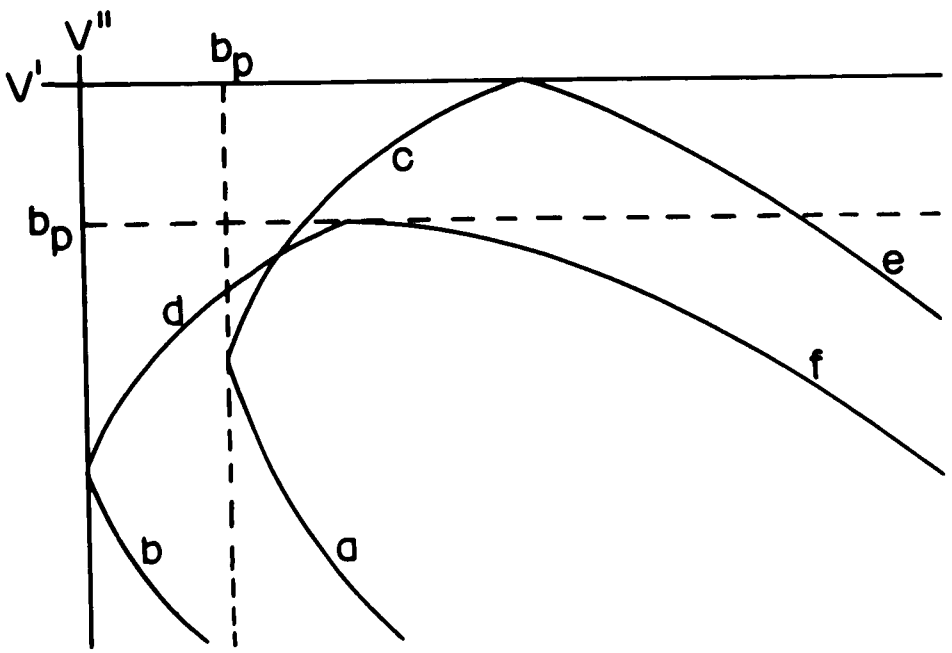

Fig.3.3 Positioning of antinode coincidence on v'v'' plane for $r_e'' < r_e'$

For p = 1 eq. 3.19 contains the four identities of eq. 3.15. Three of these are physically achievable. When $r_e'' < r_e'$ the three cases are:

$$\begin{aligned} &\text{a and b)} \quad r'_{1,1} = r''_{1,1} \\ &\text{c and d)} \quad r'_{1,1} = r''_{2,1} \\ &\text{e and f)} \quad r'_{2,1} = r''_{2,1} \end{aligned} \tag{3.24}$$

These cases are illustrated by the transition in fig. 3.4 and in the Deslandres diagram of fig. 3.5.

3.4 The Form of the Loci of Antinode Coincidence

The loci arising from the coincidence of pairs of antinodes has been calculated for the transitions listed in table 3.2 by solving eq. 3.19 numerically for pairs of v'v'' values. If coincidence of pairs of antinodes alone controls the magnitude of the overlap integral, then the largest values will occur when terminal antinodes coincide (p = 1, i.e. eq. 3.24). There will be lesser maximum values when a terminal antinode coincides with a subsidiary ($p \neq 1$ in eq. 3.23). Nicholls (1963a) suggests that this describes the pth Condon locus.

The graphical appearance of the solution to eq. 3.19 is largely dependent on the size of Δr_e. Eight transitions have been studied with Δr_e ranging from zero to 0.397 Å. Three cases representative of small (0.049 Å and 0.051 Å), medium (0.1069 Å) and large (0.2233 Å)

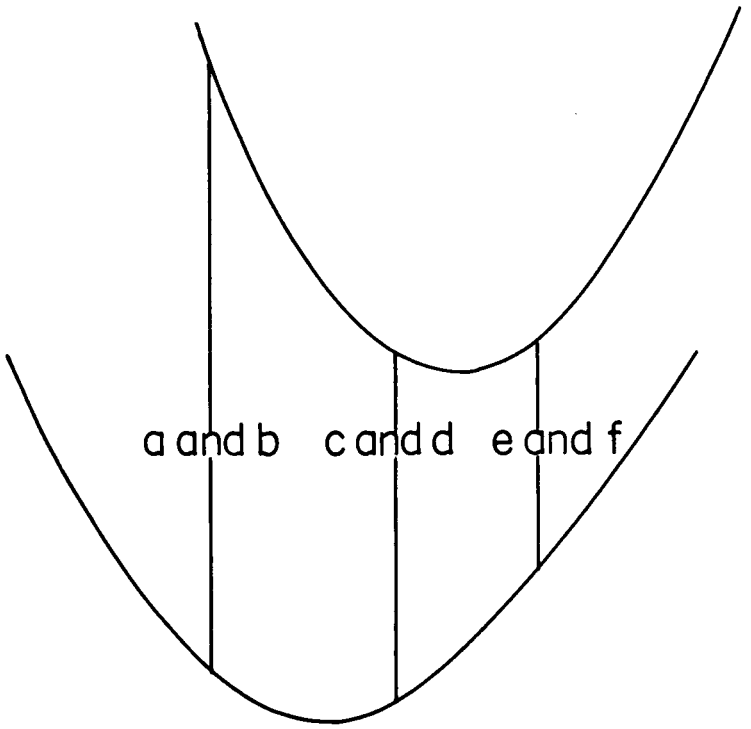

Fig.3.4 Transition illustrating primary locus

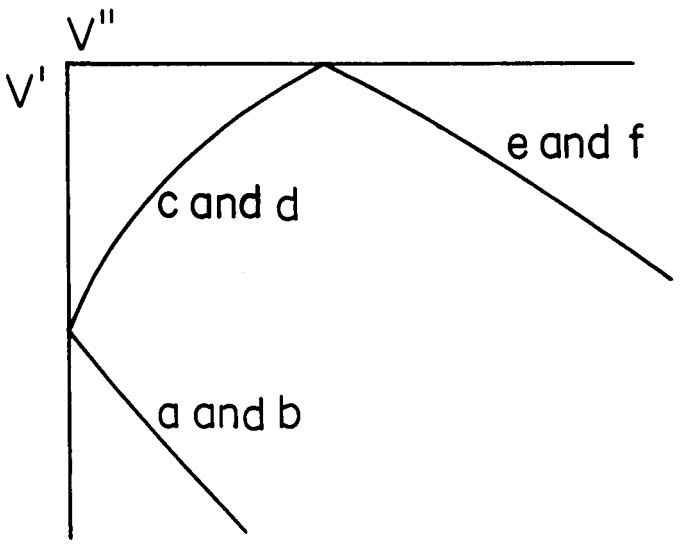

Fig.3.5 Segments of primary locus

Table 3.2

Data for Transitions examined with SHO Model (from Herzberg 1950)

MOLECULE	μ Atomic wt. units	Upper State	Lower State	ω_e' cm^{-1}	ω_e'' cm^{-1}	r_e' Å	r_e'' Å	Δr_e Å
GaI	44.682	$A^3\Pi_o^+$	$X^1\Sigma^+$	193.2	216.4			0
MgH	0.967480	$C^2\Pi$	$X^2\Sigma^+$	1740	1495.7	1.682	1.7306	0.049
MgH	0.967480	$A^2\Pi$	$X^2\Sigma^+$	1611.3	1495.7	1.6795	1.7306	0.0511
CH^+	0.930021	$A^1\Pi$	$X^1\Sigma^+$	1850.02	2739.54	1.23439	1.13083	0.10356
CO	6.85841	$A^1\Pi$	$X^1\Sigma^+$	1515.61	2170.21	1.2351	1.12819	0.1069
CO^+	6.85823	$A^2\Pi$	$X^2\Sigma$	1562.06	2214.24	1.24368	1.11506	0.12862
C_2	6.00194	$B^3\Pi_g$	$X^3\Pi_u$	1106.56	1641.35	1.5350	1.13117	0.2233
O_2	8	$B^3\Sigma_u^-$	$X^3\Sigma_g^-$	700.36	1580.3613	1.604	1.207398	0.397

values of Δr_e are discussed in detail in section 3.5, the other cases are discussed in Appendix 1.

The results may be summarised as follows:

At zero Δr_e (eg. GaI Appendix 1.4) there are no c and d segments, but a and e, and b and f which are separated for all but the coincidence of terminal antinodes. The sections a and e are coincident due to the symmetry of the antinode loci, as are b and f. The primary locus ($p = 1$) is a single line on the $v'v''$ plane close to $v' = v''$. The secondary locus ($p = 2$) consists of a line on each side of the primary locus. The subsequent subsidiary loci ($p = 3, 4 \ldots$) are pairs of lines external to the lower order loci. There is no nesting of loci.

At slightly larger Δr_e (eg. MgH section 3.5.1) segments c and d are very short, and sections a and e slightly separated, as are b and f. The primary locus consists of two lines which are very close near $v' = v'' = 0$ and open out at larger v' and v''. Each subsidiary locus consists of two slightly open three-segment loci, one each side of the primary locus.

At larger Δr_e (eg. CH^+ Appendix 1.1 and CO section 3.5.2) the loci become broader and cross each other. The internal limbs of the secondary locus, for example, lie for the most part inside the primary locus.

This trend is continued with increasing Δr_e (eg. CO^+ Appendix 1.2 and C_2 section 3.5.3), segments c and d increasing in length and the internal limbs of each subsidiary locus crossing inside the region described by the primary locus.

At very large Δr_e (eg. O_2 Appendix 1.3) segments c and d occupy most of the v'v" array and each segment is crossed many times.

In the remaining part of this chapter the three representative transitions are discussed in detail. The suggestions put forward in their discussion are also based on the transitions discussed in Appendix 1. The arrays of calculated loci of antinode pair coincidence are compared with the arrays of overlap integral and measured band intensities where available. The overlap integral arrays are those calculated by Aiken (1951). The entries which are of large modulus compared with their neighbours are underlined and connected by curves which are the Condon loci. The Condon loci are also indicated on the intensity arrays.

3.5 Detailed Examination of Representative Types of Transition

3.5.1 MgH $C^2\Pi \rightarrow X^2\Sigma$ and $A^2\Pi \rightarrow X^2\Sigma$

These two band systems are very similar and will be examined together. The Δr_e values are very small (0.049 Å and 0.051 Å respectively) and have been chosen to illustrate the validity of our approximate form of the Franck-Condon Principle in this region.

The systems occur in the flame of burning magnesium in air, and in the absorption spectra of sunspots. No intensity measurements are available but five bands of the $C \rightarrow X$ system, and eight bands of the $A \rightarrow X$ system are known (tables 3.3 and 3.4). The former lie in the ultra-violet region of the spectrum ($\lambda \sim 2500$ Å) and the latter in the red ($\lambda \sim 6000$ Å).

Table 3.3

Observed Bands of MgH C→X (Pearse and Gaydon 1950)

v' \ v''	0	1	2
0	X	X	
1	X	X	X
2			

Table 3.4

Observed Bands of MgH A→X (Pearse and Gaydon 1950)

v' \ v''	0	1	2	3
0	X	X	X	
1	X	X	X	
2			X	X
3				

On the arrays of overlap integral (tables 3.5 and 3.6) both systems show a primary "closed" Condon locus, typical of small Δr_e. This locus lies along the main diagonal for the A → X system, and slightly inclined to higher v" for C → X. An interesting difference between the two arrays is the occurrence of a subsidiary locus of high overlap integral entries in the C → X transition array. This lies along the $\Delta v = v' - v'' = -3$ sequence.

Figs. 3.6 and 3.7 show the loci of antinode coincidence calculated by the method outlined in section 3.3 of this thesis. Both systems exhibit slightly open loci of the coincidence of pairs of primary antinodes straddling the main diagonal. That of A → X is almost symmetrical about the main diagonal, but that of C → X is slightly inclined to lower v", i.e. in the opposite direction to the overlap locus. The loci of coincidence of terminal antinodes with internal antinodes lie outside the primary locus due to the shortness of the curved sections c and d.

The relationship between the calculated loci and the Condon loci is not immediately apparent and it is necessary to examine each contribution to the overlap integral. v" progression plots of overlap integral for the C → X array are given in fig. 3.8. The systematic progression of the shape of the plot is due to the consistent nature of the entries on each diagonal. Table 3.7 is an examination of each entry of the overlap integral array. The signs of the wave functions at the relevant antinodes are given, the sign of the product of the antinodes in coincidence, and the sign of the overlap integral.

Table 3.5

Overlap Integrals of MgH C → X

v' \ v''	0	1	2	3	4	5	6	7
0	0.9717	-0.2353	-0.0116	0.0161	-0.0012	-0.0010	0.0002	0.0001
1	0.2181	0.9161	-0.3344	-0.0164	0.0319	-0.0029	-0.0023	0.0005
2	0.0865	0.2867	0.8598	-0.4101	-0.0181	0.0498	-0.0053	-0.0042
3	0.0247	0.1434	0.3242	0.8032	-0.4726	-0.0171	0.0694	-0.0086
4	0.0084	0.0471	0.1937	0.3433	0.7467	-0.5255	-0.0134	0.0902
5	0.0025	0.0182	0.0711	0.2383	0.3492	0.6907	-0.5707	-0.0074
6	0.0008	0.0059	0.0303	0.0956	0.2775	0.3450	0.6355	-0.6901
7	0.0002	0.0021	0.0107	0.0446	0.1200	0.3114	0.3325	0.5815

Table 3.6

Overlap Integrals of MgH A → X

v' \ v''	0	1	2	3	4	5	6	7
0	0.9710	-0.2384	0.0158	0.0050	-0.0011	-0.0000	0.0000	-0.0000
1	0.2297	0.9140	-0.3332	0.0286	0.0097	-0.0025	-0.0001	0.0001
2	0.0640	0.3089	0.8580	-0.4028	0.0420	0.0149	-0.0044	-0.0002
3	0.0157	0.1069	0.3591	0.8033	-0.4588	0.0562	0.0205	-0.0067
4	0.0039	0.0304	0.1456	0.3928	0.7498	-0.5055	0.0710	0.0263
5	0.0009	0.0085	0.0466	0.1810	0.4151	0.6977	-0.5451	0.0865
6	0.0002	0.0022	0.0144	0.0637	0.2132	0.4289	0.6470	-0.5792
7	0.0001	0.0006	0.0041	0.0213	0.0815	0.2425	0.4359	0.5977

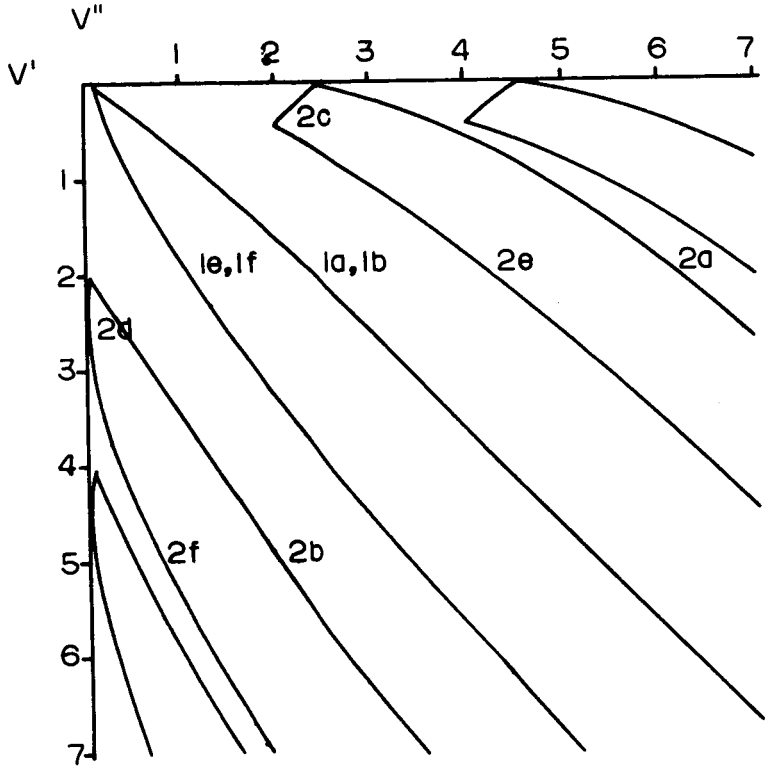

Fig.3.6 Loci of coincidence of antinode pairs,

MgH C→X

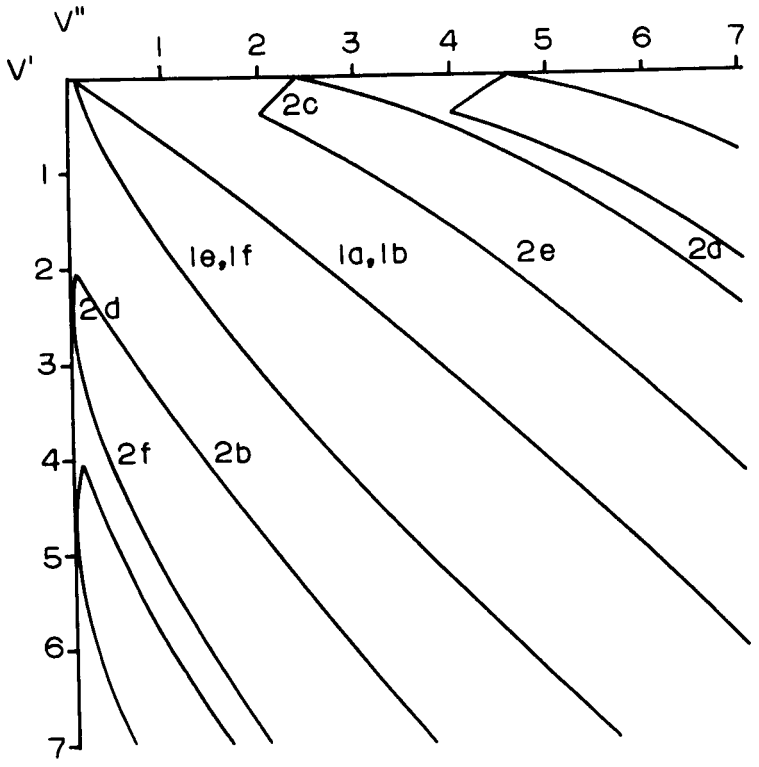

Fig. 3.7 Loci of coincidence of antinode pairs,

MgH A→X

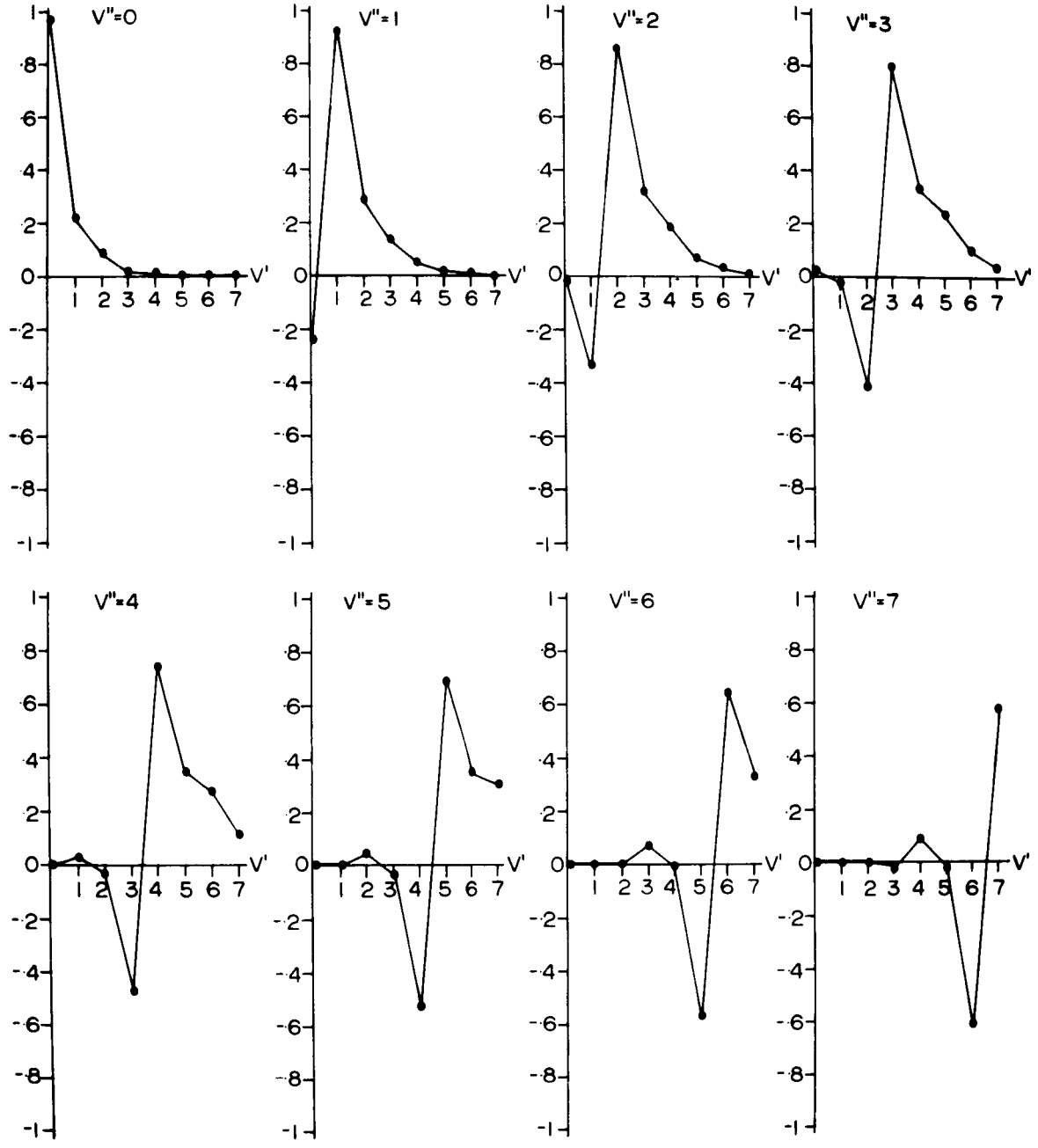

Fig. 3.8 Progression plots of overlap integral of MgH C→X

Table 3.7

Examination of Contributions to the Overlap Integral

of MgH C → X system

v'	v''	Close to:	Section	Sign of $\psi_{v'}$ $\psi_{v''}$ at antinode		Sign of $\psi_{v'} \times \psi_{v''}$ at coincidence of antinodes	Sign of $\int \psi_{v'} \psi_{v''} dr$
0	0	Primary	a,b & e,f	+	+	+	+
1	0	Primary	e,f	+	+	+	+
2	0	Secondary	b	−	+	−	+
2	0	Primary	e,f	+	+	+	+
3	0	Secondary	f	−	+	−	+
3	0	Primary	e,f	+	+	+	+
4	0	Tertiary	b	+	+	+	+
5	0	Tertiary	f	+	+	+	+
0	1	Primary	a,b	+	−	−	−
1	1	Primary	a,b	−	−	+	+
2	1	Primary	e,f	+	+	+	+
3	1	Primary	e,f	+	+	+	+
3	1	Secondary	b	+	−	−	+
4	1	Secondary	b	−	−	+	+
5	1	Secondary	f	−	+	−	+
6	1	Secondary	f	−	+	−	+
6	1	Tertiary	b	+	−	−	+
7	1	Tertiary	b	−	−	+	+
7	1	Tertiary	f	+	+	+	+
0	2	Secondary	e	+	−	−	−
1	2	Primary	a,b	−	+	−	−
2	2	Primary	a,b	+	+	+	+
3	2	Primary	e,f	+	+	+	+
4	2	Primary	e,f	+	+	+	+
5	2	Secondary	b	+	+	+	+
6	2	Secondary	f	−	+	−	+
6	2	Primary	e,f	+	+	+	+
7	2	Secondary	f	−	+	−	+
7	2	Tertiary	b	−	+	−	+
7	2	Primary	e,f	+	+	+	+
0	3	Secondary	a	+	+	+	+
1	3	Secondary	e	+	−	−	−
1	3	Primary	a,b	−	−	+	−
2	3	Primary	a,b	+	−	−	−
3	3	Primary	a,b	−	−	+	+
4	3	Primary	e,f	+	+	+	+

5	3	Primary	e,f	+	+	+	+
6	3	Secondary	b	-	-	+	+
6	3	Primary	e,f	+	+	+	+
7	3	Secondary	b	+	-	-	+
7	3	Primary	e,f	+	+	+	+
0	4	Tertiary	e	+	+	+	+
1	4	Secondary	e	+	-	-	+
1	4	Secondary	a	-	-	+	+
2	4	Secondary	e	+	-	-	-
3	4	Primary	a,b	-	+	-	-
4	4	Primary	a,b	+	+	+	+
5	4	Primary	e,f	+	+	+	+
6	4	Primary	e,f	+	+	+	+
7	4	Secondary	b	+	+	+	+
7	4	Primary	e,f	+	+	+	+
0	5	Tertiary	a	+	-	-	-
1	5	Tertiary	e	+	+	+	-
1	5	Secondary	a	-	+	-	-
2	5	Secondary	a	+	+	+	+
2	5	Secondary	e	+	-	-	+
3	5	Secondary	e	+	-	-	-
4	5	Primary	a,b	+	-	-	-
5	5	Primary	a,b	-	-	+	+
6	5	Primary	e,f	+	+	+	+
7	5	Primary	e,f	+	+	+	+
0	6	Tertiary	a	+	+	+	+
1	6	Tertiary	a	-	+	-	-
1	6	Tertiary	e	+	+	+	-
2	6	Secondary	a	+	-	-	-
3	6	Secondary	a	-	-	+	+
3	6	Secondary	e	+	-	-	+
4	6	Secondary	e	+	-	-	-
5	6	Primary	a,b	-	+	-	-
6	6	Primary	a,b	+	+	+	+
7	6	Primary	a,b	-	+	-	+
7	6	Primary	e,f	+	+	+	+
1	7	Tertiary	a	-	-	+	+
2	7	Tertiary	e	+	+	+	-
2	7	Secondary	a	+	+	+	-
3	7	Secondary	a	-	+	-	-
4	7	Secondary	a	+	+	+	+
4	7	Secondary	e	+	-	-	+
5	7	Secondary	e	+	-	-	-
5	7	Primary	a,b	-	-	+	-
6	7	Primary	a,b	+	-	-	-
7	7	Primary	a,b	-	-	+	+

3.5.1a The Comparison of Overlap Integral with Antinode Coincidence

The bands on the main diagonal all have large positive overlap integrals (table 3.5). They all closely represent coincidence of pairs of left hand terminal antinodes (table 3.7), which give a positive contribution to the overlap integral (eg. band 3, 3). The coincidence of right hand pairs of terminal antinodes also gives a positive contribution (eg. band 4, 3), but in this case $\Delta v \neq 0$ so the contribution is less and no second arm of the primary Condon locus appears.

Below the main diagonal ($v' > v''$) all the overlap integrals are of positive sign, while above ($v' < v''$) there are both positive and negative values. It is suggested here that the contribution to the overlap integral due to partial overlap between terminal antinodes is greater than that due to the overlap of a subsidiary antinode with a terminal antinode (eg. the value for 7, 3 is +ve, while -ve is expected if the overlap integral is dominated by the overlap of a terminal and secondary antinode).

The sequence $\Delta v = v' - v'' = -1$, also represents close coincidence of pairs of left hand terminal antinodes. The contribution to the overlap integral is large and negative, the overlap integral array showing the same feature (eg. 2, 3).

The coincidence of the right hand terminal antinode of the upper state with the right hand secondary antinode of the lower state adequately represents the form of the overlap integrals of the $\Delta v = v' - v'' = -2$ sequence. This contribution which is negative appears to be much larger than the positive contribution due to the partial overlap of pairs of left hand terminal antinodes (eg. 1, 3).

The adjacent sequence $\Delta v = -3$ is notable due to the overlap integrals of its members being larger than those of their neighbours. This is the general criterion for the specification of a Condon locus. This diagonal is associated with the partial overlap of two pairs of antinodes; the terminal left antinode of the upper state with the secondary left antinode of the lower state, giving a positive contribution to overlap integral; and the terminal right antinode of the upper state with the secondary right antinode of the lower state, giving a negative contribution to the overlap integral (eg. 2, 5). The former case of coincidence appears to give the larger contribution as the overlap integrals are all positive. This is probably due to the smaller value of v' involved and hence greater size of the loop of the wave function.

The sequence $\Delta v = v' - v'' = -4$ is adequately represented by the coincidence of left hand primary and secondary antinodes mentioned in the previous paragraph (eg. 1, 5).

The apparent Condon locus at $\Delta v = -3$ must be concluded to be due to the abnormally small overlap integrals along the $\Delta v = -2$ diagonal caused by the opposing contributions of the partial overlap of two pairs of antinodes.

A similar study has been made of the $A \rightarrow X$ transition, but from it nothing can be added to the comments above.

We are able to conclude that the primary Condon locus in the case of small change in internuclear separation is due to the coincidence of pairs of terminal antinodes. The size of other overlap

integrals on the array can be interpreted as the overlapping of other pairs of antinodes. Apparent external Condon loci are due to the smallness of neighbouring overlap integrals, rather than the magnitude of their own entries.

3.5.2 CO $A^1\Pi \rightarrow X^1\Sigma$ Fourth Positive System

This well-known system has been chosen to illustrate the validity of the approximation at intermediate values of Δr_e ($\Delta r_e = 0.1069$ Å).

Over one hundred bands of this system are found in emission. They lie in the ultra-violet region of the spectrum ($\lambda \sim 2500$ Å). Some of the short wave length bands are found in absorption.

The overlap integral array, table 3.8, of this transition shows the familiar nested Condon loci, the primary locus comprising the largest entries. Primary, secondary and tertiary Condon loci are also clearly defined on the array of observed bands of table 3.9.

The coincidence of antinode pairs has been calculated to high quantum numbers ($v' = 20$, $v'' = 30$) and high antinode numbers ($p = 8$). The calculated loci are given in fig. 3.9. The primary Condon locus is closely represented by the coincidence of terminal antinodes; the secondary by the internal segments (a and f) of the coincidence of a terminal antinode ($p = 1$) of the vibrational wave function of one state with a secondary antinode ($p = 2$) of the other state as suggested by Nicholls (1963a); the tertiary by a similar coincidence of primary and tertiary antinodes.

Table 3.8

Overlap Integrals of CO A → X

v' \ v''	0	1	2	3	4	5	6	7
0	0.3516	0.4593	0.4683	0.4198	0.3462	0.2689	0.1995	0.1427
1	-0.5496	-0.3718	-0.0928	0.1422	0.2851	0.3415	0.3363	0.2964
2	0.5632	-0.0292	-0.3221	-0.3217	-0.1607	0.0325	0.1853	0.2737
3	-0.4285	0.4003	0.2807	-0.0473	-0.2619	-0.2830	-0.1708	-0.0115
4	0.2483	-0.5192	0.1087	0.3256	0.1828	-0.0720	-0.2361	-0.2555
5	-0.1055	0.4086	-0.4437	-0.1372	0.2004	0.2752	0.1146	-0.0946
6	0.0270	-0.2189	0.4976	-0.2740	-0.2678	0.0161	0.2360	0.2236
7	0.0014	0.0722	-0.3362	0.5050	-0.0786	-0.2775	-0.1436	0.1158

Table 3.9: Observed Bands of CO A → X (Estey 1930 and Headrick and Fox 1930)

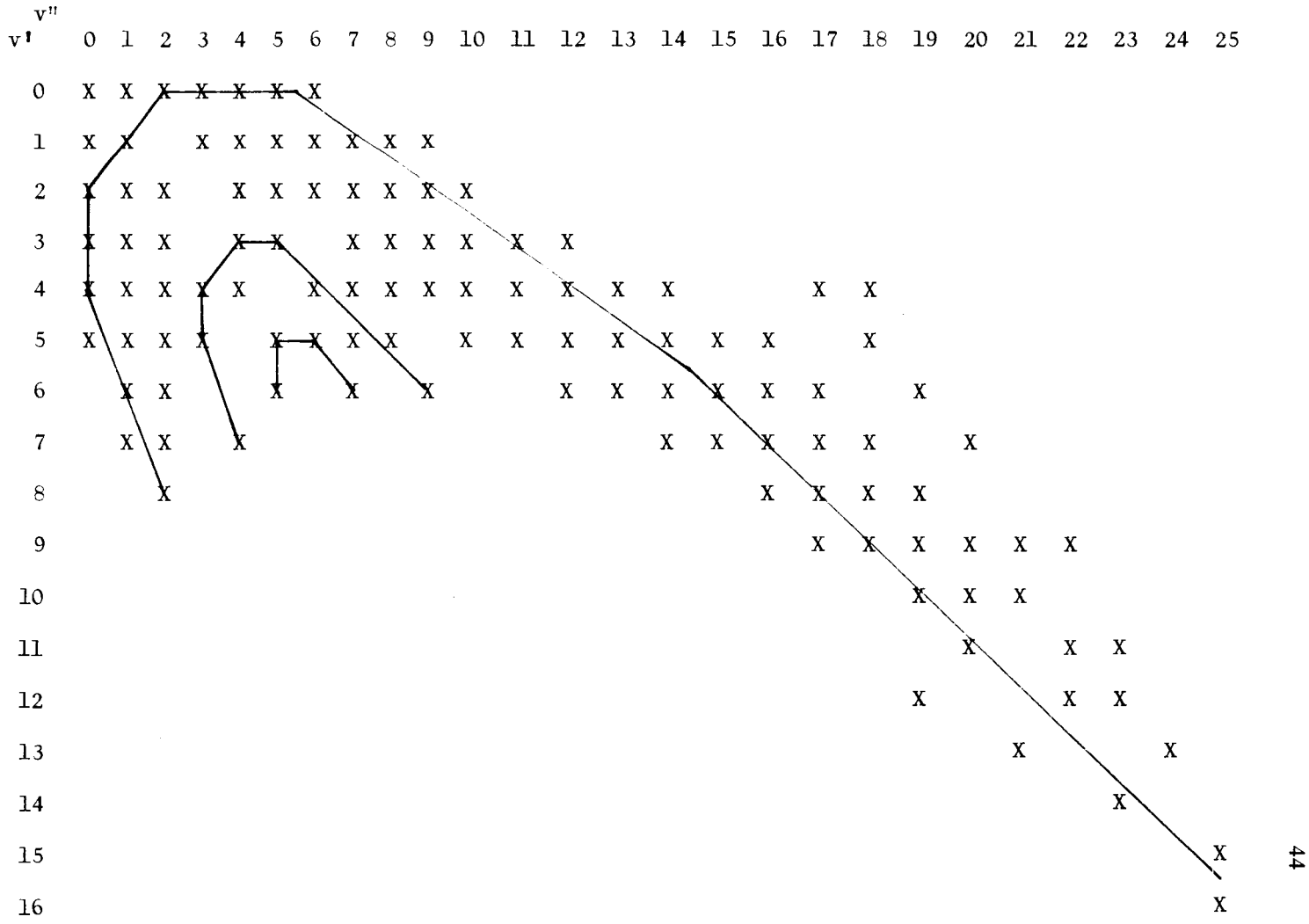

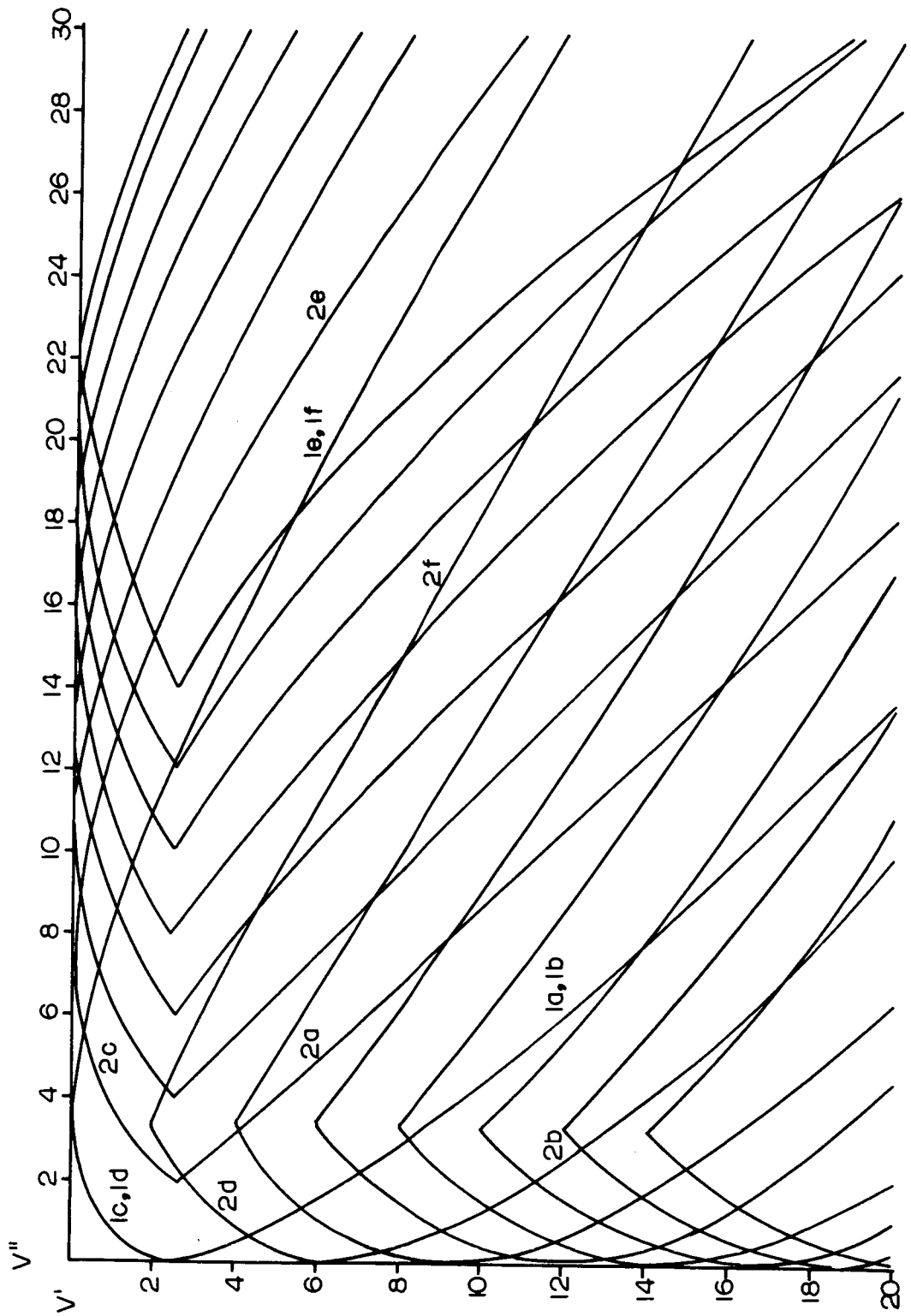

Fig.3.9 Loci of coincidence of antinode pairs, CO A→X

3.5.3 C_2 $B^3\Pi \rightarrow X^3\Pi$ Fox-Herzberg System

This ultra-violet system of C_2 ($\lambda \sim 3000$ Å) has been chosen to illustrate the validity of the approximation at large values of Δr_e, ($\Delta r_e = 0.2233$ Å).

No intensity measurements are available but the fourteen observed bands (table 3.10) fall on a broad curve at low v'. The overlap integral array (table 3.11) exhibits broad nested Condon loci. It appears that the primary Condon locus suffers a change in direction at $v' = 6$, $v'' = 0$; the secondary at $v' = 6$, $v'' = 2$.

The primary Condon locus is successfully represented by the calculated locus of the coincidence of terminal antinodes (fig. 3.10). The sharp turn at 6,0 is the junction point of the curved sections c,d and a,b. The secondary Condon locus is represented by the calculated sections c,d and a of the coincidence of a terminal and secondary antinode. Again the sharp turn in the Condon locus comes at a junction point. The tertiary Condon locus is similarly well represented by the calculated locus involving a tertiary antinode.

3.6 Additional Remarks on the Geometry of the Primary Condon Locus

The primary Condon locus proposed by Nicholls (1962b) arose from a simple consideration of the coincidence of classical turning points of a simple harmonic oscillator. The locus is described in terms of a single skewed displaced parabola. On the other hand the locus described by eq. 3.24 is more realistic as it represents the coincidence of terminal antinodes of the vibrational wave functions.

Table 3.10

Observed Bands of C_2 B → X (Phillips 1949)

v' \ v''	0	1	2	3	4	5	6
0			X	X	X	X	X
1			X	X	X		
2		X	X	X			
3		X	X				
4		X					

Table 3.11

Overlap Integrals of C_2 B → X

v' \ v''	0	1	2	3	4	5	6	7
0	0.0527	0.1146	0.1834	0.2484	0.3008	0.3356	0.3513	0.3491
1	-0.1396	-0.2517	-0.3265	-0.3459	-0.3091	-0.2287	-0.1234	-0.0124
2	0.2540	0.3585	0.3391	0.2210	0.0574	-0.0975	-0.2058	-0.2514
3	-0.3660	-0.3641	-0.1792	0.0498	0.2117	0.2580	0.1989	0.0778
4	0.4417	0.2419	-0.0724	-0.2554	-0.2409	-0.0930	0.0813	0.1976
5	-0.4592	-0.0293	0.2670	0.2387	0.0243	-0.1712	-0.2308	-0.1530
6	0.4177	-0.1952	-0.2923	-0.0274	0.2077	0.2233	0.0671	-0.1143
7	-0.3352	0.3555	0.1420	-0.2033	-0.2325	-0.0203	0.1772	0.2077

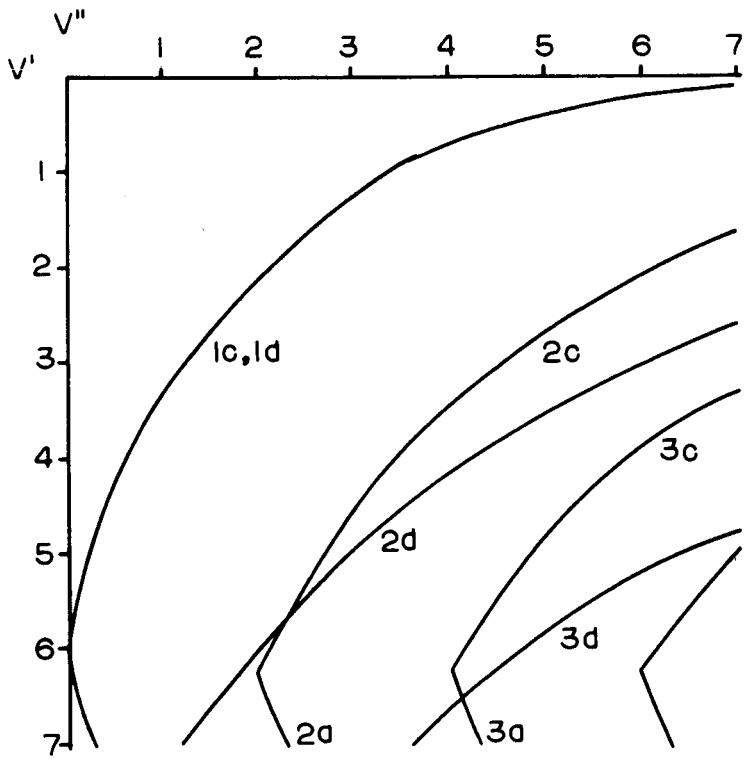

Fig. 3.10 Loci of coincidence of antinode pairs,

C_2 B→X

This locus consists of three distinct sections which join smoothly. Their slopes change rapidly near the junction points giving an appearance of discontinuity of slope. This point is of no practical value as points on the Condon loci are defined only at integral values of v' and v". However, it is clearly not feasible to describe the Condon locus defined by the three parts of eq. 3.24 by a single equation.

The form of the locus has been shown in fig. 3.5 which is repeated here (fig. 3.11) for convenience. We have seen that this corresponds closely to the primary Condon locus except when Δr_e is very small and when v is large assuming that a simple harmonic potential is valid. It is possible that important information concerning the two states of the transition may be found from the triangle AOB (fig. 3.11). The point A is given by

$$|\Delta r_e| = K' \, V_A'^{\,\alpha_1} \quad , \tag{3.25}$$

and B by

$$|\Delta r_e| = K'' \, V_B''^{\,\alpha_1} \quad . \tag{3.26}$$

The sides of the triangle are

$$OA = v' = \Delta r_e^{n_1} \, k^{n_1/2} \, \omega_e'^{\,n_1/2} \, a_1 , \tag{3.27}$$

$$OB = v'' = \Delta r_e^{n_1} \, k^{n_1/2} \, \omega_e''^{\,n_1/2} \, a_1 , \tag{3.28}$$

and

$$AB = \left[\Delta r_e^{2n_1} \, k^{n_1} \, a_1^2 \, (\omega_e'^{\,n_1} + \omega_e''^{\,n_1}) \right]^{\frac{1}{2}} . \tag{3.29}$$

Equations 3.27 and 3.28 give a method of finding Δr_e, a parameter which is not known for all transitions. The equilibrium internuclear

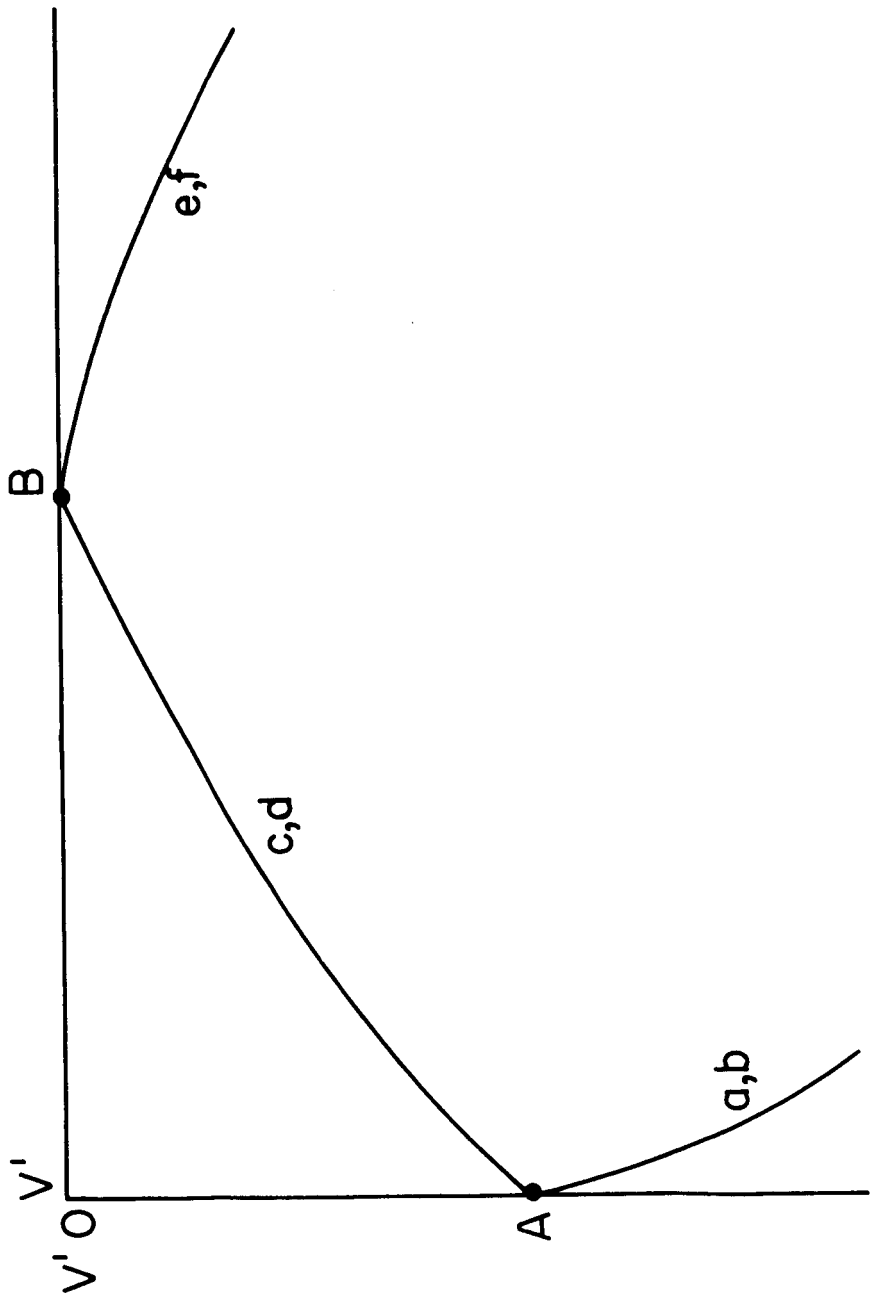

Fig.3.11 Primary Condon locus

separation is usually known for the ground state of a molecule from the infrared spectrum, hence the value of r_e for the upper state may be found. Such calculations have been found to be of little value as the points A and B are never clearly defined on an intensity array.

The ratio of the sides OA and OB of the triangle gives the tangent of the angle ABO or the inclination of the locus in the v'v" plane;

$$\tan ABO = \left(\frac{\omega_e'}{\omega_e''}\right)^{n_1/2} \tag{3.30}$$

n_1 is given as 1.79 (table 3.1) giving an inclination of $\left(\frac{\omega_e'}{\omega_e''}\right)^{.895}$ instead of $\left(\frac{\omega_e'}{\omega_e''}\right)^{0.5}$ as found by Manneback (1951).

The width of the locus can be measured in terms of the length of the side AB of the triangle (eq. 3.29). This is a function of Δr_e, μ, ω_e' and ω_e'' , not Δr_e alone as is generally understood. We propose this length as a realistic transition parameter which describes the shape of the primary Condon locus.

3.7 A Simple Method of Finding the Subsidiary Condon Loci

In the identification of bands of a spectral system the positions of the Condon loci are of greater practical interest to many users than the Franck-Condon factors. We therefore suggest a simple method of locating the Condon loci without the lengthy and costly computation of wave functions and overlap integrals. For simplicity we chose a parabolic potential.

Firstly the potential curves of the upper and lower states must be plotted on a scale of v versus r. Using the equations

$$U = 2\pi^2 \mu c^2 \omega_e^2 (r - r_e)^2 , \tag{3.31}$$

and

$$E = h c \omega_e (v + \tfrac{1}{2}) \tag{3.32}$$

for one state a point on the parabola is found at a convenient value of v. Another point is made at $v = -\frac{1}{2}$, $r = r_e$. From these two points the potential parabola is easily constructed graphically. The potential curve of the other state is similarly constructed.

The positions of the antinodes are now found for each value of v by dividing the width of the parabola by v and marking off the distance between the points on the parabola. The points on the parabola approximately represent the positions of the terminal antinodes, and the points made between them represent the internal antinodes. In this way all the antinodes of both states may be found.

A procedure described in detail in Chapter 4 section 4.4 is now followed to locate the values of v' and v'' at the coincidence of relevant pairs of antinodes. The loci drawn on the $v'v''$ plane closely represent the Condon loci calculated by more sophisticated and costly methods.

Our method has been tried for the CO Fourth Positive System. The results are shown in fig. 3.12 which is in very good agreement with fig. 3.9.

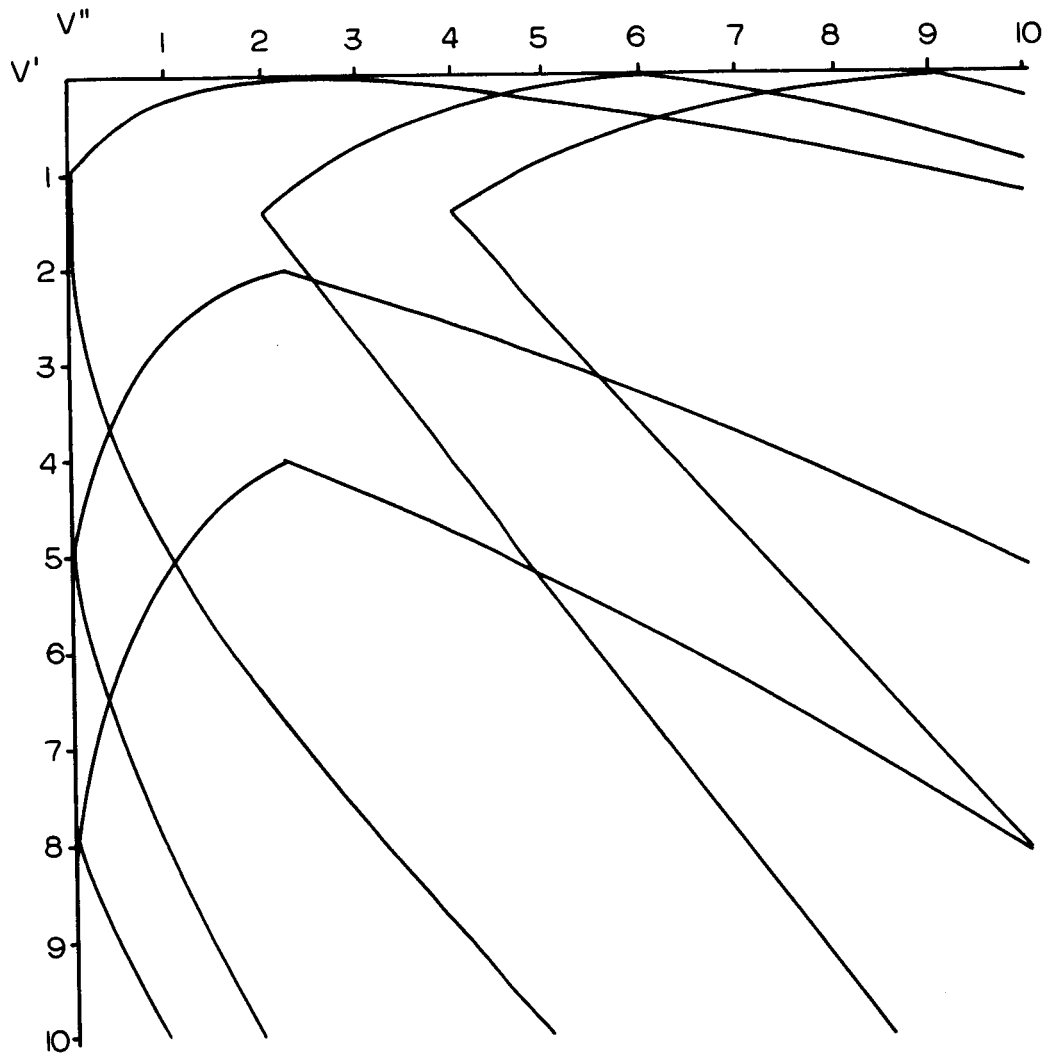

Fig.3.12 Approximate loci of coincidence of antinode pairs,

CO $A \rightarrow X$

CHAPTER 4

CONDON LOCI AND THE MORSE POTENTIAL MODEL

4.1 The Morse Model of a Diatomic Molecule

The motion of a diatomic molecule can be safely represented by a harmonic oscillator only close to the equilibrium position and for low quantum numbers. The expression

$$U(r - r_e) = D\,(1 - e^{-\beta(r - r_e)})^2 \qquad (4.1)$$

proposed by Morse (1929) is a closer representation of the potential at other values of r. In this expression D is the dissociation energy referred to the minimum (fig. 4.1) and β is an anharmonicity parameter given by

$$\beta = (2\pi^2 c \mu/Dh)^{\frac{1}{2}}\ \omega_e\ . \qquad (4.2)$$

A solution of the one-dimensional Schrodinger equation when U(r) is of the form of eq. (4.1) is the set of vibrational wave functions (Morse 1929),

$$\psi_v(r) = N_v\, e^{-z/2}\, z^{(k-2v-1)/2}\, L_{k-v-1}^{k-2v-1}(z) \qquad (4.3)$$

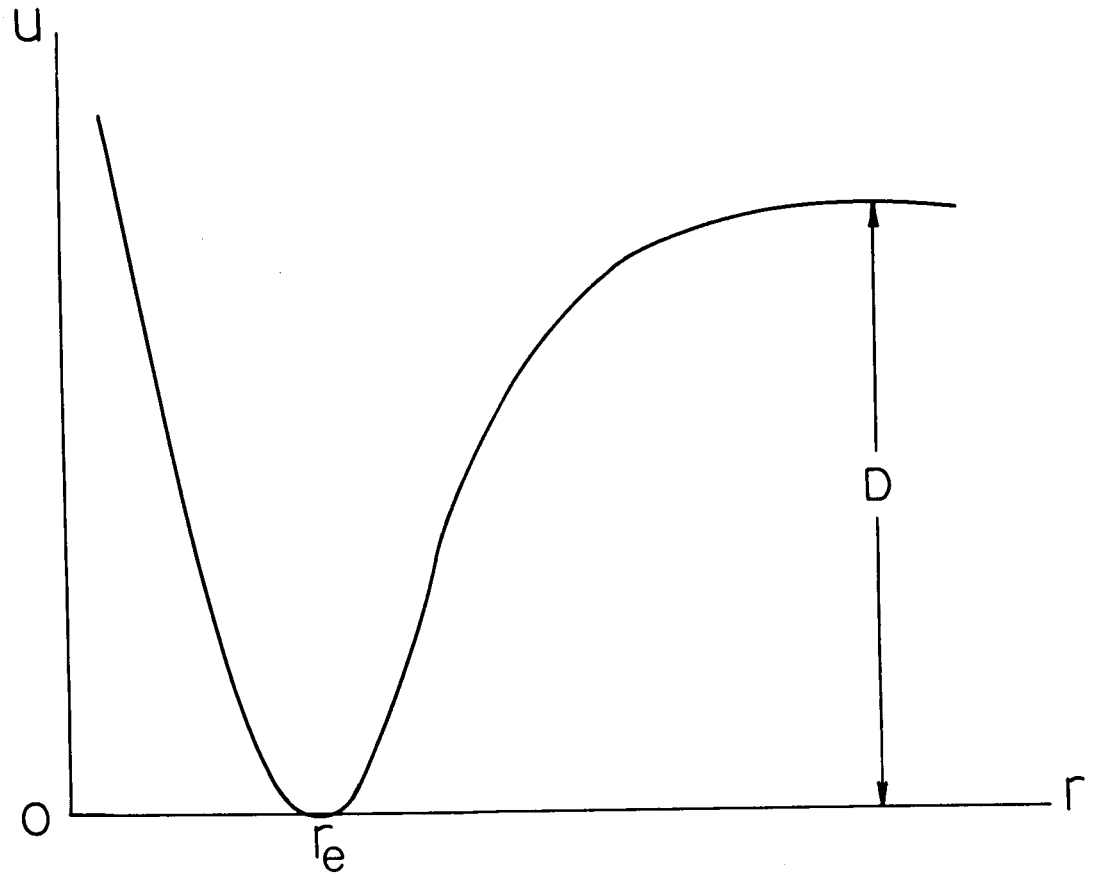

Fig.4.1 Potential energy of a Morse diatomic molecule

where $$L^{k-2v-1}_{k-v-1}(z) = (-1)^v \sum_{p=0}^{v} (-1)^p \binom{v}{p} \frac{\Gamma(k-v)}{\Gamma(k-v-p)} z^{v-p} , \quad (4.4)$$

$$N_v = \left[\alpha (k - 2v - 1)/v! \quad \Gamma (k - v) \right]^{\frac{1}{2}} , \quad (4.5)$$

$$z = k\, e^{-\beta (r - r_e)} , \quad (4.6)$$

$$k = \omega_e / \omega_e x_e , \quad (4.7)$$

and $$D = \omega_e^2 / 4 \omega_e x_e . \quad (4.8)$$

4.2 Wave Functions, Overlap Integrals and Franck-Condon Factors

The Morse wave functions of many molecular states (Nicholls 1962a) up to the highest vibrational levels known have been calculated at 0.01 Å intervals at the Computing Center of the National Bureau of Standards, Washington. Overlap integrals between all possible pairs of wave functions of a transition were evaluated and squared. These data were kindly made available for the present work.

4.3 Reduction of Antinode Position to Algebraic Form

In an attempt to follow the same procedure as section 3.2 the wave functions ψ_v of all the bound vibrational levels computed for the $X^3\Sigma$ and $B^3\Sigma$ states of the O_2 molecule were plotted against r to find the positions of the antinodes, r_p. Attempts were made to find a simple empirical algebraic relationship between r_p and v in analogy with the expression $v - b_p = a_p |\xi|^{n_p}$ (eq. 3.8) found for the antinodes of the harmonic wave functions. No simple expression was found which would apply to all values

of v and p for all molecular states. It was thus found necessary to resort to a graphical method for locating the coincidence of antinode pairs.

4.4 Graphical Method for Locating the Coincidence of Antinode Pairs

A graphical method for locating the coincidence of the turning points of the classical motion of an anharmonic oscillator was used by Condon (1926). The method has been extended here for use with any desired pair of antinodes. The positions of the antinodes were found from the calculated wave functions either by plotting them or by inspection, and plotted on a graph of v against r. The points of each antinode number p were joined by straight lines (fig. 4.2).

For each transition studied the antinode positions of the upper state were plotted on transparent paper, of the lower state on opaque paper. The v' and v'' values (not necessarily integral) corresponding to the alignment of antinode pairs could them be easily found. This alignment was found, as in the harmonic case, for the terminal antinode of one state with terminal and subsidiary antinodes of the other state.

4.5 Loci of Antinode Coincidence

The loci of antinode coincidence are again six-segment curves on the $v'v''$ plane as shown in fig. 3.3 for $p = 2, 3 \ldots$ and three-segment curves for $p = 1$ (fig. 3.5). The terminology used is that

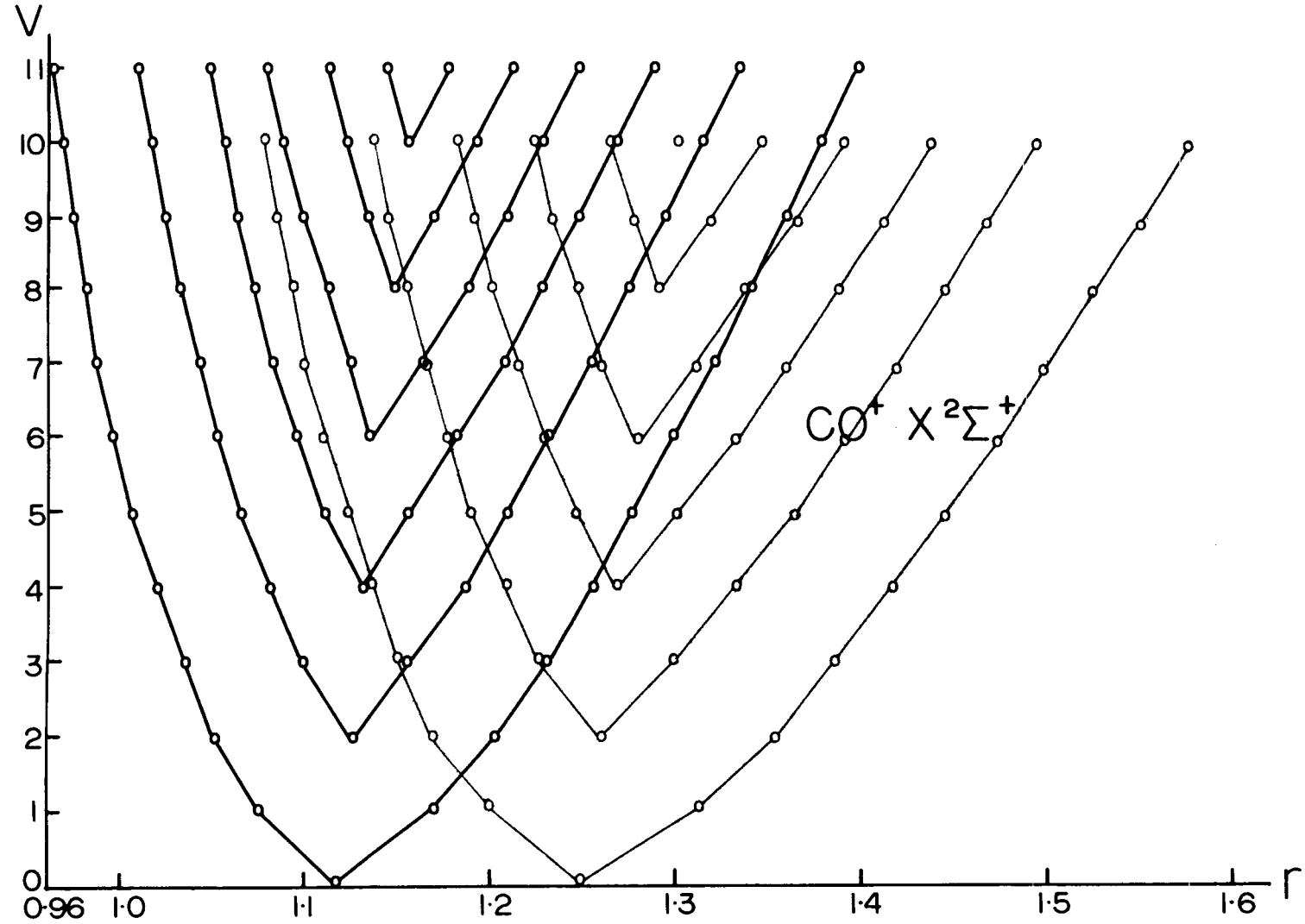

Fig.4.2 Antinode positions of CO^+ A and X states

shown in figs. 3.2 and 3.3. In the following section of this chapter the loci are examined for three transitions representative of small (0.012 Å), medium (0.1069 Å) and large (0.2233 Å) Δr_e. Our conclusions are based on these transitions and seven others discussed in Appendix 2.

The data for the transitions studied are given in table 4.1. The loci of antinode coincidence are compared with the Condon loci found from the Franck-Condon factor arrays and the band intensity arrays. The negative number following each entry in the factor arrays is the power of ten by which the entry is multiplied. Arrays of measured emission band intensity are given where available unless already given in Chapter 3 or Appendix 1.

4.6 Detailed Examination of Representative Types of Transition

4.6.1 MgO $B^1\Sigma \rightarrow X^1\Sigma$ Green System

Twenty-three bands of this system lying in the visible region ($\lambda \sim 5000$ Å) are known in emission. The system is typical of a small Δr_e ($\Delta r_e = 0.012$ Å) having a marked 0,0 sequence. The observed bands (table 4.2) all belong to the 0,0 and 0,1 sequences. The Condon locus of the Franck-Condon factor array (table 4.3) is confined to the main diagonal.

The calculated loci of antinode coincidence are shown on fig. 4.3. The subsidiary loci are in pairs external to the primary locus which lies about the main diagonal. The contribution to the overlap integral due to the coincidence of terminal pairs of antinodes along the calculated primary locus add to give high values along

Table 4.1

Data for transitions studied with Morse Model (from Herzberg 1950)

MOLECULE	μ atomic wt. units	Upper State	Lower State	ω_e' cm^{-1}	ω_e'' cm^{-1}	$\omega_e' x_e'$ cm^{-1}	$\omega_e'' x_e''$ cm^{-1}	r_e' Å	r_e'' Å	Δr_e Å
GaI	44.682	$A^3\Pi_o^+$	$X^1\Sigma^+$	193.2	216.4	2.4	0.5	*2.577	2.575	0.002
MgO	9.59888	$B^1\Sigma$	$X^1\Sigma$	824.1	785.1	4.76	5.18	1.737	1.749	0.012
$N_2^+ \leftarrow N_2$	N_2:7.00377 N_2^+:7.00363	$B^2\Sigma_u^+$	$X^1\Sigma_g^+$	2419.84	2358.07	23.19	14.19	1.075	1.0976	0.023
CO	6.85841	$A^1\Pi$	$X^1\Sigma^+$	1515.61	2170.21	17.2505	13.461	1.2351	1.12819	0.1069
MgO	9.59888	$B^1\Sigma$	$A^1\Pi$	824.1	664.4	4.76	3.91	1.737	1.864	0.127
CO^+	6.85823	$A^2\Pi$	$X^2\Sigma$	1562.06	2214.24	13.532	15.164	1.24368	1.11506	0.12862
$N_2^+ \leftarrow N_2$	N_2:7.00377 N_2^+:7.00363	$C^2\Sigma^+$	$X^1\Sigma_g^+$	2061	2358.07	11.0	14.19	1.262	1.0976	0.164
C_2	6.00194	$B^3\Pi_g$	$X^3\Pi_u$	1106.56	1641.35	39.26	11.67	1.5350	1.3117	0.2233
$N_2^+ \leftarrow N_2$	N_2:7.00377 N_2^+:7.00363	$D^2\Pi_g$	$X^1\Sigma_g^+$	919.2	2358.07	13.8	14.19	1.481	1.0976	0.383
O_2	8	$B^3\Sigma_u^-$	$X^3\Sigma_g^-$	700.36	1580.3613	8.0023	12.073	1.604	1.207398	0.397

* assumed value

Table 4.2

Band Intensities of MgO B → X (Mahanti 1932)

v' \ v"	0	1	2	3	4	5	6	7	8	9	10	11	12	13
0	10	4												
1		9	4											
2			8	3										
3				7	3									
4					6	3								
5						5	2							
6							4	1						
7								3	1					
8									2	0				
9										2				
10											2			
11												1		
12													0	
13														0

Table 4.3

Franck-Condon Factors for MgO $B^1\Sigma \rightarrow X^1\Sigma$ System (Nicholls 1962c)

v' \ v''	0	1	2	3	4	5	6	7
0	9.8232−1	1.7569−2	1.1034−4	2.7888−10	2.8250−8	9.1065−10	8.1415−15	3.6788−12
1	1.7438−2	9.4488−1	3.7280−2	4.1029−4	1.3180−7	1.2865−7	6.6214−9	1.0895−11
2	2.4248−4	3.6760−2	9.0300−1	5.9003−2	1.0008−3	1.3207−6	3.3386−7	2.7033−8
3	1.4216−6	7.9743−4	5.7857−2	8.5681−1	8.2536−2	2.0054−3	6.3316−6	6.2908−7
4	4.8725−9	6.6725−6	1.7456−3	8.0571−2	8.0651−1	1.0759−1	3.5689−3	2.1258−5
5	3.4746−11	3.0167−8	1.9510−5	3.1787−3	1.0469−1	7.5242−1	1.3381−1	5.8559−3
6	8.2972−13	2.3129−10	1.1174−7	4.5491−5	5.1989−3	1.2992−1	6.9496−1	1.6073−1
7	1.1138−13	4.9809−12	9.0730−10	3.2099−7	9.2529−5	7.9185−3	1.5594−1	6.3468−1

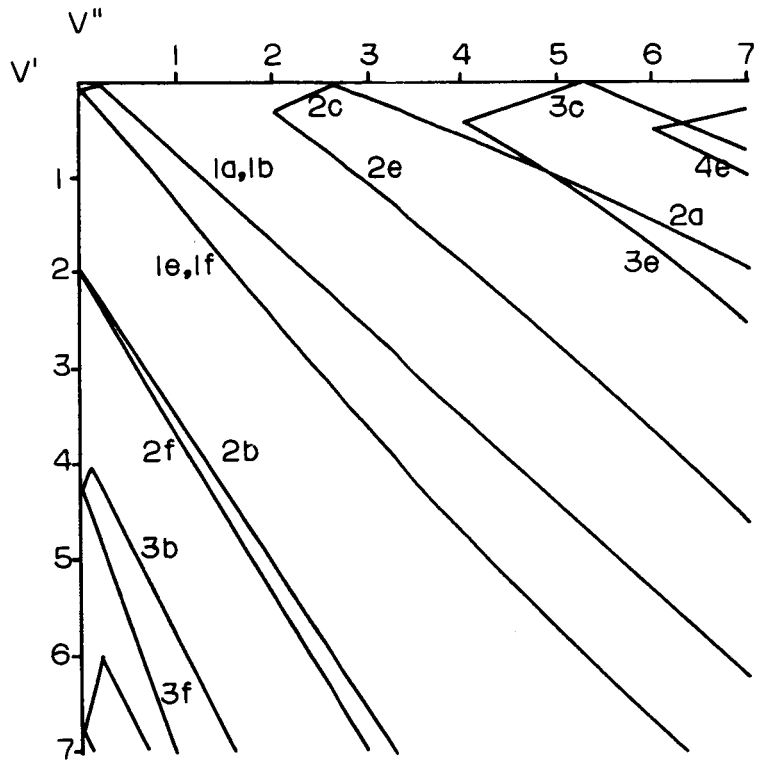

Fig.4.3 Loci of coincidence of antinode pairs,

MgO B→X

the main diagonal. Thus the primary Condon locus is well explained as due to the large contribution of overlapping terminal loops of the vibrational wave functions.

4.6.2 CO $A^1\Pi \rightarrow X^1\Sigma$ Fourth Positive System

The simple harmonic oscillator model of this system was discussed in Chapter 3 section 3.5.2 and the semi-quantum form of the Franck-Condon Principle found to apply well with a medium value of Δr_e ($\Delta r_e = 0.1069$ Å). The positions of observed bands will be found in table 3.9. Franck-Condon factors of the Morse model and the calculated loci of antinode coincidence are given in table 4.4 and fig. 4.4 respectively.

The primary Condon locus lies very close to the locus of the coincidence of terminal antinode pairs. The secondary Condon locus lies along the internal branches of the calculated secondary locus. The tertiary and quaternary Condon loci are equally well given by branches of the loci of coincidence of terminal and relevant subsidiary antinode pairs.

4.6.3 C_2 $B^3\Pi \rightarrow X^3\Pi$ Fox-Herzberg System

This system was discussed in Chapter 3 (section 3.5.3) and is representative of large values of Δr_e ($\Delta r_e = 0.2233$ Å). The location of observed bands is to be found in table 3.10. Franck-Condon factors for the Morse oscillator model are given in table 4.5. The calculated loci of antinode coincidence are shown in fig. 4.5. The primary Condon locus is well represented by the sections c, d and e, f only of the locus of coincidence of terminal antinode pairs

Table 4.4

Franck-Condon Factors for CO $A^1\Pi \rightarrow X^1\Sigma^+$ System (Nicholls 1962a)

v' \ v''	0	1	2	3	4	5	6	7	8	9	10	11	12	13	14	15	16	17	18	19	20	21	22	23	24
0	1.1319-1	2.6087-1	2.8477-1	1.9629-1	9.6040-2	3.5535-2	1.0340-2	2.4282-3	4.6859-4	7.5264-5	1.0151-5	1.1568-6	1.1181-7	9.1869-9	6.4215-10	3.7782-11	1.8874-12	9.6394-14	1.9682-15	1.7458-16	6.9579-16	8.4461-18	4.7739-16	2.2078-16	2.3198-17
1	2.1614-1	1.5487-1	3.0508-3	7.6435-2	1.9313-1	1.8569-1	1.0829-1	4.4465-2	1.3804-2	3.3745-3	6.6637-4	1.0812-4	1.4579-5	1.6462-6	1.5635-7	1.2525-8	8.4721-10	4.8179-11	2.2816-12	8.8683-14	3.5241-15	5.5781-16	1.8542-16	1.2590-16	7.7682-16
2	2.2997-1	1.2179-2	9.0126-2	1.1607-1	5.0832-3	5.7179-2	1.6502-1	1.6681-1	9.9629-2	4.1314-2	1.2831-2	3.1152-3	6.0724-4	9.6710-5	1.2731-5	1.3957-6	1.2800-7	9.8388-9	6.3250-10	3.4137-11	1.5954-12	5.3403-14	8.4261-16	2.1479-16	5.7173-19
3	1.8128-1	2.0493-2	1.1704-1	6.4536-4	8.9569-2	8.4157-2	4.7128-4	6.7660-2	1.5884-1	1.4862-1	8.4545-2	3.3725-2	1.0112-2	2.3717-3	4.4621-4	6.8445-5	8.6524-6	9.0748-7	7.9258-8	5.7731-9	3.5084-10	1.7696-11	7.0676-13	2.3445-14	2.0941-15
4	1.1879-1	8.7285-2	3.4433-2	5.7630-2	6.6561-2	6.1711-3	9.8034-2	5.1406-2	2.7202-3	8.9110-2	1.5679-1	1.2914-1	6.7610-2	2.5283-2	7.1696-3	1.5970-3	2.8572-4	4.1658-5	4.9963-6	4.9572-7	4.0797-8	2.7859-9	1.5695-10	7.2888-12	3.0315-13
5	6.8846-2	1.2304-1	3.2357-4	9.1254-2	1.3841-5	8.2359-2	2.2684-2	3.1553-2	9.4377-2	2.1092-2	1.8021-2	1.1299-1	1.5095-1	1.0784-1	5.1173-2	1.7696-2	4.6884-3	9.8077-4	1.6515-4	2.2666-5	2.5551-6	2.3757-7	1.8248-8	1.1565-9	6.0027-11
6	3.6675-2	1.1603-1	3.2109-2	4.2201-2	4.2898-2	4.2285-2	2.1776-2	7.2885-2	5.9304-4	6.3519-2	7.2827-2	2.4331-3	4.5471-2	1.3211-1	1.3855-1	8.5849-2	3.6707-2	1.1654-2	2.8628-3	5.5819-4	8.7798-5	1.1256-5	1.1833-6	1.0227-7	7.2653-9
7	1.8429-2	8.8057-2	7.3469-2	2.2336-3	7.3886-2	4.2668-5	6.9877-2	2.9021-3	5.8181-2	3.7499-2	1.0104-2	8.2806-2	4.0479-2	2.7402-3	7.8643-2	1.4142-1	1.2017-1	6.4922-2	2.4980-2	7.2532-3	1.6441-3	2.9713-4	4.3394-5	5.1631-6	5.0252-7
8	8.8974-3	5.8371-2	9.0972-2	9.8994-3	4.4622-2	3.2779-2	2.9742-2	3.0612-2	4.2672-2	9.8388-3	6.8218-2	6.0752-3	4.0752-2	7.7972-2	1.1842-2	2.2424-2	1.0892-1	1.3911-1	9.8285-2	4.6607-2	1.6147-2	4.2794-3	8.9197-4	1.4877-4	2.0069-5
9	4.1842-3	3.5370-2	8.4527-2	4.0627-2	7.9687-3	6.0808-2	3.8286-5	3.8344-2	1.6689-5	5.8879-2	5.9671-3	4.3499-2	4.4543-2	2.4546-3	6.9276-2	5.2619-2	1.8350-5	5.4755-2	1.2915-1	1.2656-1	7.5863-2	3.1782-2	9.9277-3	2.3987-3	4.5850-4
10	1.9367-3	2.0162-2	6.6327-2	6.4755-2	1.4618-3	4.5052-2	2.4181-2	2.3731-2	3.2522-2	2.3741-2	2.4797-2	4.1697-2	4.7082-3	6.2178-2	1.2255-2	2.6202-2	7.6757-2	2.1822-2	1.0029-2	8.9341-2	1.3590-1	1.0721-1	5.5381-2	2.0615-2	5.8141-3
11	8.8941-4	1.1024-2	4.6641-2	7.1751-2	1.9480-2	1.4504-2	4.9695-2	1.1030-5	4.9442-2	1.0943-3	4.9911-2	5.7511-6	5.1872-2	8.4925-3	3.3523-2	4.8135-2	1.3307-4	5.7040-2	6.0094-2	2.2404-3	3.7582-2	1.1651-1	1.2977-1	8.5100-2	3.8334-2
12	4.0787-4	5.8643-3	3.0446-2	6.5086-2	4.1768-2	1.7143-4	4.4180-2	1.6298-2	2.1594-2	3.0204-2	1.4383-2	3.1435-2	2.0623-2	2.0729-2	4.0979-2	1.9786-3	5.6287-2	1.8132-2	1.6192-2	7.2885-2	3.1097-2	3.3754-3	7.2539-2	1.3088-1	1.1416-1
13	1.8773-4	3.0666-3	1.8881-2	5.2041-2	6.5313-2	6.7201-3	2.0995-2	3.9190-2	4.2287-4	4.2877-2	1.7179-3	4.1004-2	2.1272-3	4.4591-2	6.1243-6	4.6549-2	1.1148-2	2.5596-2	5.0261-2	4.4292-4	4.5885-2	6.4819-2	6.9871-3	2.4538-2	1.0405-1
14	8.7084-5	1.5891-3	1.1304-2	3.8223-2	5.7629-2	2.3102-2	3.3642-3	4.1680-2	9.2001-3	2.1882-2	2.5544-2	1.0672-2	3.1550-2	1.0101-2	2.9406-2	1.9578-2	1.6848-2	4.0913-2	4.4129-4	5.0304-2	2.4094-2	8.8213-3	6.7352-2	3.9879-2	3.6765-4
15	4.0846-5	8.2117-4	6.6118-3	2.6471-2	5.1936-2	3.7973-2	7.3801-4	2.6615-2	2.8617-2	1.9365-3	3.7513-2	1.2081-3	3.4831-2	4.0014-3	3.5446-2	2.3548-3	4.1117-2	1.5983-4	4.1675-2	1.4535-2	1.8411-2	5.1503-2	2.7558-3	3.5154-2	6.7555-2
16	1.9425-5	4.2525-4	3.8121-3	1.7597-2	4.2528-2	4.5927-2	9.4788-3	9.4220-3	3.6896-2	3.5232-3	2.3565-2	1.9485-2	1.0192-2	2.8332-2	6.0848-3	3.0450-2	8.6642-3	2.6350-2	2.0329-2	1.2562-2	4.1355-2	2.6062-5	4.3585-2	3.0498-2	3.4547-3
17	9.3867-6	2.2157-4	2.1816-3	1.1373-2	3.2596-2	4.6731-2	2.1795-2	6.1450-4	3.0143-2	1.8049-2	5.1274-3	3.2376-2	2.6912-4	3.1077-2	3.7993-3	2.9198-2	4.8212-3	3.2361-2	1.7042-3	3.8687-2	8.6115-4	3.6321-2	1.9083-2	1.1515-2	5.1596-2
18	4.6172-6	1.1653-4	1.2459-3	7.2159-3	2.3851-2	4.2574-2	3.1818-2	1.6937-3	1.6581-2	2.9379-2	3.2516-4	2.5475-2	4.2637-2	1.1864-2	2.3360-2	5.3800-3	2.7723-2	4.6775-3	2.7916-2	9.2564-3	2.2094-2	2.2721-2	7.8327-3	4.1710-2	1.2774-3

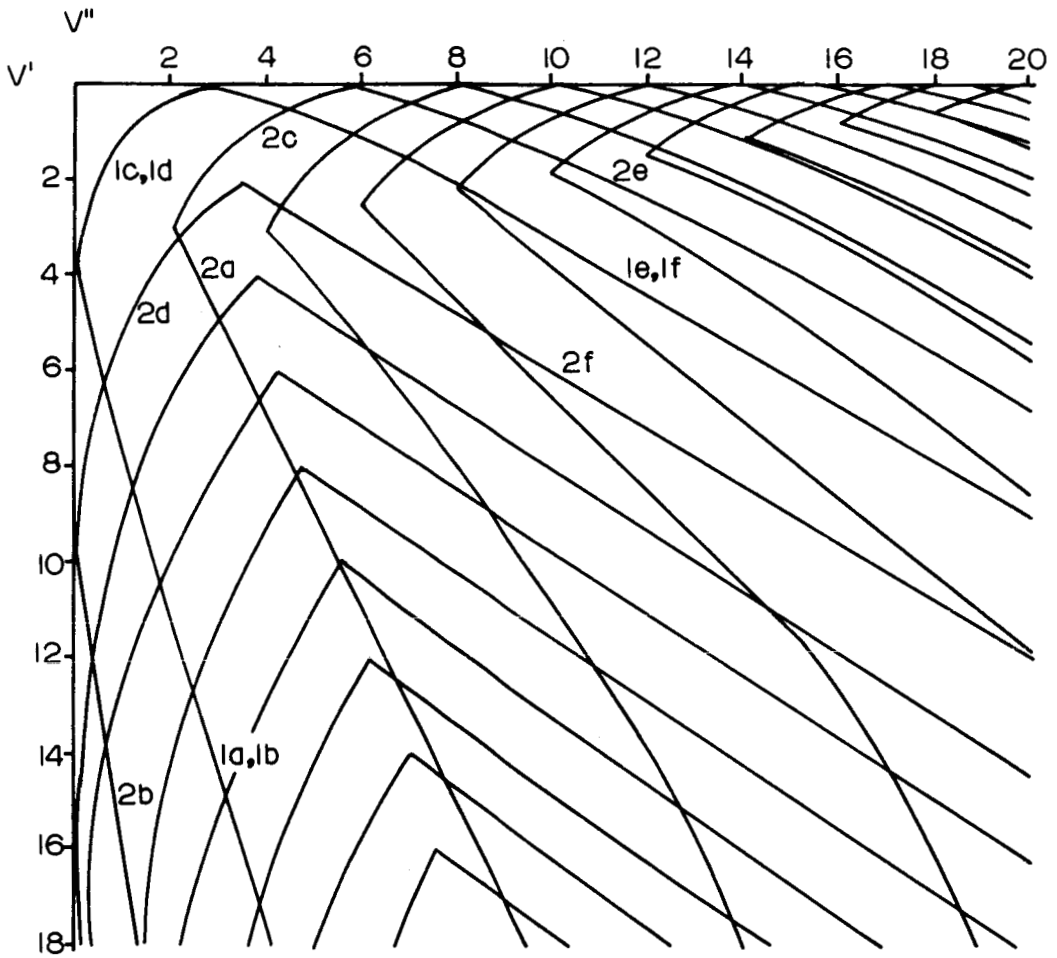

Fig.4.4 Loci of coincidence of antinode pairs,

CO A→X

Table 4.5

Franck-Condon Factors for C_2 $B^3\Pi \rightarrow X^3\Pi$ System (Nicholls 1964a)

	v"	0	1	2	3	4	5	6	7	8	9	10	11	12	13
v'	0	1.4369-3	1.2826-2	5.1012-2	1.2046-1	1.9023-1	2.1504-1	1.8236-1	1.2034-1	6.3754-2	2.7861-2	1.0281-2	3.2669-3	9.0834-4	2.2386-4
	1	4.9176-3	3.3567-2	9.2494-2	1.2742-1	8.1493-2	9.9149-3	1.6509-2	9.7844-2	1.6238-1	1.5926-1	1.1155-1	6.0802-2	2.7111-2	1.0217-2
	2	9.7331-3	5.1224-2	9.5733-2	6.5454-2	3.5013-3	3.0368-2	9.1015-2	6.3191-2	3.9953-3	2.5140-2	1.0327-1	1.4992-1	1.3578-1	9.0583-2
	3	1.4669-2	6.0055-2	7.3803-2	1.6848-2	1.1130-2	6.5229-2	3.9538-2	2.8033-4	5.0808-2	8.1780-2	3.0748-2	8.0493-4	4.9589-2	1.1695-1
	4	1.8718-2	6.0202-2	4.6500-2	4.6442-4	3.4636-2	4.5646-2	1.0560-2	3.4079-2	5.7214-2	8.2749-3	1.7440-2	7.1192-2	5.6860-2	6.7070-3

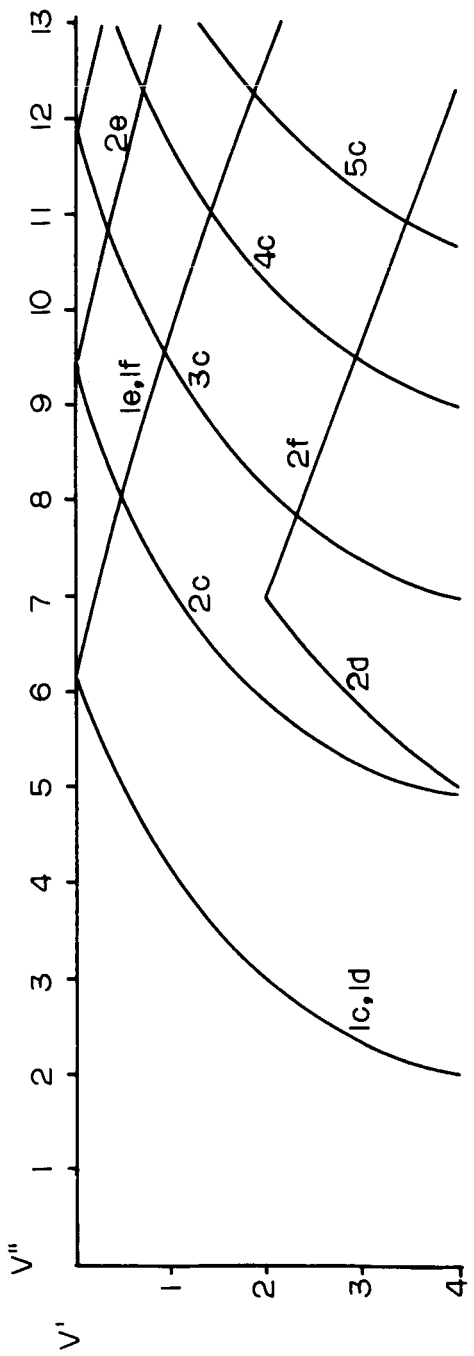

Fig.4.5 Loci of coincidence of antinode pairs, C_2 B→X

giving the asymmetrical nature of the Condon locus. The subsidiary Condon loci are equally well represented by the d and f sections of the calculated subsidiary loci.

CHAPTER 5

CONCLUSIONS

The study of Condon loci of diatomic molecular spectra described here has shown that the location of strong bands of a system is largely determined by the overlapping of pairs of antinodes of the vibrational wave functions. As stated by Condon the strongest bands occur at the condition of maximum overlap of terminal antinodes. These bands define the primary Condon locus. We have found that the subsidiary Condon loci are defined by the maximum overlap of a terminal antinode of one vibrational state and an inner antinode of the other state. Thus the largest contribution to the overlap integral is from a single pair of overlapping loops of the vibrational wave functions.

In the extreme and unusual cases of very small and very large equilibrium internuclear separation difference these general conclusions are not applicable. In the former case there is cancellation in the overlap integral between wave functions with an odd difference in vibrational quantum number. No nested Condon loci can be defined. In the latter case the important vibrational quantum numbers are so high that the individual loops of the wave functions are of minor significance. Here nested loci are not clearly defined. In both

these cases the complete overlap integral must be considered in locating the strong bands of a system.

A transition parameter depending on the equilibrium internuclear separation of the two electronic states, their classical vibrational frequencies, and the reduced mass of the molecule has been defined. This parameter describes the shape of the primary Condon locus.

A method has been described for finding the approximate positions of the Condon loci for the wide range of Δr_e in which the maximum contribution to the Franck-Condon factor is from the overlapping of a pair of antinodes of the vibrational wave functions. This approach can be of use in the identification of observed bands of a system, and in the observation of unrecorded bands.

APPENDIX 1

A1 Further Results of the Examination of Condon Loci Using the Simple Harmonic Oscillator Model

The transitions discussed in Chapter 3 (section 3.5) are representative of small, medium and large values of Δr_e. The conclusions concerning them are based on a study of four more transitions which are included in this Appendix. They are:

GaI $A^3\Pi_o^+ \rightarrow X^1\Sigma^+$,

CH^+ $A^1\Pi \rightarrow X^1\Sigma^+$,

CO^+ $A^2\Pi \rightarrow X^2\Sigma$,

and O_2 $B^3\Sigma_u^- \rightarrow X^3\Sigma_g^-$

the molecular data for which are given in table 3.2. The transitions are treated in order of increasing Δr_e but the apparently anomalous case of zero Δr_e is treated last.

From this section of the study we base our conclusions that the approximation we have made to the Franck-Condon principle breaks down at very small and very large values of Δr_e for the reasons outlined in the relevant sections.

A1.1 $\underline{CH^+ \quad A^1\Pi \rightarrow X^1\Sigma^+}$ ($\Delta r_e = 0.10356$ Å)

Four bands lying in the violet region of the spectrum are observed in emission. Their location on the v'v" plane is given in table A1.1, no intensities being available. This system is of astrophysical interest because certain lines are observed in the absorption spectra of some stars and interstellar space.

The overlap integral array (table A1.2) shows a slightly open primary Condon locus. One branch lies along the $\Delta v = v' - v'' = 1$ diagonal and has negative overlap integrals. The other branch of the primary Condon locus is inclined to the main diagonal with $v'' > v'$, and has positive overlap integrals. There are two apparent external loci along the $\Delta v = v' - v'' = 4$ and 6 diagonals. The $\Delta v = 4$ diagonal has negative entries, the $\Delta v = 6$ diagonal positive.

The Condon loci given in table A1.2 correspond closely to the loci of antinode coincidence shown in fig. A1.1 as follows:

(a) the $\Delta v = 1$ branch of the primary with coincidence between pairs of left hand terminal antinodes (segment a,b) and coincidence between right hand pairs of antinodes (segment f) the secondary antinode of the upper state, and the primary antinode of the lower state.

(b) the $v'' > v'$ branch of the primary with coincidence between left hand pairs of antinodes (segment a) the primary antinode of the upper state with the secondary antinode of the lower state.

Table A1.1

Observed Bands of CH^+ A → X (Pearse and Gaydon 1950)

v' \ v''	0	1	2
0	X	X	
1	X		
2	X		

Table A1.2

Overlap Integrals of CH^+ A → X

v' \ v''	0	1	2	3	4	5	6	7
0	0.8412	0.4317	0.2719	0.1489	0.0838	0.0450	0.0243	0.0128
1	-0.5253	0.5557	0.4291	0.3691	0.2397	0.1558	0.0931	0.0550
2	0.1167	-0.6689	0.3185	0.3322	0.3947	0.2969	0.2203	0.1448
3	0.0411	0.2193	-0.7185	0.1342	0.1961	0.3682	0.3178	0.2692
4	-0.0324	0.0640	0.3230	-0.7082	0.0042	0.0503	0.3062	0.3041
5	0.0019	-0.0701	0.0740	0.4200	-0.6565	-0.0737	-0.0866	0.2239
6	0.0052	0.0073	-0.1157	0.0696	0.5030	-0.5781	-0.1044	-0.2026
7	-0.0016	0.0128	0.0179	-0.1661	0.0507	0.5667	-0.4849	-0.0948

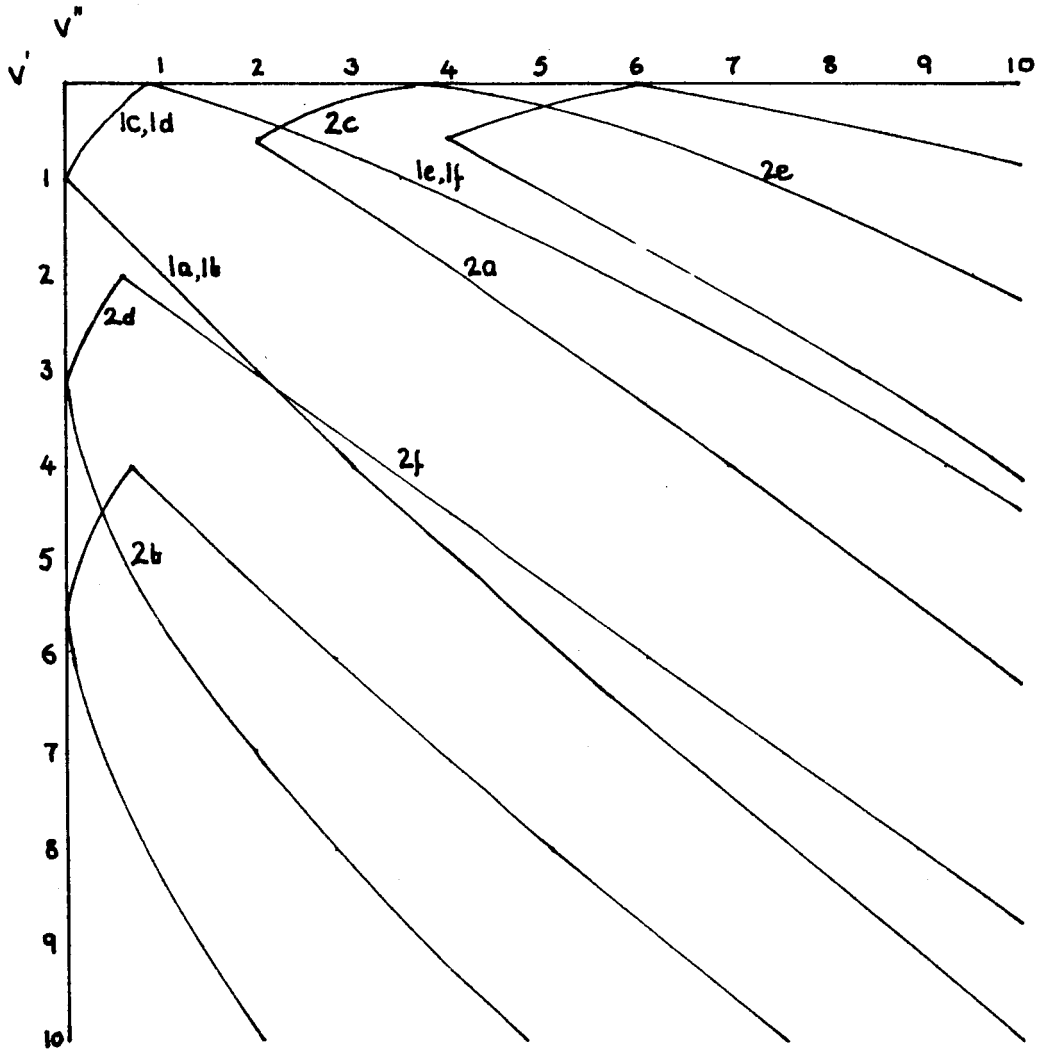

Fig. A 1.1 Loci of coincidence of antinode pairs,

CH^+ $A \rightarrow X$

(c) the $\Delta v = 4$ diagonal with coincidence between left hand pairs of antinodes (segment b) the secondary antinode of the upper state with the primary antinode of the lower state, and with coincidence between right hand pairs of antinodes (segment f) the tertiary antinode of the upper state and the primary antinode of the lower state.

(d) the $\Delta v = 6$ diagonal is also associated with the coincidence between the left hand pairs of antinodes (segment b) mentioned above and with the coincidence of left hand pairs of antinodes the upper antinode being the tertiary, the lower antinode the primary (segment b).

Table A1.3 is an examination of the sign of the contribution to the overlap integral due to the coincidence of pairs of antinodes for $v' = 0 - 7$, $v'' = 0 - 2$. It is clear that the above comments concerning the primary Condon locus are substantiated, while the apparent subsidiaries are due to the cancellation of opposing contributions in neighbouring entries. These conclusions are identical to those reached in the study of the MgH transitions discussed in section 3.5.1.

A1.2 CO^+ $A^2\Pi \rightarrow X^2\Sigma$ Comet Tail System ($\Delta r_e = 0.12862$ Å)

This system is of astrophysical importance as it is emitted by the tails of comets. Twenty-nine bands lying throughout the visible and in the near ultra violet region of the spectrum ($\lambda \sim 6000 - 3000$ Å) are known in emission. Their intensities are given in table A1.4.

Table A1.3

Examination of Contributions to Overlap Integral of CH^+ $A \rightarrow X$

v'	v''	Close to:	Section	$\psi_{v'}$	$\psi_{v''}$	$\psi_{v'} \times \psi_{v''}$	$\int \psi_{v'} \psi_{v''} dr$
0	0	Primary	c,d	+	+	+	+
1	0	Primary	c,d	−	+	−	−
2	0	Primary	c,d	+	+	+	+
3	0	Secondary	d	+	+	+	+
4	0	Secondary	b	−	+	−	−
5	0	Tertiary	d	−	+	−	+
5	0	Secondary	b	+	+	+	+
6	0	Tertiary	b	+	+	+	+
7	0	Tertiary	b	−	+	−	−
0	1	Primary	e,f	+	+	+	+
1	1	Primary	e,f	+	+	+	+
1	1	Primary	a,b	−	−	+	+
2	1	Primary	a,b	+	−	−	−
2	1	Secondary	f	−	+	−	−
3	1	Primary	a,b	−	−	+	+
3	1	Secondary	f	−	+	−	+
4	1	Tertiary	f	+	+	+	+
4	1	Primary	a,b	+	−	−	+
5	1	Secondary	b	+	−	−	−
5	1	Tertiary	f	+	+	+	−
6	1	Secondary	b	−	−	+	+
6	1	Tertiary	f	+	+	+	+
6	1	Tertiary	b	+	−	−	+
7	1	Secondary	b	+	−	−	+
7	1	Tertiary	b	−	−	+	+
7	1	Quarternary	f	−	+	−	+
0	2	Primary	e,f	+	+	+	+
1	2	Primary	e,f	+	+	+	+
1	2	Secondary	c	−	−	+	+
2	2	Primary	e,f	+	+	+	+
2	2	Primary	a,b	+	+	+	+
2	2	Secondary	f	−	+	−	+
3	2	Primary	a,b	−	+	−	−
3	2	Secondary	f	−	+	−	−
4	2	Primary	a,b	+	+	+	+
4	2	Secondary	f	−	+	−	+
5	2	Tertiary	f	+	+	+	+
5	2	Primary	a,b	−	+	−	+
5	2	Secondary	f	−	+	−	+
5	2	Secondary	b	+	+	+	+
6	2	Tertiary	f	+	+	+	−
6	2	Secondary	b	−	+	−	−
7	2	Secondary	b	+	+	+	+

Table A1.4

Band Intensities of CO^+ A → X (Pearse and Gaydon 1950)

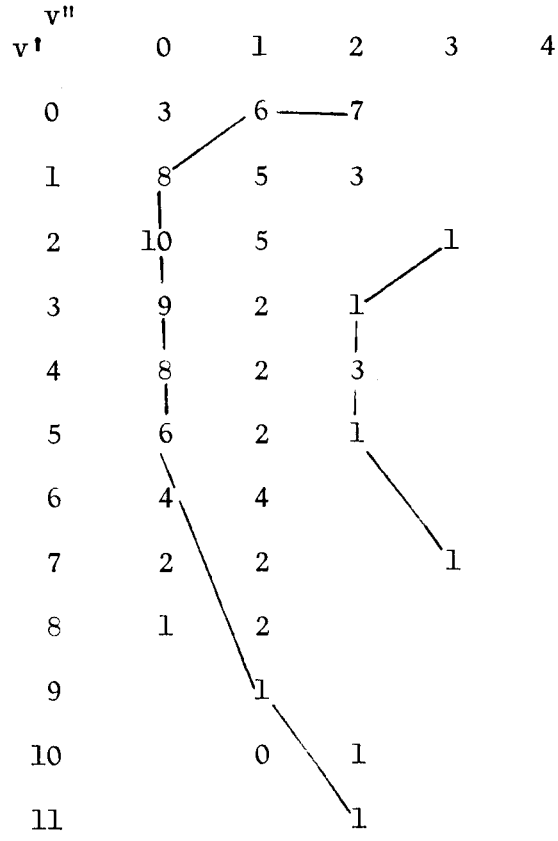

The observed bands are confined to the left hand portion of the Deslandres table and it is possible to distinguish the paths of primary and secondary Condon loci.

The overlap integral array (table A1.5) shows three Condon loci nested in the conventional manner typical of the medium Δr_e value. The loci are, however, not symmetrical about the main diagonal, or even roughly so, as much of the literature infers (Herzberg 1950 p. 198). The primary Condon locus is confined to the $v' = 0$ progression from $v'' = 2 - 5$. From $v' = 2$, $v'' = 0$ the locus drops steeply to $v' = 7$, $v'' = 2$. Thus there is a distinct "corner" at $v' = 2$. The subsidiary loci are of similar shape.

Fig. A1.2 shows the loci of antinode coincidence from which the Condon loci can be interpreted. The locus of the coincidence of terminal antinode pairs closely follows the primary Condon locus. The "corner" at $v' = 2$, $v'' = 0$ already mentioned is close to the junction of the branches a, b and c, d of the calculated locus.

The secondary Condon locus follows closely the sections a, c and d, and f of the locus of coincidence between a secondary and a terminal antinode. The remaining coincidences of this locus are understood to contribute little to the overlap integral due to the shortness of the overlapping regions of the vibrational wave functions and to the large difference in loop sizes of the wave functions resulting from large difference in vibrational quantum number.

The tertiary Condon locus can be similarly interpreted in terms of the large contribution to the overlap integral at the coincidence of a tertiary antinode and a terminal antinode.

Table A1.5

Overlap Integral of CO^+ A → X

v' \ v''	0	1	2	3	4	5	6	7
0	0.2126	0.3394	0.4092	0.4251	0.4006	0.3517	0.2924	0.2327
1	-0.4041	-0.4359	-0.3051	-0.1100	0.0759	0.2137	0.2927	0.3196
2	0.5173	0.2630	-0.0692	-0.2721	-0.3042	-0.2119	-0.0646	0.0812
3	-0.5108	0.0670	0.3305	0.2459	0.0137	-0.1843	-0.2656	-0.2314
4	0.4081	-0.3546	-0.2571	0.0889	0.2747	0.2219	0.0398	-0.1383
5	-0.2681	0.4708	-0.0533	-0.3097	-0.1574	0.1104	0.2467	0.1996
6	0.1437	-0.4173	0.3497	0.1892	-0.1703	-0.2622	-0.0890	0.1293
7	-0.0604	0.2780	-0.4624	0.1390	0.2884	0.0290	-0.2146	-0.2125

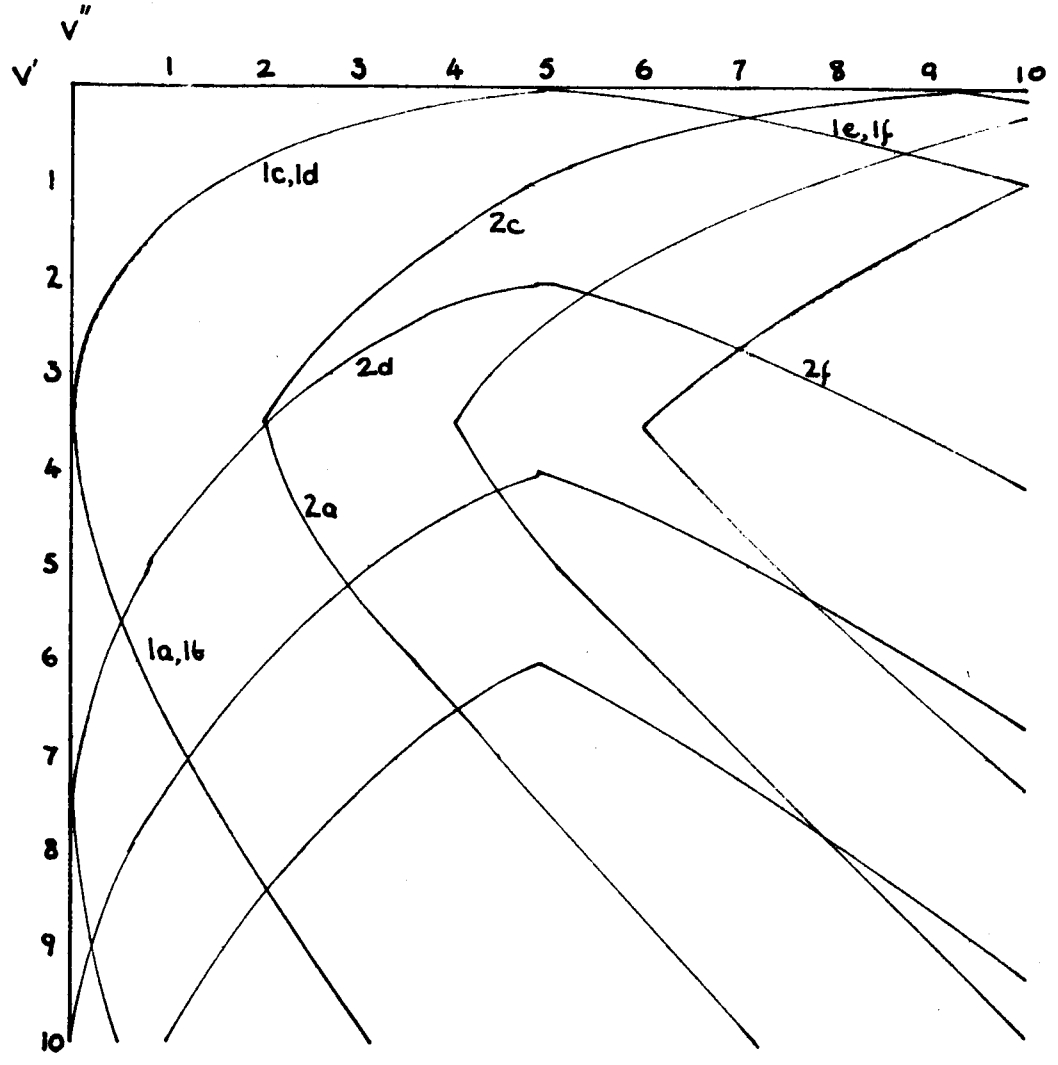

Fig. A1.2 Loci of coincidence of antinode pairs.

CO^+ $A \rightarrow X$

Al.3 O_2 $B^3\Sigma_u^- \rightarrow X^3\Sigma_g^-$ Schumann-Runge System ($\Delta r_e = 0.397$ Å)

This extensive system of O_2 exists throughout the ultra-violet region of the spectrum in both emission and absorption. Twenty-nine emission bands up to λ 4372 Å are well known. Continuum appears below λ 1759 Å setting the ultra-violet limit to spectroscopy in air. Measured band intensities are given in table Al.6. Most of the observed bands fall on a primary Condon locus, with two bands (2,15 and 2,16) possibly indicating a secondary Condon locus.

The overlap integral array for this transition using the harmonic oscillator model is not available. The transition is of very large Δr_e giving the strongest bands at high v" values for which the harmonic oscillator model is a very poor approximation. However, as a matter of interest, this transition has been studied with both a harmonic and an anharmonic potential.

The calculations of antinode coincidence were carried out to high quantum numbers (v' = 20, v" = 30) and high antinode number (p = 8). The results are shown in fig. Al.3.

Because of the above mentioned features of this transition it is not possible to relate the loci of antinode pair coincidence with the Condon loci. It must be concluded that the approximate form of the Franck-Condon Principle is inadequate at very large Δr_e values.

Al.4 GaI $A^3\Pi \rightarrow X^1\Sigma$ System A ($\Delta r_e = 0$)

Sixty bands in the blue region ($\lambda \sim 4000$ Å) of the spectrum are known to belong to this system, which is however overlapped by the B → X system of the same molecule.

Table A1.6

Band Intensities of O_2 B → X (Hébert and Nicholls 1961)

v' \ v''	5	6	7	8	9	10	11	12	13	14	15	16	17	18	19	20	21	22	23	24	25
0					71	58	64	48	38	30	17	10	7	3	2						
1				79	95	89	67	26				4	6	8	4	2					
2			58	100	97						3	2			1	3	2				

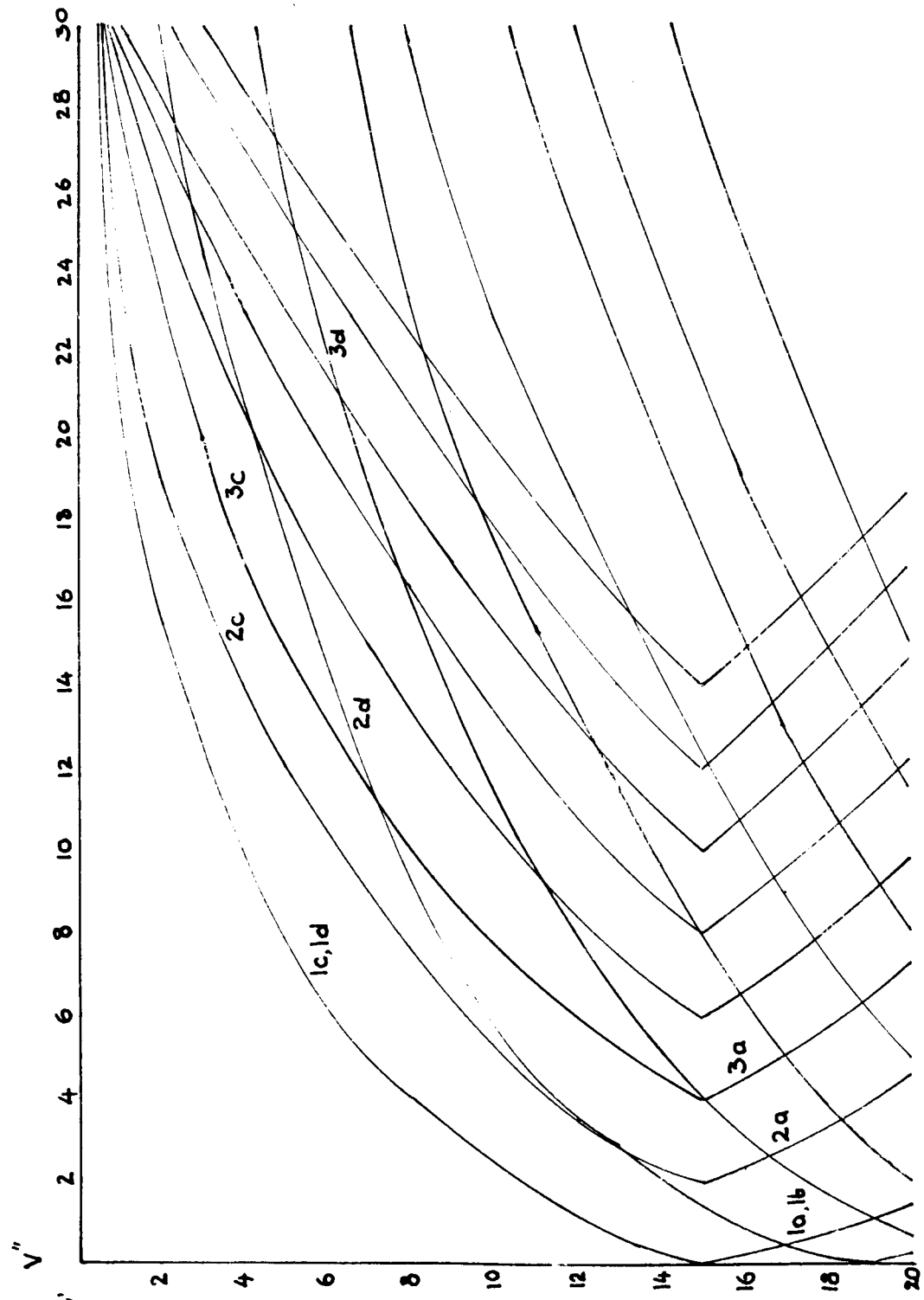

Fig.A1.3 Loci of coincidence of antinode pairs, O_2 $B \rightarrow X$

This system was studied in detail by Wehrli (1934) in relation to the Franck-Condon Principle. It has been included in our study in order to assess his conclusion that only the complete quantum mechanical analysis of vibrational overlap is valid when $\Delta r_e = 0$, this system being one of the few with zero or very near zero difference in equilibrium internuclear separation.

The overlap integral array for zero Δr_e is not available but is indicated qualitatively in table A1.7. The unusual appearance is due to the symmetry of the vibrational wave functions. Odd Δv entries have zero overlap integral (cancellation of odd and even functions). Even Δv entries have finite overlap integral the value decreasing from the main diagonal. Thus odd Δv transitions are forbidden; even Δv transitions allowed.

The array of measured band intensity (table A1.8) shows that the GaI transition $A \rightarrow X$ is closely one of zero change in equilibrium internuclear separation. The strong bands appear on the even Δv diagonals and no nested Condon loci can be drawn. However we shall associate the main diagonal with the primary Condon locus, and pairs of external diagonals with the subsidiary loci.

The coincidence of antinode pairs calculated by our algebraic method with $\Delta r_e = 0$ is shown in fig. A1.4. There is coincidence of primary antinodes along the line close to the main diagonal of the array. It is important to note that this line coincides with the main diagonal only if $\omega_e' = \omega_e''$. The inclination of the line to the v' axis is $\tan^{-1}(\omega_e''/\omega_e')^{n1/2}$. The coincidence of central modes or antinodes, rather than of terminal antinodes, describe the diagonals.

Table Al.7

Overlap Integrals of GaI A → X (Wehrli 1934)

v' \ v''	0	1	2	3	4	5	6	7	8	9	10	11	12	13	14	15
0	X	-	X													
1	-	X	-	X												
2	X	-	X	-	X											
3		X	-	X	-	X	-	X								
4			X	-	X	-	X	-	X							
5				X	-	X	-	X	-	X						
6					X	-	X	-	X	-	X					
7				X	-	X	-	X	-	X	-	X				
8					X	-	X	-	X	-	X	-	X			
9						X	-	X	-	X	-	X	-	X		
10							X	-	X	-	X	-	X	-	X	
11								X	-	X	-	X	-	X	-	X

legend X non-zero overlap integral

\- zero overlap integral

Table A1.8

Band Intensities of GaI A → X (Miescher and Wehrli 1934)

v' \ v''	0	1	2	3	4	5	6	7	8	9	10	11	12	13	14	15	16
0	10	5	2														
1	8	9	5	2	0												
2	4	9	8	5	2	1	1										
3			10	7	4	3	0	1									
4				7	7	2	4	0	1								
5			3		6	6		3	0	1							
6				4			6	1	3		0						
7								6	1	4	0	1					
8									5	1	3	1	1				
9										3	2	2	0	1			
10											1		2	0	1		
11												1		2	0	1	
12													1			1	
																	1

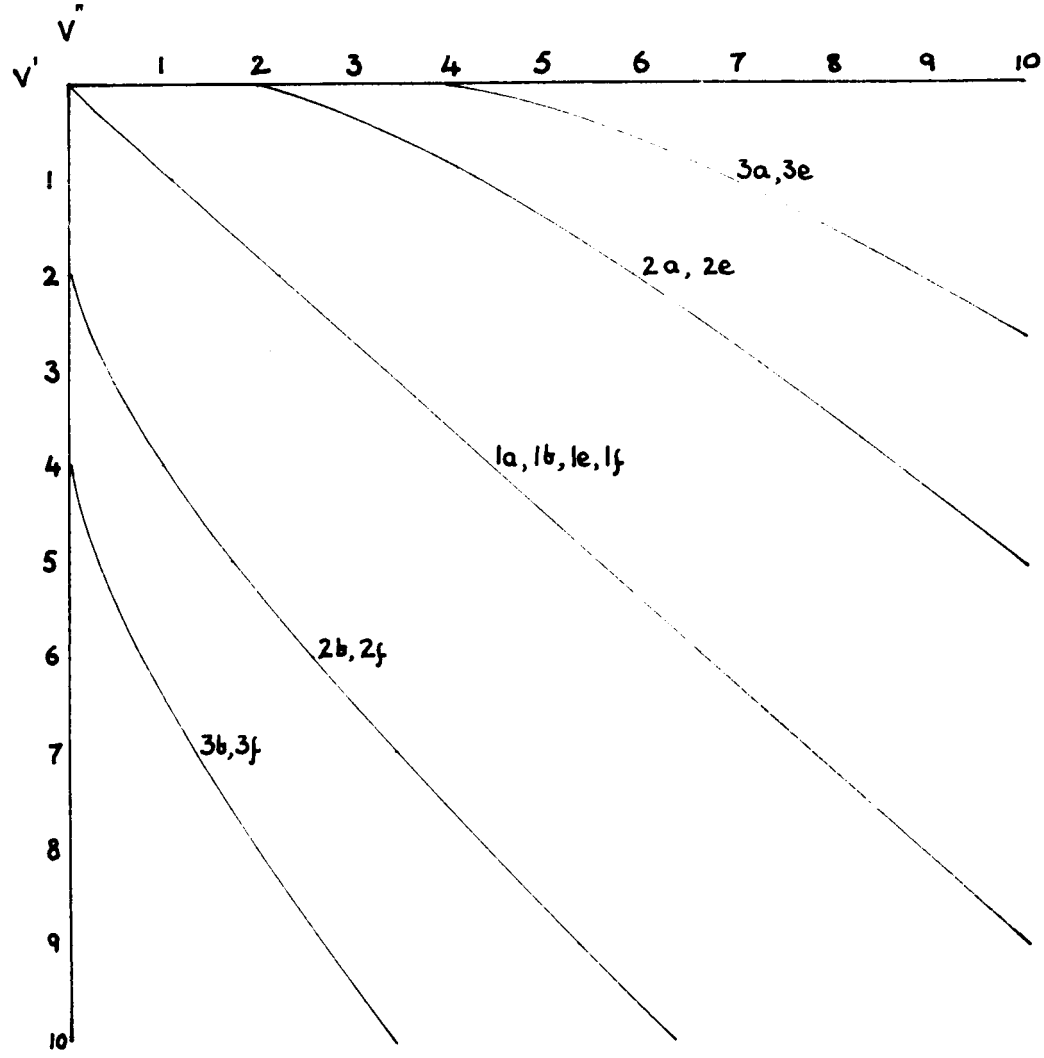

Fig. AI.4 Loci of coincidence of antinode pairs,

GaI $A \rightarrow X$

The pair of lines in fig. A1.4 one on each side of the main diagonal, describe the coincidence of a terminal antinode of one state with a secondary antinode of the other. These lines are far from the $\Delta v = 2$ lines of the overlap integral array, and cannot be associated with the secondary Condon locus. There is also lack of similarity between the lines of primary and tertiary antinode coincidence, and the $\Delta v = 4$ diagonals.

The effect of a very small Δr_e on the loci of antinode coincidence has been investigated. Calculations of the loci with $\Delta r_e = 0.002$ Å yield six-segmented loci with the c and d sections very short (~ 0.1 quantum number) and the a and e, b and f sections very close. The nature of the loci is unchanged.

This system is discussed further in Appendix 2.7 where the Morse model is studied.

APPENDIX 2

A2 Further Results of the Examination of Condon Loci Using the Morse Oscillator Model

This appendix relates to the results of Chapter 4. Its arrangement and purpose is similar to that of Appendix 1 and the conclusions concerning the validity of our approximation to the Franck-Condon Principle are the same. Seven transitions are examined in detail; these are:

GaI	$A^3\Pi^* \rightarrow X^1\Sigma^+$,
N_2 ionisation	$N_2^+B^2\Sigma_u^+ \leftarrow N_2\ X^1\Sigma_g^+$,
MgO	$B^1\Sigma \rightarrow A^1\Pi$,
CO^+	$A^2\Pi \rightarrow X^2\Sigma$,
N_2 ionisation	$N_2^+C^2\Sigma^* \leftarrow N_2X^1\Sigma_g^+$,
N_2 ionisation	$N_2^+D^2\Pi_g \leftarrow X^1\Sigma_g^+$
and O_2	$B^3\Sigma_u^- \rightarrow X^3\Sigma_g^-$

the molecular data for which are given in table 4.1.

A2.1 $N_2^+\ B^2\Sigma_u^+ \leftarrow N_2\ X^1\Sigma_g^+$ Rydberg System ($\Delta r_e = 0.023$ Å)

The ionization transitions of nitrogen have been included in our study due to interesting features in their Franck-Condon factor arrays.

Some of the transitions have been observed in emission by Takamine et al. (1938). Five emission and ten absorption bands have been observed in the vacuum ultra-violet ($\lambda \sim 700 - 800$ Å). There has been no vibrational analysis.

The Franck-Condon factor array (table A2.1) shows a narrow primary Condon locus lying entirely along the main diagonal up to $v' = v'' = 10$. The locus broadens at higher quantum numbers and an inner secondary locus runs from $v' = v'' = 12$. External to these loci are many entries which are large in comparison with their neighbours. Of these many lie along diagonals of the Deslandres table defining additional subsidiary Condon loci. The Franck-Condon factors involved are, however, very much smaller than those of the generally recognized Condon loci.

The calculated loci of antinode coincidence are shown in fig. A2.1. The primary locus is unusual in that it becomes narrow at high quantum numbers. The subsidiary loci are in pairs each side of the primary. Their branches intersect considerably.

The e,f branch of the calculated primary locus lies close to the main diagonal and hence to the primary Condon locus up to its point of broadening. From $v' = v'' = 12$ the secondary Condon locus lies along the main diagonal and may be associated with the calculated primary locus. The a,b branch lies along the primary locus from its point of broadening.

The external Condon loci lie along branches of the calculated subsidiary loci. The existence of these minor Condon loci can be

Table A2.1

Franck–Condon Factors for N_2^+ $B^2\Sigma_u^+ \leftarrow N_2$ $X^1\Sigma_g^+$ System (Nicholls 1962a)

v' \ v''	0	1	2	3	4	5	6	7	8	9	10	11	12	13	14
0	8.9119-1	9.7304-2	1.0474-2	9.4914-4	7.2849-5	4.1719-6	1.1411-7	7.4131-10	4.0546-9	1.7257-9	4.3749-10	8.3964-11	1.2776-11	1.4485-12	9.2064-14
1	1.0703-1	7.1633-1	1.4924-1	2.4218-2	2.8875-3	2.7556-4	1.8965-5	6.2483-7	2.9900-8	2.5030-8	1.2117-8	3.4178-9	7.2475-10	1.2182-10	1.5561-11
2	1.7514-3	1.8270-1	5.9899-1	1.7279-1	3.7606-2	5.4970-3	6.2445-4	4.9978-5	1.9210-6	6.9500-7	8.6547-8	4.6938-8	1.4576-8	3.3839-9	6.2427-10
3	2.6855-5	3.5203-3	2.3645-1	5.2279-1	1.7860-1	4.9048-2	8.3782-3	1.0989-3	9.9719-5	4.3554-6	1.2691-6	2.2153-7	1.3270-7	4.4942-8	1.1327-8
4	1.7966-6	1.4796-4	4.3907-3	2.7414-1	4.7695-1	1.7330-1	5.8086-2	1.1174-2	1.6550-3	1.6678-4	8.0945-6	2.1182-8	4.6891-7	3.0588-7	1.1198-7
5	6.5482-8	5.7324-6	4.6203-4	4.0522-3	2.9916-1	4.5442-1	1.6096-1	5.6851-2	1.3609-2	2.2400-3	2.4621-4	1.3021-5	3.5426-8	8.7019-7	6.1001-7
6	1.0485-9	5.3631-7	8.8267-6	1.0709-3	2.6997-3	3.1313-1	4.5064-1	1.4407-1	6.9768-2	1.5497-2	2.8034-3	3.3060-4	1.8720-5	6.2242-8	1.4669-6
7	3.3727-10	1.4116-9	2.2552-6	6.6161-6	2.0360-3	9.8996-4	3.1643-1	4.6253-1	1.2419-1	7.3394-2	1.6717-2	3.3053-3	4.1139-4	2.4548-5	1.1509-7
8	5.2112-12	2.7128-9	9.3400-10	6.4549-6	4.6160-7	3.3256-3	6.3250-6	3.0870-1	4.8779-1	1.0244-1	7.6337-2	1.7202-2	3.7206-3	4.8011-4	2.9760-5
9	1.8534-13	1.1244-10	1.0491-8	5.9233-8	1.3888-5	1.0128-5	4.7685-3	1.1786-3	2.8927-1	5.2424-1	7.9801-2	7.9230-2	1.6920-2	4.0408-3	5.2926-4
10	4.9245-14	1.0207-13	9.6809-10	2.4304-8	4.6098-7	2.3178-5	8.7719-5	6.0358-3	6.1037-3	2.5782-1	5.6915-1	5.7376-2	8.2727-2	1.5863-2	4.2752-3
11	5.0633-17	5.3826-13	5.3210-12	4.9481-9	3.2181-8	1.9582-6	2.9402-5	3.2400-4	6.6828-3	1.6220-2	2.1498-1	6.1869-1	3.6519-2	8.7517-2	1.4050-2
12	1.0188-15	1.8996-14	1.9769-12	1.3185-10	1.7295-8	1.3557-8	5.8447-6	2.5412-5	8.3368-4	6.2839-3	3.2318-2	1.6313-1	6.6753-1	1.8875-2	9.4347-2
13	3.3279-16	5.4799-15	2.9464-13	2.0798-12	1.1339-9	4.3420-8	1.2278-8	1.3367-5	9.4334-6	1.7067-3	4.6711-3	5.3931-2	1.0707-1	7.0857-1	6.2550-3
14	5.4866-17	5.3805-15	3.9593-16	1.6457-12	2.3559-12	5.8518-9	7.6828-8	3.4640-7	2.4031-5	1.1931-6	2.9234-3	2.2431-3	7.8749-2	5.4367-2	7.3328-1
15	1.7921-17	6.6602-16	1.8022-14	3.1687-14	4.4747-12	1.4779-10	2.1131-8	8.3850-8	1.9185-6	3.3288-5	6.2841-5	4.2595-3	2.3617-4	1.0234-1	1.5011-2
16	2.8420-20	8.5038-17	1.0164-14	4.2038-14	4.9708-13	3.6233-12	1.4432-9	5.6056-8	2.8740-8	6.2837-6	3.2341-5	3.0962-4	5.2417-3	7.3647-2	1.1857-1
17	2.9486-17	2.1789-16	2.0012-15	4.3395-14	2.2960-14	2.3944-12	6.2867-12	7.7213-9	1.0868-7	3.2478-8	1.4732-5	1.5464-5	8.8324-4	5.2690-3	6.3520-3
18	1.0171-16	1.3487-17	6.0425-17	1.5492-14	1.1034-13	4.2613-15	5.2199-12	3.0184-10	2.8176-8	1.4119-7	7.2983-7	2.5794-5	6.7688-8	1.8614-3	3.9390-3
19	1.3940-16	6.7739-17	6.7072-17	1.7595-15	7.8144-14	2.0259-13	4.1500-13	6.0798-13	2.6790-9	7.5066-8	8.5565-8	3.5956-6	3.2399-5	5.6319-5	3.1096-3
20	2.0681-17	1.6193-16	4.9803-17	9.8874-19	3.2294-14	2.1040-13	2.8352-13	2.2894-12	6.3737-11	1.3294-8	1.4512-7	9.2392-10	1.0404-5	2.4035-5	3.2271-4
21	3.5482-17	5.1763-17	2.4038-18	3.2078-17	7.2804-15	1.2712-13	5.6264-13	7.9931-14	1.4454-12	1.0318-9	4.5578-8	1.8453-7	4.9236-7	2.0713-5	3.1979-6
22	1.7063-16	2.2884-19	3.8032-18	9.8820-17	4.3179-16	6.3021-14	3.7941-13	1.2162-12	2.8077-13	1.9034-11	5.8774-9	1.1370-7	1.0305-7	3.1390-6	2.8083-5
23	2.6721-16	1.9869-17	2.6767-17	5.9213-16	4.0636-18	2.3755-14	2.1622-13	1.4145-12	9.7737-13	2.6944-13	5.3546-10	2.9546-8	1.9880-7	5.9462-9	9.8767-6
24	1.3949-16	3.9506-17	6.2672-17	6.6084-16	7.2364-17	5.8425-15	1.1945-13	5.4780-13	2.3281-12	3.5369-13	2.1374-11	4.5833-9	8.8000-8	2.0095-7	7.9024-7
25	5.5412-19	1.6361-17	1.1615-16	3.4968-16	9.0760-16	1.1283-15	5.1642-14	2.3050-13	1.8880-12	4.1776-12	4.3061-12	4.8151-10	2.1669-8	1.7701-7	4.2742-8
26	9.7988-17	2.2193-19	1.3806-16	8.0335-17	2.1322-15	4.1104-16	1.0749-14	1.1153-13	1.1372-12	7.6723-12	1.1400-11	4.7898-11	3.3351-9	6.6409-8	2.2189-7
27	3.1142-16	2.0150-17	8.0677-17	5.8638-18	2.3089-15	4.3035-16	1.1745-17	6.8490-14	8.3183-13	8.6581-12	1.9476-11	9.4822-12	2.3305-10	1.4786-8	1.5305-7
28	4.3268-16	5.2950-17	2.7932-17	3.3630-18	1.3045-15	3.9918-16	2.4451-15	5.4145-14	9.4617-13	7.9598-12	1.8429-11	1.8347-12	5.7147-12	1.8066-9	6.1577-8
29	2.8228-16	4.3013-17	2.0285-18	2.8264-17	2.6401-16	5.4263-17	2.1394-15	6.5662-14	1.3502-12	6.3545-12	9.3813-12	1.2213-12	8.6121-11	6.1068-11	2.0922-8

v' \ v''	15	16	17	18	19	20	21	22	23	24	25	26	27
0	1.6729-16	2.6309-15	2.1657-15	6.5954-16	1.0585-16	1.0150-17	3.3945-18	1.0440-20	5.5059-19	3.8570-18	1.6211-17	4.5833-17	7.9011-17
1	1.2238-12	1.4381-14	1.9287-14	2.1956-14	9.1312-15	2.0004-15	2.0219-16	2.3298-17	1.3474-16	6.5214-16	9.9128-16	6.1761-16	5.1300-17
2	8.8749-11	8.1569-12	1.8991-13	6.6126-14	1.0784-13	5.7938-14	2.4999-14	1.0996-14	4.7852-15	1.7298-15	4.9505-16	3.2110-16	3.6068-16
3	2.2706-9	3.5573-10	3.8046-11	1.4259-12	1.7315-13	5.0340-13	3.2867-13	1.3601-13	4.8978-14	1.9795-14	9.7078-15	4.0730-15	7.1274-16
4	3.0447-8	6.5945-9	1.1239-9	1.3416-10	6.6658-12	2.7138-13	1.5039-12	1.2211-12	6.1524-13	2.3416-13	7.0593-14	1.7841-14	5.4427-15
5	2.3934-7	6.9697-8	1.6196-8	2.9850-9	3.9489-10	2.4321-11	3.0663-13	3.8351-12	3.4465-12	1.8416-12	1.5807-13	2.7130-13	1.1102-13
6	1.0907-6	4.5507-7	1.4110-7	3.4972-8	6.9125-9	1.0014-9	7.4721-11	7.8794-14	8.1314-12	8.4499-12	5.0667-12	2.6857-12	1.6595-12
7	2.2991-6	1.7914-6	7.8860-7	2.5877-7	6.8113-8	1.4371-8	2.2574-9	1.9787-10	2.2181-13	1.5795-11	2.1863-11	1.7145-11	1.1264-11
8	2.1893-7	3.4031-6	2.7481-6	1.2677-6	4.3760-7	1.2175-7	2.7347-8	4.6222-9	4.4876-10	1.3704-12	3.6025-11	5.5607-11	3.8990-11
9	3.3671-5	4.1665-7	4.8118-6	3.9855-6	1.9150-6	6.9188-7	2.0219-7	4.7937-8	8.5761-9	8.7456-10	3.6325-12	5.1525-11	4.8864-11
10	5.5276-4	3.5808-5	7.7599-7	6.5536-6	5.5143-6	2.7430-6	1.0318-6	3.1445-7	7.7899-8	1.4809-8	1.8154-9	8.1290-11	1.8140-13
11	4.4507-3	5.4616-4	3.6023-5	1.3962-6	8.6456-6	7.3276-6	3.7481-6	1.4605-6	4.6420-7	1.2220-7	2.6388-8	4.5836-9	5.8446-10
12	1.1547-2	4.6125-3	5.0662-4	3.4561-5	2.4157-6	1.1079-5	9.4005-6	4.9262-6	1.9922-6	6.6817-7	1.9074-7	4.5418-8	7.3576-9
13	1.0403-1	8.4984-3	4.8260-3	4.3318-4	3.2095-5	4.0297-6	1.3845-5	1.1742-5	6.3038-6	2.6495-6	9.2438-7	2.6281-7	5.0258-8
14	3.0950-4	1.1742-1	5.1936-3	5.1839-3	3.2794-4	2.9624-5	6.5689-6	1.6965-5	1.4373-5	7.8185-6	3.3128-6	1.1103-6	2.6698-7
15	7.3256-1	2.0083-3	1.3534-1	2.1485-3	5.8192-3	1.9933-4	2.8463-5	1.0593-5	2.0237-5	1.6964-5	9.0437-6	3.7016-6	1.1800-6
16	3.0735-6	6.9857-1	1.0987-2	1.5833-1	2.0467-4	6.9328-3	7.1139-5	3.0910-5	1.6735-5	2.2756-5	1.8889-5	9.8853-6	4.2716-6
17	1.2097-1	1.8644-2	6.2714-1	2.4980-2	1.8628-1	6.0714-4	8.8453-3	2.8249-7	4.2191-5	2.5969-5	2.4101-5	2.1392-5	1.2224-5
18	1.8821-2	1.0540-1	7.4710-2	5.2047-1	3.9689-2	2.1784-1	2.4977-1	1.5121-2	1.7421-2	6.3245-4	1.4695-4	8.3541-5	3.1439-5
19	1.6311-3	3.7817-2	7.3208-2	1.6254-1	3.8902-1	4.9485-2	4.9272-2	2.7637-1	3.2479-2	2.5880-2	2.0767-3	3.1703-4	1.6470-4
20	4.1577-3	1.7341-5	5.9209-2	3.3803-2	2.6482-1	2.5127-1	1.2992-1	3.7395-2	2.8937-1	5.7424-2	3.8671-2	5.2523-3	7.6910-4
21	9.5974-4	4.2794-3	2.0261-3	7.5083-2	4.4432-3	3.5433-1	4.0097-1	4.4780-2	1.8237-2	2.7997-1	8.7663-2	5.7364-2	1.1123-2
22	2.0201-5	1.9999-3	2.9745-3	1.0630-2	7.6295-2	5.4445-3	5.0307-2	3.8350-1	4.7731-3	3.2855-3	2.4332-1	1.1653-1	8.3229-2
23	2.1108-5	2.0615-4	3.1371-3	8.2331-4	2.6359-2	5.8166-2	2.7016-2	1.3415-1	3.0278-1	2.4185-3	3.5123-3	1.8217-1	1.3447-1
24	1.9702-5	1.7681-6	7.4606-4	3.6519-3	1.7188-4	4.4771-2	5.6328-2	2.2303-3	2.2898-1	1.8709-1	1.5469-2	3.1224-2	1.0720-1
25	4.4649-6	2.3735-5	3.0729-5	1.7109-3	2.7881-3	4.6600-3	1.6720-2	5.0861-2	9.7615-3	2.9273-1	7.9698-2	2.0613-2	7.9418-2
26	1.5745-7	1.1965-5	1.0806-5	2.6660-4	2.7510-3	8.1059-4	1.9626-4	3.3112-2	2.7216-2	6.5460-2	2.8925-1	1.4942-2	1.1193-2
27	1.3111-7	1.9018-6	1.8537-5	2.0447-6	8.8360-4	3.0047-3	1.8390-3	4.8818-3	4.3149-2	2.9179-3	1.5466-1	2.1212-1	4.2500-4
28	2.8340-7	1.0232-9	7.0980-6	1.4511-5	9.7121-5	1.8143-3	2.5479-3	1.8296-4	1.6292-2	3.6050-2	8.6058-3	2.2609-1	1.0112-1
29	2.1962-7	2.9253-7	9.4223-7	1.5973-5	6.5843-7	4.7819-4							

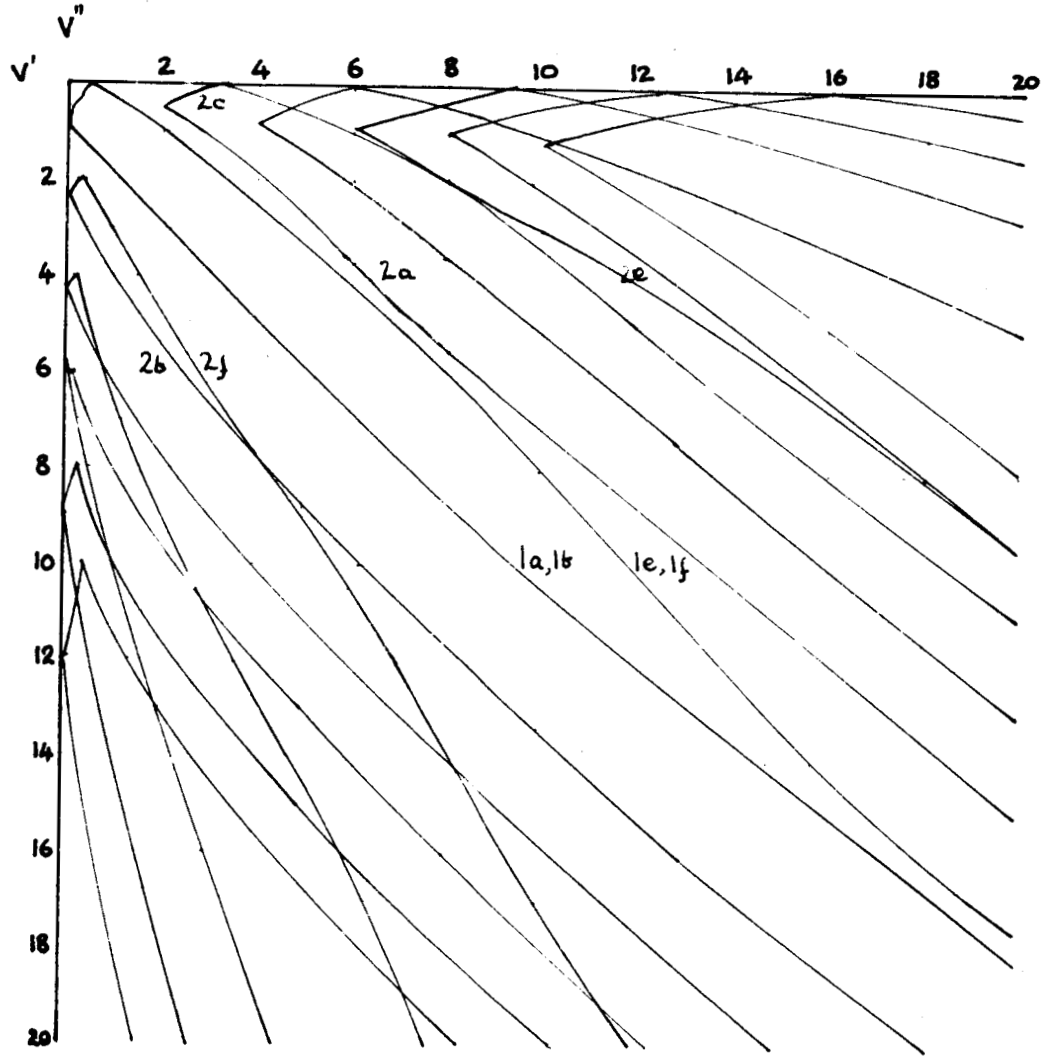

Fig. A2.1 Loci of coincidence of antinode pairs,

$N_2^+ B \leftarrow N_2 X$

assumed to be due to the contributions to the overlap integral of overlapping pairs of loops of the vibrational wave functions.

A2.2 MgO $B^1\Sigma \rightarrow A^1\Pi$ Red System ($\Delta r_e = 0.127$ Å)

Forty-six bands lying in the red region of the spectrum ($\lambda \sim 6000$ Å) are known in emission. The transition is of medium Δr_e giving well-defined nested Condon loci on the Franck-Condon factor array (table A2.2). The strongest bands are also seen to lie on the conventional form of Condon locus (table A2.3).

The calculated loci of the coincidence of antinode pairs are shown on fig. A2.2. The primary Condon locus is well represented by the locus of the coincidence of terminal antinode pairs. The secondary Condon locus is represented by the internal branches of the locus of coincidence of a terminal and a secondary antinode.

This case is very similar to that of the CO Fourth Positive System. The loci of the MgO system are slightly broader due to a larger Δr_e value.

A2.3 CO^+ $A^2\Pi \rightarrow X^2\Sigma$ Comet Tail System ($\Delta r_e = 0.12862$ Å)

The harmonic oscillator model of this system was studied in section A1.2 of this thesis. The measured band intensities will be found in table A1.4. The Franck-Condon factors for the Morse oscillator model are given in table A2.4 where broad nested Condon loci are clearly defined.

The calculated loci of antinode coincidence are given in fig. A2.3. As in the previous cases discussed the Condon loci of this system can be well represented by selected branches of the calculated loci.

Table A2.2

Franck-Condon Factors for MgO $B^1\Sigma \rightarrow A^1\Pi$ System (Nicholls 1962c)

v' \ v''	0	1	2	3	4	5	6	7
0	1.8306-1	2.8220-1	2.4205-1	1.5297-1	7.9650-2	3.6252-2	1.4952-2	5.7236-3
1	3.3956-1	8.8133-2	6.1050-3	9.9418-2	1.5503-1	1.3574-1	8.8549-2	4.8027-2
2	2.8256-1	2.6356-2	1.6410-1	5.5441-2	1.9893-3	6.2800-2	1.1491-1	1.1356-1
3	1.3872-1	2.0777-1	3.1342-2	6.0528-2	1.1484-1	2.9167-2	3.6489-3	5.3219-2
4	4.4545-2	2.3041-1	5.5960-2	1.1420-1	4.6824-4	8.1395-2	7.8915-2	1.1928-2
5	9.8033-3	1.1987-1	2.1144-1	8.4384-6	1.1876-1	2.7056-2	2.2178-2	8.3053-2
6	1.5068-3	3.6920-2	1.8561-1	1.2679-1	3.3018-2	6.3150-2	7.3658-2	5.0713-5
7	1.6178-4	7.3153-3	7.9740-2	2.1189-1	4.3965-2	8.5851-2	1.2438-2	8.7185-2

Table A2.3

Band Intensities of MgO B → A (Mahanti 1932)

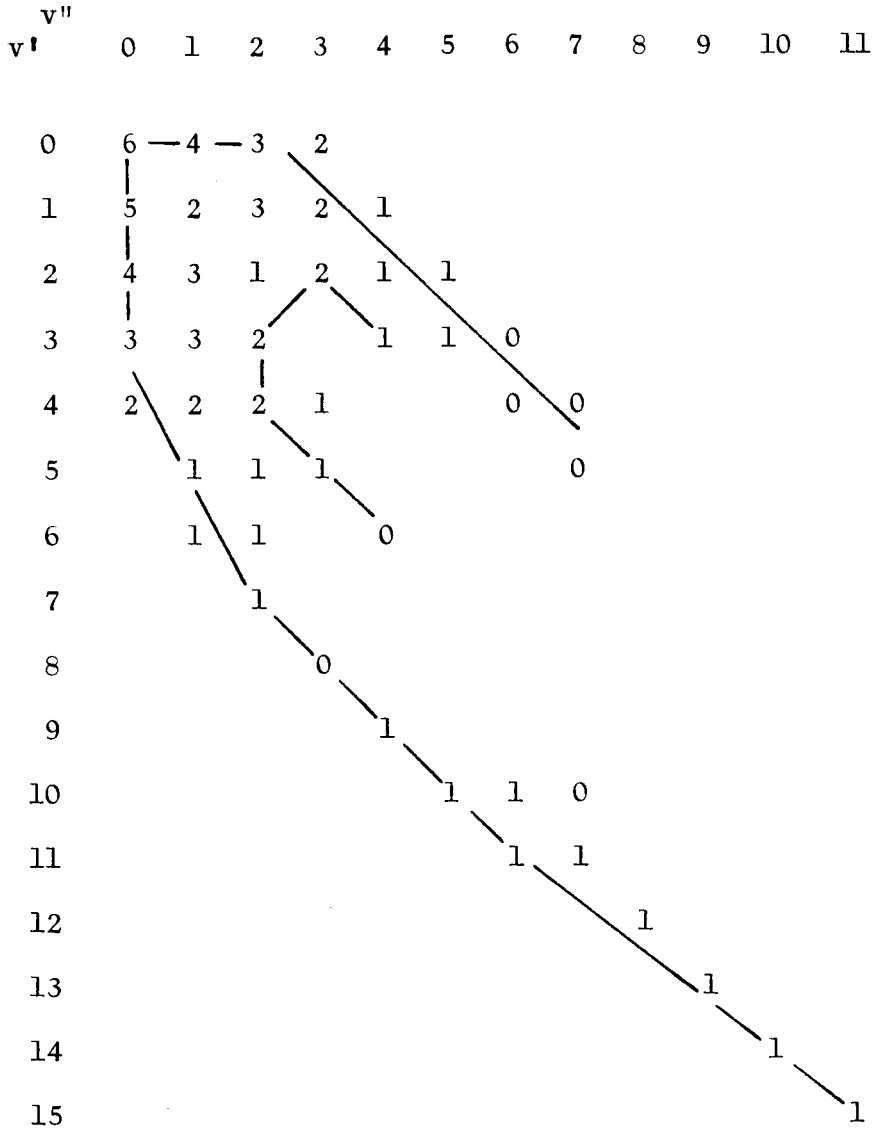

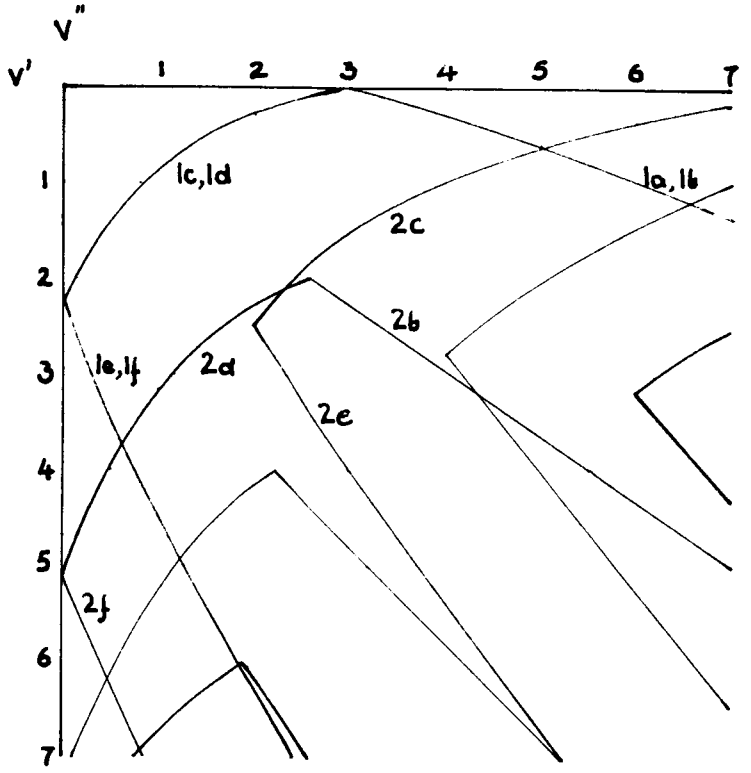

Fig. A2.2 Loci of coincidence of antinode pairs,

MgO B → A

Table A2.4

Franck-Condon Factors for CO^+ $A^2\Pi \rightarrow X^2\Sigma^+$ System (Nicholls 1962c)

v' \ v''	0	1	2	3	4	5	6	7	8	9	10	11	12	13
0	4.2745-2	1.5201-1	2.4987-1	2.5157-1	1.7335-1	8.6541-2	3.2330-2	9.2074-3	2.0181-3	3.4136-4	4.4433-5	4.4130-6	3.2957-7	1.8103-8
1	1.1506-1	1.9325-1	8.0462-2	5.6766-4	9.1665-2	1.9053-1	1.7595-1	9.9924-2	3.8971-2	1.0969-2	2.2812-3	3.5380-4	4.0879-5	3.4847-6
2	1.6979-1	9.7458-2	3.2276-3	1.0830-1	8.4544-2	3.5046-4	7.2252-2	1.7243-1	1.6130-1	8.8296-2	3.2140-2	8.2237-3	1.5168-3	2.0329-4
3	1.8244-1	1.2721-2	7.4829-2	6.8836-2	4.1855-3	9.7419-2	6.2065-2	1.0539-3	9.1449-2	1.7241-1	1.3941-1	6.6706-2	2.1102-2	4.6305-3
4	1.6004-1	5.7963-3	9.6177-2	5.7868-4	7.7853-2	3.5317-2	1.9930-2	9.8372-2	2.9637-2	1.6384-2	1.2684-1	1.6791-1	1.0874-1	4.2944-2
5	1.2187-1	4.5371-2	4.7189-2	3.3357-2	5.5935-2	9.2749-3	7.8567-2	5.5694-3	5.3829-2	8.1631-2	2.9760-3	5.7725-2	1.5869-1	1.4625-1
6	8.3692-2	8.3590-2	4.9733-3	7.1968-2	2.7299-3	6.3553-2	1.3161-2	4.3797-2	5.0731-2	4.9493-3	8.5397-2	4.0134-2	8.7396-3	1.1564-1
7	5.3165-2	9.8536-2	5.1549-3	5.6486-2	1.6807-2	4.5990-2	1.3848-2	5.5377-2	2.2886-3	6.9170-2	9.5381-3	4.3949-2	7.9079-2	3.0458-3
8	3.1817-2	9.1846-2	3.2115-2	1.8802-2	5.2375-2	4.0655-3	5.4195-2	3.7020-3	5.2171-2	1.3426-2	3.8243-2	4.6432-2	5.7134-3	8.3059-2
9	1.8182-2	7.3806-2	5.9270-2	2.3453-4	5.4271-2	9.0054-3	3.8654-2	1.6939-2	3.6070-2	1.4865-2	4.6950-2	4.2012-3	6.4832-2	4.4651-3
10	1.0025-2	5.3529-2	7.2508-2	8.8302-3	2.8246-2	3.8194-2	4.8691-3	4.7003-2	4.9856-4	4.9408-2	5.7364-4	5.1822-2	5.7995-3	4.6167-2

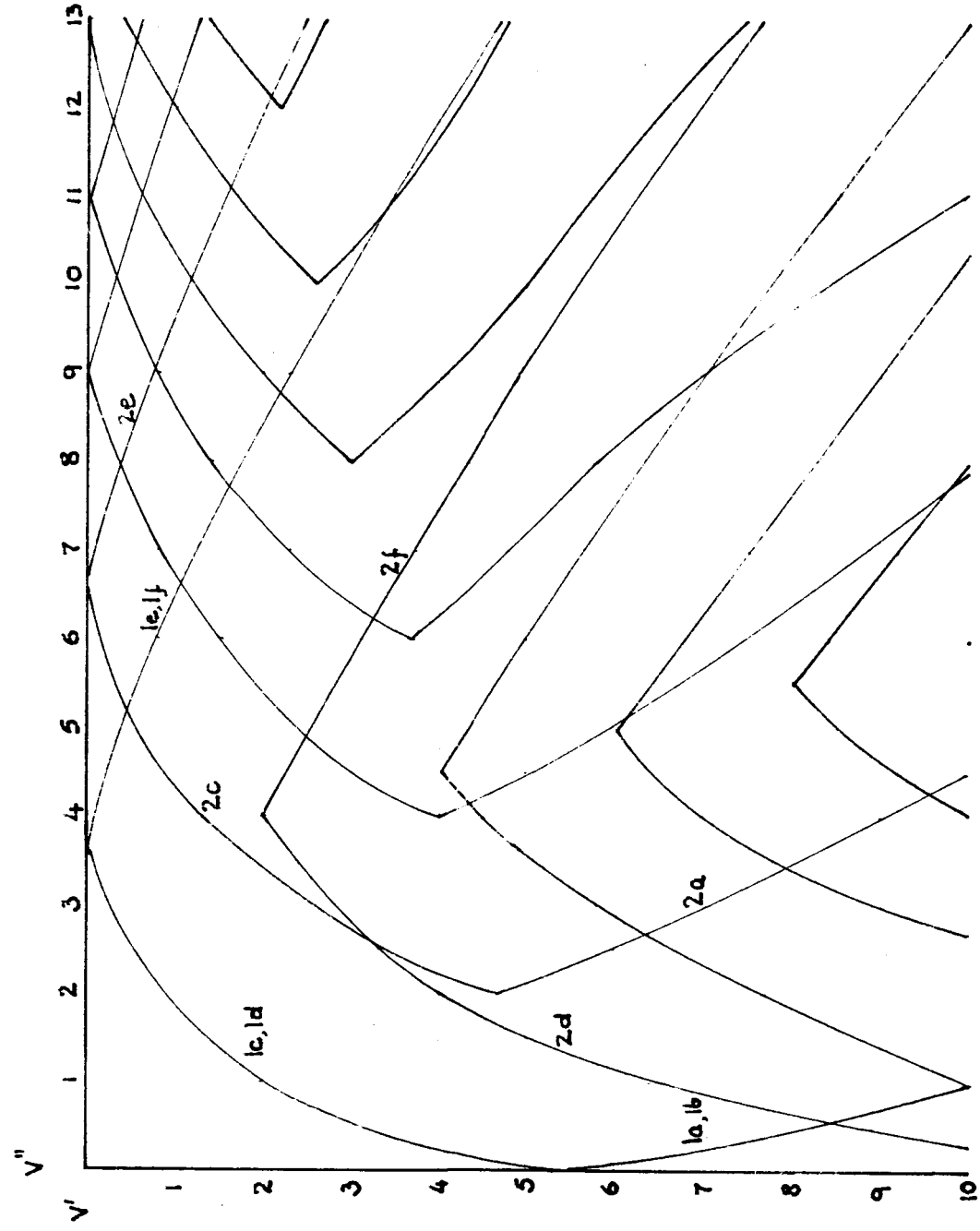

Fig. A2.3 Loci of coincidence of antinode pairs, CO^+ $A \rightarrow X$

A2.4 $\underline{N_2^+ \; C^2\Sigma^+ \leftarrow N_2 \; X^1\Sigma_g^+}$ ($\Delta r_e = 0.164$ Å)

The Franck-Condon factor array (table A2.5) shows broad nested Condon loci which are asymmetrical about the main diagonal of the Deslandres table. At high v" there are additional external Condon loci lying roughly along the diagonals. The Franck-Condon factors involved are very small, being much smaller than those of the internal subsidiary loci.

The calculated loci of antinode coincidence are shown in fig. A2.4. The primary Condon locus lies close to the c,d and e,f branches of the locus of the coincidence of terminal antinodes. The a,b branch exists at higher v' values than those considered. The appearance of only two of the sections of the primary locus explains the asymmetrical nature of the Condon array. The internal subsidiary Condon loci are well represented by the internal sections (d and f) of the calculated loci.

The external Condon loci are well represented by the external branches (e) of the calculated loci.

A2.5 $\underline{N_2^+ \; D^2\Pi_g \leftarrow N_2 \; X^1\Sigma_g^+}$ ($\Delta r_e = 0.383$ Å)

The Condon loci (table A2.6) of this system are very broad and far separated from the main diagonal of the Deslandres table. The calculated loci of antinode coincidence are shown in fig. A2.5.

The primary Condon locus is well represented by sections c,d and e,f of the locus of terminal antinode coincidence. The secondary Condon locus lies close to sections c and f of the calculated secondary locus. The tertiary locus lies close to sections d of the calculated

Table A2.5

Franck-Condon Factors for $N_2^+ C^2\Sigma_u^+ \leftarrow N_2 X^1\Sigma_g^+$ System (Nicholls 1962a)

v'\v''	0	1	2	3	4	5	6	7	8	9	10	11	12	13	14	15	16	17	18	19	20	21	22	23	24	25	26	27
0	2.1958-3	1.8586-2	7.0292-2	1.5688-1	2.2982-1	2.3246-1	1.6623-1	8.4533-2	3.0292-2	7.4482-3	1.1919-3	1.1172-4	4.7624-6	2.9246-8	2.5985-9	1.9018-10	1.6540-12	6.2254-13	3.1389-15	6.3459-15	3.4470-17	1.5680-15	3.4020-17	1.1327-15	7.6660-16	1.3898-16	1.4228-15	3.1632-16
1	1.0020-2	5.8698-2	1.3427-1	1.3968-1	4.6885-2	2.6849-3	9.4429-2	1.9453-1	1.8118-1	9.7843-2	3.2513-2	6.5471-3	7.3133-4	3.5129-5	2.0002-7	2.8946-8	1.8472-9	3.2756-11	6.8454-12	1.7178-13	2.4870-14	1.8632-15	7.8082-18	2.2499-17	3.5219-19	1.1118-16	5.0557-17	2.5816-17
2	2.5033-2	9.8313-2	1.2035-1	3.0665-2	1.3293-2	9.8576-2	7.0716-2	2.7749-5	8.1904-2	1.9238-1	1.6890-1	7.7448-2	1.9695-2	2.6140-3	1.4054-4	7.1139-7	1.7069-7	9.4196-9	2.9883-10	4.1660-11	1.9656-12	1.8397-13	2.8079-14	2.3856-15	1.4799-15	4.1988-17	2.1755-16	5.6056-17
3	4.5382-2	1.1403-1	5.7369-2	2.4560-3	7.5492-2	4.5375-2	5.5481-3	8.8136-2	5.4704-2	3.6630-3	1.2189-1	2.0497-1	1.3289-1	4.2974-2	6.7651-3	4.0454-4	1.7210-6	7.0985-7	3.3158-8	1.8144-9	1.6622-10	1.4437-11	5.3900-13	2.0245-13	1.9518-15	7.3659-15	1.4254-16	2.1971-15
4	6.6827-2	1.0013-1	8.8092-3	4.1287-2	3.7411-2	5.6992-4	6.6713-2	2.9309-2	1.8305-2	9.1633-2	1.9478-2	3.9839-2	1.8542-1	1.8311-1	7.6094-2	1.4196-2	9.3838-4	3.0994-6	2.3354-6	8.9906-8	8.3069-9	4.9901-10	7.6680-11	1.0062-12	1.0414-12	4.9246-15	1.7665-14	3.1858-16
5	8.4885-2	6.7729-2	2.1502-3	6.4637-2	8.8827-3	3.8571-2	3.9392-2	8.1830-3	6.7282-2	4.6392-3	5.5072-2	6.8372-2	1.2052-3	1.3125-1	2.1420-1	1.1609-1	2.5660-2	1.8635-3	4.2255-6	6.4680-6	1.9731-7	3.0891-8	1.1621-9	3.2176-10	8.7457-13	4.1358-12	1.3317-13	3.7592-14
6	9.6507-2	3.3445-2	2.3477-2	4.7118-2	4.2107-3	5.3544-2	3.2396-4	5.1434-2	1.1808-2	3.6240-2	4.3359-2	8.7804-3	8.6050-2	1.2243-2	6.8804-2	2.1962-1	1.5833-1	4.1481-2	3.2879-3	4.1109-6	1.5666-5	3.5777-7	9.7576-8	2.0741-9	1.1252-9	1.8501-14	1.3113-11	9.8318-13
7	1.0066-1	9.4888-3	4.6254-2	1.5996-2	3.0531-2	2.3566-2	2.0024-2	3.3651-24	1.0297-2	4.5929-2	1.7372-3	6.0990-2	3.1574-3	6.2595-2	4.6508-2	2.1948-2	2.0102-1	1.9791-1	6.1498-2	5.2835-3	2.1848-6	3.4037-5	5.3377-7	2.6950-7	2.6130-9	3.3934-9	1.1787-11	3.4720-11
8	9.8035-2	2.0303-4	5.4154-2	3.4962-4	4.5333-2	6.7612-4	4.2595-2	1.5580-3	4.2115-2	4.0111-3	4.1896-2	1.0809-2	3.8616-2	2.9132-2	2.5412-2	7.4333-2	1.2170-3	1.6576-1	2.3084-1	8.5141-2	7.8680-3	3.5434-8	6.7524-5	6.3001-7	6.6352-7	1.6748-9	8.9871-9	1.2893-10
9	9.0305-2	3.5455-3	4.5804-2	6.1791-3	3.4711-2	8.5686-3	3.0209-2	1.0362-2	2.8847-2	1.1792-2	3.0812-2	1.1579-2	3.7594-2	8.7347-3	5.2600-2	2.4734-3	5.0576-2	4.3979-3	1.2324-1	2.5469-1	1.1156-1	1.0995-2	4.3024-6	1.2389-4	5.2004-7	1.4755-6	6.2766-15	2.0945-8
10	7.9463-2	1.4411-2	2.8980-2	2.2285-2	1.4085-2	2.7945-2	6.5408-3	3.2159-2	2.6224-3	3.5631-2	8.7107-4	3.9356-2	3.2548-4	4.4740-2	4.9686-4	5.3548-2	3.0525-3	6.6389-2	2.2048-2	8.1876-2	2.6868-1	1.3981-1	1.4554-2	3.0772-5	2.1220-4	1.8187-7	2.9935-6	8.5227-9

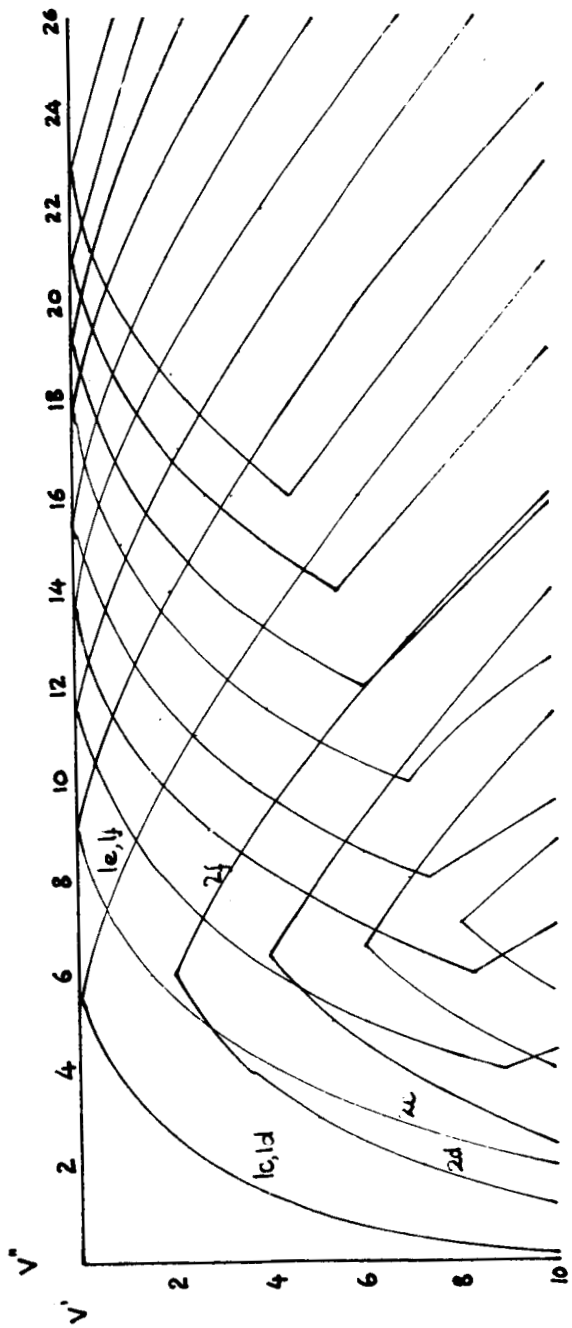

Fig. A2.4 Loci of coincidence of antinode pairs,

$N_2^+ C \leftarrow N_2\ X$

Table A2.6

Franck-Condon Factors for $N_2^+ \; D^2\Pi_g \leftarrow N_2 \; X^1\Sigma_g^+$ System (Nicholls 1962a)

v' \ v''	0	1	2	3	4	5	6	7
0	1.3213-10	4.1224-9	6.2577-8	6.1580-7	4.4160-6	2.4597-5	1.1076-4	4.1433-4
1	1.6230-9	4.6973-8	6.5715-7	5.9153-6	3.8469-5	1.9237-4	7.6848-4	2.5146-3
2	1.0374-8	2.7885-7	3.5983-6	2.9639-5	1.7473-4	7.8323-4	2.7666-3	7.8692-3
3	4.5969-8	1.1489-6	1.3687-5	1.0320-4	5.5125-4	2.2107-3	6.8763-3	1.6869-2
4	1.5871-7	3.6931-6	4.0654-5	2.8069-4	1.3576-3	4.8605-3	1.3246-2	2.7741-2
5	4.5507-7	9.8711-6	1.0050-4	6.3562-4	2.7817-3	8.8670-3	2.1040-2	3.7119-2
6	1.1278-6	2.2835-5	2.1525-4	1.2474-3	4.9353-3	1.3963-2	2.8624-2	4.1776-2
7	2.4826-6	4.6988-5	4.1050-4	2.1806-3	7.7917-3	1.9492-2	3.4188-2	4.0245-2
8	4.9516-6	8.7731-5	7.1112-4	3.4638-3	1.1166-2	2.4590-2	3.6439-2	3.3337-2
9	9.0825-6	1.5087-4	1.1360-3	5.0760-3	1.4743-2	2.8431-2	3.5016-2	2.3495-2
10	1.5500-5	2.4178-4	1.6932-3	6.9437-3	1.8144-2	3.0448-2	3.0489-2	1.3586-2
11	2.4837-5	3.6444-4	2.3769-3	8.9510-3	2.1010-2	3.0446-2	2.4040-2	5.8389-3

v' \ v''	8	9	10	11	12	13	14	15	16	17
0	1.3133-3	3.5800-3	8.4883-3	1.7665-2	3.2499-2	5.3163-2	7.7694-2	1.0182-1	1.2004-1	1.2761-1
1	6.8530-3	1.5724-2	3.0554-2	5.0330-2	6.9944-2	8.0900-2	7.5615-2	5.3482-2	2.3977-2	2.9346-3
2	1.8242-2	3.4592-2	5.3373-2	6.5792-2	6.2090-2	4.0482-2	1.3101-2	5.9864-6	1.2501-2	4.0632-2
3	3.2783-2	5.0012-2	5.8149-2	4.7925-2	2.2836-2	2.1409-3	5.1670-3	2.8939-2	4.7008-2	5.7770-2
4	4.4292-2	5.2119-2	4.1361-2	1.6843-2	3.8018-4	9.4525-3	3.2663-2	3.9161-2	1.9120-2	4.8892-4
5	4.7277-2	3.9907-2	1.7092-2	4.6315-4	9.0198-3	3.0424-2	3.2743-2	1.1498-2	2.8650-4	1.8184-2
6	4.0554-2	2.1235-2	1.8778-3	5.5578-3	2.5742-2	2.9868-2	1.0195-2	5.3252-4	1.8552-2	3.1160-2
7	2.7564-2	6.0773-3	1.5349-3	1.8997-2	2.8585-2	1.2580-2	4.5148-5	1.5011-2	2.7735-2	1.1957-2
8	1.3865-2	7.5749-5	1.0508-2	2.5949-2	1.7311-2	6.6147-4	9.2316-3	2.4832-2	1.3538-2	1.2645-5
9	4.0675-3	2.7100-3	1.9475-2	2.1958-2	4.5923-3	3.0903-3	2.0203-2	1.7138-2	6.9751-4	9.7013-3
10	1.1556-4	9.5846-3	2.2438-2	1.2007-2	3.6354-6	1.2494-2	2.0018-2	4.3749-3	3.6400-3	1.9850-2
11	1.3096-3	1.5901-2	1.8879-2	3.3443-3	3.8127-3	1.8336-2	1.1073-2	7.1619-5	1.3461-2	1.6389-2

v' \ v''	18	19	20	21	22	23	24	25	26	27
0	1.2256-1	1.0650-1	8.3811-2	5.9772-2	3.8640-2	2.2639-2	1.2017-2	5.7743-3	2.5089-3	9.8422-4
1	3.2441-3	2.6402-2	6.1418-2	9.1817-2	1.0527-1	9.9144-2	7.9312-2	5.4906-2	3.3261-2	1.7750-2
2	5.9646-2	5.2096-2	2.4584-2	2.1638-3	6.0499-3	3.6303-2	7.4076-2	9.8027-2	9.8681-2	8.0650-2
3	1.1513-2	3.0610-4	1.9521-2	4.8266-2	5.3875-2	3.0184-2	3.9263-3	4.8803-3	3.6439-2	7.6120-2
4	1.1094-2	3.6765-2	4.0123-2	1.5886-2	3.9994-6	1.7802-2	4.7467-2	5.0511-2	2.3418-2	7.3781-4
5	3.5814-2	2.2936-2	1.4168-3	9.5589-3	3.5678-2	3.6502-2	1.0470-2	1.3724-3	2.7323-2	5.2096-2
6	1.4193-2	4.4771-5	1.7282-2	3.3918-2	1.7771-2	3.0351-5	1.6761-2	3.9226-2	2.6586-2	1.7528-3
7	2.8561-4	1.8159-2	2.8562-2	9.1349-3	1.6916-3	2.4134-2	3.0397-2	7.1353-3	3.6962-3	3.0550-2
8	1.5074-2	2.5173-2	7.0134-3	2.7110-3	2.3796-2	2.2433-2	1.5477-3	1.0439-2	3.1530-2	1.8021-2
9	2.3078-2	8.3947-3	1.5739-3	2.0516-2	1.9212-2	7.1011-4	1.1884-2	2.7183-2	9.3178-3	2.2313-3
10	1.2136-2	1.0341-4	1.5453-2	1.9072-2	1.4069-3	9.3697-3	2.3702-2	7.1518-3	3.2615-3	2.4468-2
11	1.0011-3	8.7160-3	1.9370-2	4.0407-3	4.8848-3	2.0838-2	8.4838-3	1.9070-3	2.0917-2	1.4545-2

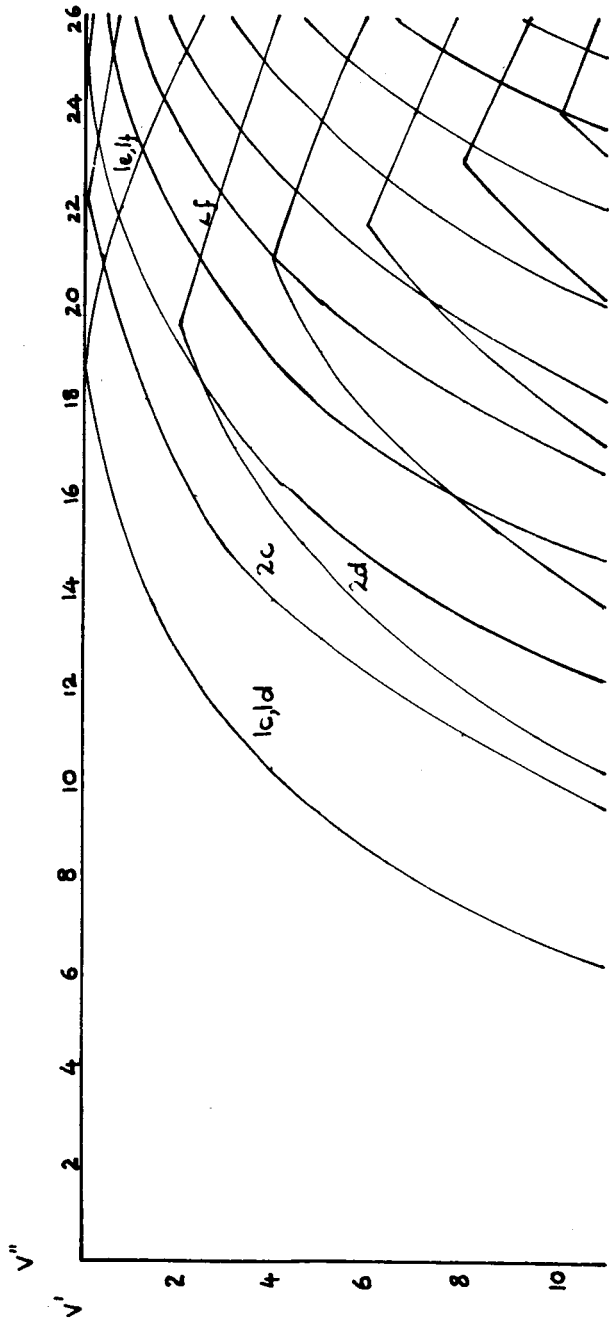

Fig. A2.5 Loci of coincidence of antinode pairs, $N_2^+ D \leftarrow N_2 X$

tertiary locus and c of the quaternary, and close to section f of the tertiary. The quaternary Condon locus lies close to sections d and f of the calculated quaternary.

In cases where Δr_e is large the sections c and d are large and these intersect other calculated loci on the v'v" plane. It is thus difficult to associate a subsidiary Condon locus with any single calculated locus.

A2.6 O_2 $B^3\Sigma_u^- \rightarrow X^3\Sigma_g^-$ Schumann-Runge System ($\Delta r_e = 0.397$ Å)

This system shows a confusion similar to the N_2 ionisation transition discussed in section A2.5. The Condon loci of the O_2 system (table A2.7) are very broad and crowded at high v" (~15). The positioning of the loci is ambiguous, and these are not usually drawn for this system.

The calculated loci of antinode coincidence (fig. A2.6) show that the first few loci are recognizable in the usual manner, but further subsidiary loci (~ 4 and up) are much confused by the crossing of calculated curves.

The positioning of observed bands (table A1.6) already discussed is in good agreement with the Condon loci shown in table A2.7 confirming the anharmonic nature of the potential.

A2.7 GaI $A^3\Pi \rightarrow X^1\Sigma$ System A ($\Delta r_e = 0.002$ Å)

The simple harmonic model of this system has been discussed in Appendix 1. It was pointed out that the approximate form of the Franck-Condon Principle is inadequate at zero Δr_e with a symmetrical

Table A2.7

Franck-Condon Factors for O_2 $B^3\Sigma_u^- \rightarrow X^3\Sigma_g^-$ System (Nicholls 1960)

v' \ v''	0	1	2	3	4	5	6	7	8	9	10	11	12	13	14	15	16	17	18	19	20	21
0	3.3636-9	9.7126-8	1.3505-6	1.2033-5	7.7140-5	3.7873-4	1.4800-3	4.7231-3	1.2534-2	2.8020-2	5.3261-2	8.6671-2	1.2131-1	1.4648-1	1.5285-1	1.3786-1	1.0739-1	7.2104-2	4.1588-2	2.0512-2	8.5997-3	3.0411-3
1	3.9676-8	1.0381-6	1.2945-5	1.0219-4	5.7192-4	2.4074-3	7.8855-3	2.0493-2	4.2622-2	7.0841-2	9.2709-2	9.1951-2	6.2856-2	2.1846-2	1.0257-4	1.8336-2	6.7037-2	1.1371-1	1.3009-1	1.1205-1	7.5984-2	4.1375-2
2	2.4404-7	5.7887-6	6.4721-5	4.5196-4	2.2003-3	7.8859-3	2.1377-2	4.4199-2	6.8987-2	7.8195-2	5.8045-2	2.0000-2	7.3533-7	2.1395-2	6.0732-2	6.9594-2	3.5561-2	1.9243-3	1.5355-2	7.0036-2	1.1824-1	1.2453-1
3	1.0427-6	2.2432-5	2.2478-4	1.3859-3	5.8435-3	1.7673-2	3.8964-2	6.1890-2	6.7163-2	4.2565-2	8.0346-3	3.6442-3	3.5436-2	5.6165-2	3.1874-2	1.1283-3	1.7764-2	5.9376-2	5.9716-2	1.7704-2	1.9012-3	4.6943-2
4	3.4788-6	6.7902-5	6.0943-4	3.3101-3	1.2022-2	3.0330-2	5.3060-2	6.1176-2	3.9368-2	6.5928-3	4.8018-3	3.5497-2	4.5513-2	1.5187-2	1.5192-3	3.3574-2	4.9757-2	1.6873-2	2.1202-3	4.1762-2	6.4757-2	2.8002-2
5	9.6580-6	1.7110-4	1.3745-3	6.5583-3	2.0379-2	4.2238-2	5.6541-2	4.2679-2	1.0217-2	2.3054-3	2.9646-2	4.0034-2	1.1488-2	3.1196-3	3.4247-2	3.6106-2	3.7200-3	1.3603-2	4.7615-2	2.8365-2	1.2399-3	3.3900-2
6	2.3224-5	3.7355-4	2.6835-3	1.1212-2	2.9558-2	4.9298-2	4.7668-2	1.8745-2	2.4519-3	2.0252-2	3.7544-2	1.4153-2	1.5408-3	2.9194-2	3.0501-2	1.6898-3	1.6769-2	4.0025-2	1.1688-2	6.0458-3	4.3709-2	3.1371-2
7	4.9711-5	7.2621-4	4.6605-3	1.6983-2	3.7589-2	4.9002-2	3.0940-2	2.8849-3	8.9576-3	3.3206-2	2.0936-2	3.2905-7	2.0982-2	3.0040-2	3.0113-3	1.3052-2	3.4373-2	8.0048-3	8.6070-3	3.8515-2	1.4719-2	4.9956-3
8	9.6625-5	1.2824-3	7.3428-3	2.3230-2	4.2587-2	4.1577-2	1.3901-2	7.4736-4	2.3072-2	2.8295-2	3.1437-3	1.0329-2	2.9726-2	7.8961-3	6.2085-3	3.0316-2	1.0138-2	5.7265-3	3.2809-2	1.0979-2	6.9141-3	3.7762-2
9	1.7712-4	2.0880-3	1.0652-2	2.9097-2	4.3413-2	2.9670-2	2.8284-3	8.7895-3	2.9306-2	1.3134-2	1.4009-3	2.4219-2	1.6508-2	5.8090-4	2.3815-2	1.6070-2	1.2937-3	2.6919-2	1.3395-2	3.9868-3	3.1802-2	9.4771-3
10	2.8930-4	3.1716-3	1.4394-2	3.3722-2	4.0000-2	1.7010-2	9.6842-5	1.9035-2	2.4329-2	1.7349-3	1.1939-2	2.3260-2	1.9694-3	1.2715-2	2.2466-2	4.5280-4	1.7952-2	1.9016-2	4.1577-4	2.5446-2	1.2415-2	5.5010-3
11	4.5511-4	4.5367-3	1.8283-2	3.6448-2	3.3274-2	6.8969-3	4.1499-3	2.4809-2	1.3329-2	9.7568-4	2.1221-2	1.2076-2	1.9041-3	2.2311-2	7.2076-3	6.4555-3	2.3039-2	1.4750-3	1.5844-2	1.8382-2	7.9941-4	2.6187-2
12	6.7919-4	6.1581-3	2.1993-2	3.6947-2	2.4773-2	1.1989-3	1.1258-2	2.3748-2	3.7310-3	8.0403-3	2.1145-2	1.8049-3	1.1752-2	1.7579-2	1.0621-5	1.8677-2	9.7814-3	4.5561-3	2.2209-2	1.1790-3	1.7126-2	1.4938-2
13	9.6760-4	7.9824-3	2.5206-2	3.5264-2	1.6158-2	1.2058-4	1.7641-2	1.7500-2	1.4795-5	1.5820-2	1.3387-2	7.2694-4	1.8785-2	6.1763-3	6.3663-3	1.8530-2	1.5729-4	1.6968-2	9.3470-3	5.3332-3	2.0752-2	1.1138-4
14	1.3229-3	9.9340-3	2.7664-2	3.1758-2	8.8051-3	2.5852-3	2.0894-2	9.5999-3	2.2594-3	1.8963-2	4.6266-3	6.8563-3	1.6846-2	9.8265-5	1.5285-2	8.2706-3	4.6217-3	1.7841-2	7.5768-5	1.7358-2	6.5714-3	8.5767-3
15	1.7436-3	1.1923-2	2.9199-2	2.6995-2	3.5617-3	6.9014-3	2.0397-2	3.2778-3	7.6300-3	1.6489-2	2.0345-4	1.3583-2	9.1074-3	2.8375-3	1.6729-2	5.8329-4	1.3659-2	7.9002-3	5.1625-3	1.6716-2	1.3173-4	1.8585-2
16	2.2239-3	1.3854-2	2.9744-2	2.1615-2	7.0127-4	1.1398-2	1.6938-2	2.3993-4	1.2745-2	1.0622-2	1.2745-3	1.5971-2	2.1520-3	9.5466-3	1.0663-2	1.7071-3	1.5860-2	4.4515-4	1.3908-2	5.6509-3	7.7287-3	1.2930-2
17	2.7538-3	1.5639-2	2.9329-2	1.6222-2	1.8546-5	1.4844-2	1.1986-2	5.3376-4	1.5365-2	4.6352-3	5.6573-3	1.3305-2	2.8063-5	1.3926-2	3.3389-3	7.9905-3	1.0195-2	2.0040-3	1.4795-2	1.4330-5	1.5060-2	2.3634-3
18	3.3202-3	1.7199-2	2.8067-2	1.1299-2	1.0010-3	1.6607-2	7.0243-3	3.0986-3	1.4912-2	8.6967-4	1.0193-2	7.9633-3	2.5359-3	1.2277-2	3.8679-5	1.2720-2	3.0445-3	8.3632-3	8.2711-3	3.6269-3	1.2776-2	6.6412-4
19	3.9072-3	1.8475-2	2.6120-2	7.1750-3	3.0097-3	1.6607-2	3.1183-3	6.4995-3	1.2098-2	6.0498-5	1.2642-2	2.9867-3	6.9176-3	8.5273-3	1.6452-3	1.2497-2	9.4048-6	1.2473-2	1.6953-3	1.0060-2	5.0972-3	6.8776-3
20	4.4975-3	1.9430-2	2.3682-2	4.0129-3	5.4277-3	1.5152-2	7.7456-4	9.5019-3	8.2155-3	1.6173-3	1.2353-2	3.1174-4	1.0322-2	3.9232-3	5.7175-3	8.3954-3	1.8961-3	1.1365-2	1.4158-4	1.2399-2	2.6001-4	1.2044-2
21	5.0733-3	2.0044-2	2.0949-2	1.8359-3	7.7552-3	1.2743-2	2.2666-6	1.1359-2	4.4952-3	4.3237-3	9.9517-3	2.8823-4	1.1276-2	6.9827-4	9.2104-3	3.5587-3	5.9906-3	6.8169-3	3.1689-3	9.4255-3	1.1109-3	1.1182-2

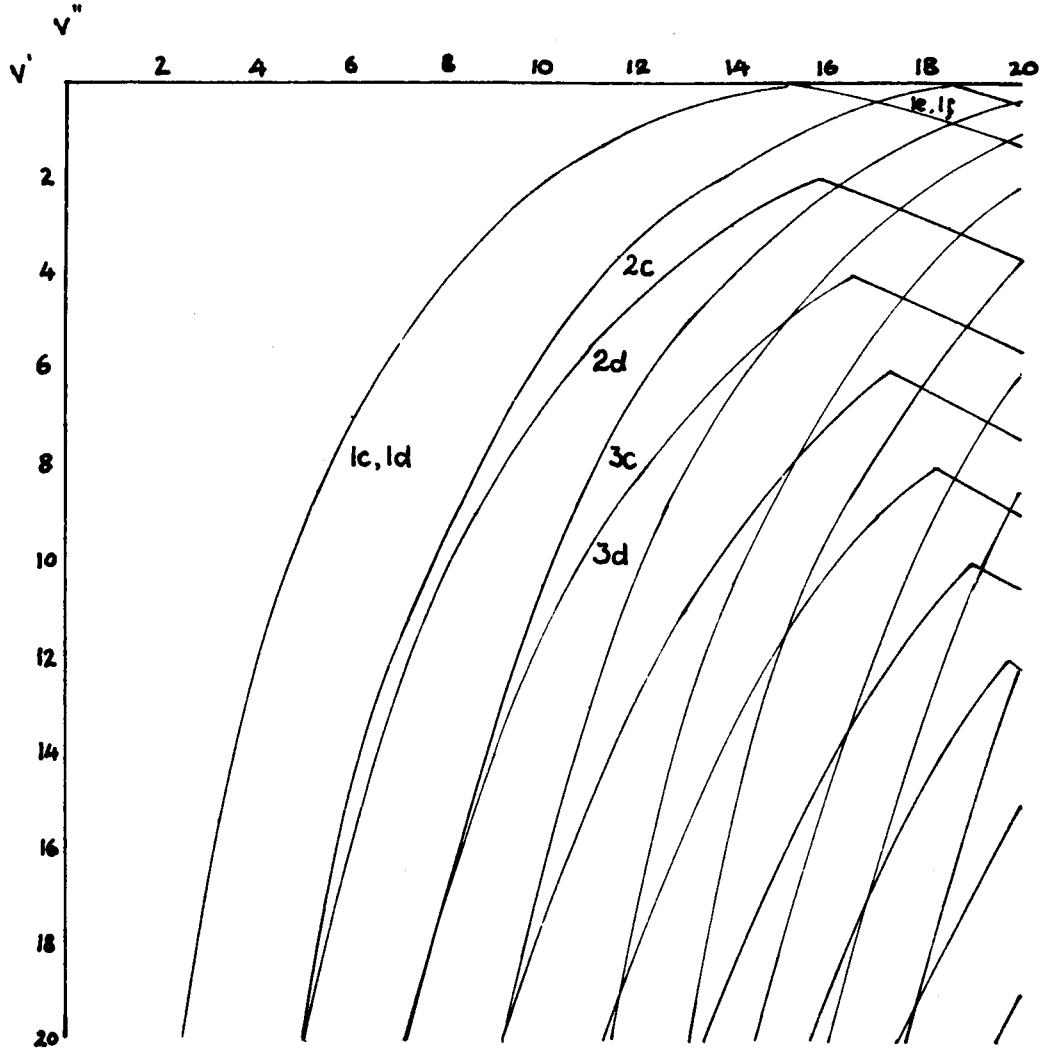

Fig. A2.6 Loci of coincidence of antinode pairs,

O_2 $B \rightarrow X$

potential function. The effect of imposing an anharmonicity and small value of Δr_e will be studied in this section.

Table A2.8 is the Franck-Condon factor array of the Morse model using measured constants and a Δr_e of 0.002 Å. The primary Condon locus lies along the main diagonal up to $v' = v'' = 4$. From this point its branches diverge, and a secondary Condon locus appears at $v' = v'' = 9$. To the high v' side of the main diagonal are isolated entries of larger Franck-Condon factors than their neighbours. These entries are of very small value compared with those defining the conventional Condon loci.

The calculated loci of antinode pair coincidence are shown in fig. A2.7. The sections c and d are very short due to the small value of Δr_e used. The sections a and e, b and f diverge from each other due to the large anharmonicity ($\omega_e x_e = 2.4$ cm^{-1}) of the upper state. The portion of the primary Condon locus lying along the main diagonal is well represented by the coincidence of left hand pairs of terminal antinodes. This coincidence at higher v values continues to represent the primary Condon locus. The high v'' branch of the Condon locus lies close to the locus of the coincidence of right hand terminal antinode pairs.

The high v'' branch of the secondary Condon locus is well represented by part of the section f of the coincidence of a secondary and primary antinode. The low v'' branch which is not clearly defined by high Franck-Condon factors, cannot be represented according to our scheme. The additional high Franck-Condon factor entries are probably due to the overlapping of terminal antinodes with subsidiary antinodes.

Table A2.8

Franck-Condon Factors for GaI $A^3\Pi \rightarrow X^1\Sigma$ System (Nicholls 1964b)

v' \ v''	0	1	2	3	4	5	6	7	8	9	10	11	12	13	14	15	16
0	9.9268-1	5.2733-3	1.8659-3	1.7505-4	3.7342-6	2.1066-6	3.9520-8	8.3209-9	1.6149-9	9.6930-13	2.9846-11	1.5071-14	4.8015-14	4.5343-14	5.1803-15	2.7047-15	1.0187-16
1	6.3716-3	9.5605-1	2.8608-2	7.6970-3	1.2034-3	6.4506-5	1.9663-5	1.1758-6	1.5892-7	3.0383-8	8.6215-10	4.8455-10	1.6165-11	2.0527-12	1.0268-12	5.9120-15	1.9637-14
2	9.0841-4	3.7387-2	8.5893-1	7.6077-2	2.1301-2	4.8135-3	4.7142-4	1.1762-4	1.2933-5	1.7868-6	3.3747-7	2.5130-8	6.0666-9	5.4044-10	5.9166-11	1.5736-11	3.6027-13
3	2.1655-5	1.0380-3	1.0985-1	6.8557-1	1.3962-1	4.6784-2	1.4298-2	2.1982-3	5.4809-4	8.8298-5	1.4223-5	2.8009-6	3.3898-7	6.5270-8	8.7762-9	1.1278-9	2.2646-10
4	1.1472-5	2.1027-4	1.4154-5	2.2541-1	4.5153-1	1.9423-1	8.4359-2	3.4063-2	7.5751-3	2.0906-3	4.4482-4	8.6525-3	1.8636-5	3.0541-6	5.9031-7	9.9420-8	1.5329-8
5	3.6939-6	2.0431-5	6.3561-4	4.1136-3	3.5581-1	2.1195-1	2.0689-1	1.2443-1	6.6693-2	2.0548-2	6.6329-3	1.7786-3	4.2033-4	1.0224-4	2.0945-5	4.4404-6	8.7979-7
6	2.1939-7	2.4829-5	2.8187-6	7.2870-4	2.9974-2	4.4143-1	4.4484-2	1.5982-1	1.4585-1	1.0709-1	4.4971-2	1.7567-2	5.8288-3	1.6725-3	4.6885-4	1.1581-4	2.7869-5
7	2.6902-9	3.9088-6	7.0068-5	3.2123-5	3.2967-5	9.7241-2	4.1973-1	1.6695-3	7.4694-2	1.2701-1	1.3760-1	7.9472-2	3.8632-2	1.5828-2	5.5187-3	1.8074-3	5.3014-4
8	2.4378-10	2.2646-7	2.5647-5	9.7326-5	1.8229-4	2.7824-3	2.0448-1	2.8017-1	6.0346-2	9.0143-3	6.9474-2	1.3363-1	1.1100-1	6.9445-2	3.5503-2	1.5125-2	5.8550-3
9	7.3642-10	1.1693-8	3.5410-6	8.8971-5	5.2294-5	1.2718-4	2.4028-2	3.0403-1	1.0059-1	1.2467-1	8.4531-3	1.2229-2	8.5878-2	1.1616-1	9.8894-2	6.4716-2	3.4139-2
10	6.2176-10	6.0081-9	3.1627-7	2.4630-5	1.7947-4	9.1846-7	2.9070-4	8.4332-2	3.1661-1	2.9561-3	1.1011-1	5.2212-2	4.6887-3	2.3594-2	8.0299-2	1.0493-1	9.2645-2
11	2.6654-10	5.9924-9	5.4449-8	3.9656-6	9.6793-5	2.0483-4	5.1602-6	7.5254-3	1.8036-1	2.0726-1	3.4423-2	3.6364-2	6.8317-2	4.6635-2	5.6669-4	2.4527-2	7.2343-2
12	8.4181-11	3.7200-9	3.2818-8	6.1907-7	2.6983-5	2.3217-4	1.1874-4	1.4577-4	4.0227.2	2.5371-1	5.6386-2	1.0291-1	1.2395-4	2.9457-2	7.3030-2	3.2947-2	1.7811-4

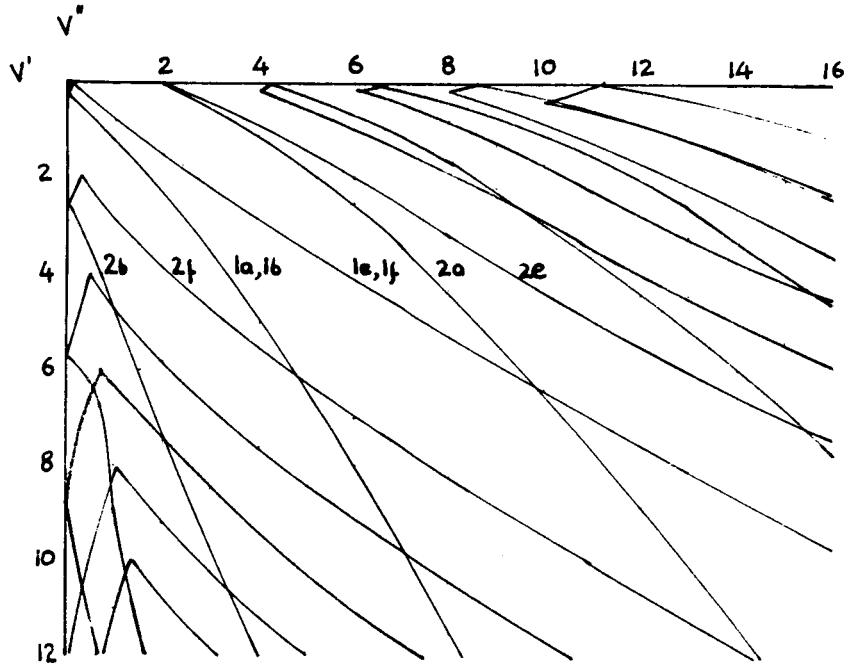

Fig. A2.7 Loci of coincidence of antinode pairs,

GaI $A \rightarrow X$

The Franck-Condon factor and intensity arrays are similar only in the predominance of the main diagonal. There are several reasons for the lack of similarity between the other diagonals:

(a) the intensity array may not be realistic. The sequences of the band system are overlapped, and the B system ($B^3\Pi \rightarrow X^1\Sigma^+$) of GaI exists in the same spectral region. The intensity measurements are only eye estimates of density and there has been no recent study.

(b) The Franck-Condon factor array may not be realistic. An arbitrary small non-zero value of Δr_e was chosen which may not have been correct. However, it is doubtful that a small change in Δr_e causes much change in the form of the array. The Morse potential model used in the calculations has a high anharmonicity constant influencing the form of the array considerably.

It is concluded that either the intensity measurements are in error, or that the electronic states are well represented by parabolic potentials with virtually identical equilibrium positions ($\Delta r_e = 0$) as discussed in Appendix 1.

REFERENCES

Aiken, H.H. 1951. Harvard Problem Report No. 27, "Computation of the Intensities of Vibrational Spectra of Electronic Bands in Diatomic Molecules (AF Problem 56)".

Allen, C.W. 1962. "Astrophysical Quantities", 2nd edition. Athlone Press, University of London.

Bates, D.R. 1952. Mon. Not. Roy. Astron. Soc. 112, 614.

Condon, E.U. 1926. Phys. Rev. 28, 1182.

Condon, E.U. 1928. Phys. Rev. 32, 858.

Condon, E.U. 1947. Am. J. Phys. 15, 365.

Estey, R.S. 1930. Phys. Rev. 35, 309.

Flinn, D.J., Spindler, R.J., Fifer, S. and Kelly, M. 1964. J. Quant. Spect. Rad. Trans. 4, 271.

Franck, J. 1926. Trans. Faraday Soc. 21, 536.

Fraser, P.A. 1954. Can. J. Phys. 32, 515.

Gaydon, A.G. and Pearse, R.W.B. 1939. Proc. Roy. Soc. 173A, 37.

Headrick, L.B. and Fox, G.W. 1930. Phys. Rev. 35, 1033.

Hébert, G.R. and Nicholls, R.W. 1961. Proc. Phys. Soc. 78, 1024.

Herzberg, G. 1950. "Molecular Spectra and Molecular Structure. I Spectra of Diatomic Molecules". 2nd edition. D. van Nostrand Company, Inc. Princetown, New Jersey.

Hutchisson, E. 1930. Phys. Rev. 36, 410.

Jarmain, W.R. 1963. Can. J. Phys. 41, 1926.

The Franck-Condon factor and intensity arrays are similar only in the predominance of the main diagonal. There are several reasons for the lack of similarity between the other diagonals:

(a) the intensity array may not be realistic. The sequences of the band system are overlapped, and the B system ($B^3\Pi \rightarrow X^1\Sigma^+$) of GaI exists in the same spectral region. The intensity measurements are only eye estimates of density and there has been no recent study.

(b) The Franck-Condon factor array may not be realistic. An arbitrary small non-zero value of Δr_e was chosen which may not have been correct. However, it is doubtful that a small change in Δr_e causes much change in the form of the array. The Morse potential model used in the calculations has a high anharmonicity constant influencing the form of the array considerably.

It is concluded that either the intensity measurements are in error, or that the electronic states are well represented by parabolic potentials with virtually identical equilibrium positions ($\Delta r_e = 0$) as discussed in Appendix 1.

REFERENCES

Aiken, H.H. 1951. Harvard Problem Report No. 27, "Computation of the Intensities of Vibrational Spectra of Electronic Bands in Diatomic Molecules (AF Problem 56)".

Allen, C.W. 1962. "Astrophysical Quantities", 2nd edition. Athlone Press, University of London.

Bates, D.R. 1952. Mon. Not. Roy. Astron. Soc. 112, 614.

Condon, E.U. 1926. Phys. Rev. 28, 1182.

Condon, E.U. 1928. Phys. Rev. 32, 858.

Condon, E.U. 1947. Am. J. Phys. 15, 365.

Estey, R.S. 1930. Phys. Rev. 35, 309.

Flinn, D.J., Spindler, R.J., Fifer, S. and Kelly, M. 1964. J. Quant. Spect. Rad. Trans. 4, 271.

Franck, J. 1926. Trans. Faraday Soc. 21, 536.

Fraser, P.A. 1954. Can. J. Phys. 32, 515.

Gaydon, A.G. and Pearse, R.W.B. 1939. Proc. Roy. Soc. 173A, 37.

Headrick, L.B. and Fox, G.W. 1930. Phys. Rev. 35, 1033.

Hébert, G.R. and Nicholls, R.W. 1961. Proc. Phys. Soc. 78, 1024.

Herzberg, G. 1950. "Molecular Spectra and Molecular Structure. I Spectra of Diatomic Molecules". 2nd edition. D. van Nostrand Company, Inc. Princetown, New Jersey.

Hutchisson, E. 1930. Phys. Rev. 36, 410.

Jarmain, W.R. 1963. Can. J. Phys. 41, 1926.

Jarmain, W.R., Fraser, P.A. and Nicholls, R.W. 1955. Astrophys. J. 122, 55.

Jenkins, F.A., Barton, H.A. and Mulliken, R.S. 1927. Phys. Rev. 30, 175.

Mahanti, P.C. 1932. Phys. Rev. 42, 609.

Manneback, C. 1951. Physica 17, 1001.

Miescher, E. and Wehrli, M. von 1934. Helv. Phys. Acta 7, 331.

Morse, P.M. 1929. Phys. Rev. 34, 57.

Nicholls, R.W. 1960. Can. J. Phys. 38, 1705.

Nicholls, R.W. 1962a. J. Quant. Spect. Rad. Transf. 2, 433.

Nicholls, R.W. 1962b. Nature 193, 966.

Nicholls, R.W. 1962c. Journ. Res. Nat. Bur. Stand. 66A, 227.

Nicholls, R.W. 1962d. Can. J. Phys. 40, 1772.

Nicholls, R.W. 1963a. Nature 199, 794.

Nicholls, R.W. 1963b. presented at C.A.P. Congress 1963.

Nicholls, R.W. 1964a. Private communication.

Nicholls, R.W. 1964b. Private communication.

Pauling, L. and Wilson, E.B. 1935. "Introduction to Quantum Mechanics". McGraw-Hill Book Company Inc., New York and London.

Pearse, R.W.B. and Gaydon, A.G. 1950. "The Identification of Molecular Spectra". Chapman and Hall, Ltd. London.

Phillips, J.G. 1949. Astrophys. J. 110, 73.

Pillow, M.E. 1949. Proc. Phys. Soc. 62A, 237.

Takamine, T., Suga, T. and Tanaka, Y. 1938. Sci. Papers Int. Phys. Chem. Research Tokyo 34, 854.

Wehrli, M. von 1934. Helv. Phys. Acta 7, 676.

VITA

NAME: Mary Frances Murty

BORN: Ruislip, Middlesex, England. 1938.

EDUCATION:
Satterthwaite School, Lancashire
Meadowside, Ruislip, England
Northwood College, Northwood, England
Battersea Polytechnic, London
Imperial College, London
University of Western Ontario, Canada

DEGREE: B.Sc. London 1961

APPOINTMENTS:
Summers 1956 and 1957. Laboratory Assistant, The Metal Box Company.

Summer 1958. Student employee, Road Research Laboratory, Department of Scientific and Industrial Research.

Summer 1959. Student employee, Hilger and Watts Limited.

Summer 1960. Student employee, Ontario Research Foundation, Toronto.

Summer 1961. Laboratory Assistant, The Metal Box Company.

1961 - 1962. Research Assistant, Molecular Excitation Group, University of Western Ontario.

1961 - 1964. Part-time Demonstrator, Department of Physics, University of Western Ontario.

PAPER GIVEN: "Condon Loci of Diatomic Molecular Spectra", Tetra-University Colloquium at the State University of New York at Buffalo, October 1963.